Population Dynamics of Stochastic Lattice Lotka–Volterra Models

Sheng Chen

Dissertation submitted to the Faculty of the
Virginia Polytechnic Institute and State University
in partial fulfillment of the requirements for the degree of

Doctor of Philosophy
in
Physics

Uwe C. Täuber, Chair
Shengfeng Cheng
Michel J. Pleimling
Eric R. Sharpe

February 5, 2018
Blacksburg, Virginia

Keywords: stochastic population dynamics, critical dynamics, aging scaling, early warning signals, spatial inhomogeneities, boundary effects, quenched disorder, Darwinian evolution, multi-species coexistence, character displacement

Population Dynamics of Stochastic Lattice Lotka–Volterra Models

Sheng Chen

(ABSTRACT)

In a stochastic Lotka–Volterra model on a two-dimensional square lattice with periodic boundary conditions and subject to occupation restrictions, there exists an extinction threshold for the predator population that separates a stable active two-species coexistence phase from an inactive state wherein only prey survive. When investigating the non-equilibrium relaxation of the predator density in the vicinity of the phase transition point, we observe critical slowing-down and algebraic decay of the predator density at the extinction critical point. The numerically determined critical exponents are in accord with the established values of the directed percolation universality class. Following a sudden predation rate change to its critical value, one finds critical aging for the predator density autocorrelation function that is also governed by universal scaling exponents. This aging scaling signature of the active-to-absorbing state phase transition emerges at significantly earlier times than the stationary critical power laws, and could thus serve as an advanced indicator of the (predator) population's proximity to its extinction threshold.

In order to study boundary effects, we split the system into two patches: Upon setting the predation rates at two distinct values, one half of the system resides in an absorbing state where only the prey survives, while the other half attains a stable coexistence state wherein both species remain active. At the domain boundary, we observe a marked enhancement of the predator population density, the minimum value of the correlation length, and the maximum attenuation rate. Boundary effects become less prominent as the system is successively divided into subdomains in a checkerboard pattern, with two different reaction rates assigned to neighboring patches.

We furthermore add another predator species into the system with the purpose of studying possible origins of biodiversity. Predators are characterized with individual predation efficiencies and death rates, to which "Darwinian" evolutionary adaptation is introduced. We find that direct competition between predator species and character displacement together play an important role in yielding stable communities.

We develop another variant of the lattice predator-prey model to help understand the killer-prey relationship of two different types of E. coli in a biological experiment, wherein the prey colonies disperse all over the plate while the killer cell population resides at the center, and a "kill zone" of prey forms immediately surrounding the killer, beyond which the prey population gradually increases outward.

(GENERAL ABSTRACT)

We utilize Monte-Carlo simulations to study population dynamics of Lotka–Volterra model and its variants. Our research topics include the non-equilibrium phase transition from a predator-prey coexistence state to an absorbing state wherein only prey survive, boundary effects in a spatially inhomogeneous system, the stabilization of a three species system with direct competition and "Darwinian" evolutionary adaption introduced, and the formation of spatial patterns in a biological experiment of two killer and prey E. coli species.

This work was supported by the U.S. Department of Energy, Office of Basic Energy Sciences, Division of Materials Sciences and Engineering, under Grant No. DE-FG02-09ER46613, and the US Army Research Office, under Grant Number W911NF-17-1-0156. The views and conclusions contained in this document are those of the author and should not be interpreted as representing the official policies, either expressed or implied, of the Army Research Office or the US Government. The US Government is authorized to reproduce and distribute reprints for Government purposes notwithstanding any copyright notation herein.

I dedicate this work to:
My beloved parents, Gengrong and Aiqin,
my loving brother and his family,
thank you for all of your support along the way,
and to my wife Yujia,
for your love, patience, kindness, and support,
and to my young boy Lucas.

Acknowledgments

I would like to express my sincere gratitude to my advisor, Prof. Uwe C. Täuber, for his continuous support of my Ph.D study and related research. His guidance helped me all the time since I joined in his group. I thank him for teaching me all about passion, curiosity, and self-discipline in research.

My sincere thanks also go to my other committee members: Prof. Eric Sharpe, Prof. Michel Pleimling, Prof. Shengfeng Cheng, and earlier also Prof. Will Mather. Their insightful comments encouraged me to widen my research from various perspectives.

My gratitude extends to Betty Wilkins and Katrina Loan for their help in all administrative issues. And I want to thank Roger Link and Travis Heath since they provided great technical assistance with computers, clusters and printers.

I would like to thank the following people: Dr. Ulrich Dobramysl, Udaya Sree Datla, Bassel Heiba and Maximilian Shafer for their excellent work in our collaboration; Dr. Hiba Assi and Dr. Ben Intoy for the help they provided when they were at Virginia Tech. I also want to thank my friends in the office: Harshwardhan Chaturvedi, Weigang Liu, Xiangwen Wang, Yanfei Tang, Chengyuan Wen, Shadi Esmaeili, John Villanova, Ahmadreza Azizi, Shannon Serrao, Bart Brown, Jacob Carrol, Riya Nandi, Ruslan Mukhamadiarov, and Ralph Romero, who made the office a great place to work in.

And finally, I am grateful to my family: my parents and my brother for supporting me spiritually and economically, and my wife who is beautiful, supportive, understanding and smart.

Contents

Chapter 1

Introduction and background

1.1 Deterministic Lotka–Volterra model

This thesis mainly focuses on the Lotka–Volterra (LV) model and its variants. In the 1920s, Lotka and Volterra proposed the original deterministic LV model in order to study fish populations [1] and chemical oscillations [2] respectively. The model was then implemented in ecology to understand the emerging coexistence of one predator species and one prey species, as a first step to investigate the coexistence of multiple species as commonly observed in natural ecosystems. The LV model assumes only two species, predator and prey, present in the system. They interact by following three kinds of reactions: a predator may remove a prey from the system and simultaneously generate a new predator particle with predation rate λ, a predator particle may spontaneously die out with death rate μ, and a prey particle may reproduce a new prey particle with reproduction rate σ. If using $a(t)$ and $b(t)$ to represent population densities of predators and prey, we write down two coupled mean-field rate equations:

$$\begin{aligned} \frac{da(t)}{dt} &= \lambda a(t)b(t) - \mu a(t)\,, \\ \frac{db(t)}{dt} &= -\lambda a(t)b(t) + \sigma b(t)\,. \end{aligned} \tag{1.1}$$

The predator population grows in the predation process, which introduces a positive term $\lambda a(t)b(t)$, and loses particles in the death process, rendering a negative term $-\mu a(t)$; the prey population decreases in the predation process as shown by $-\lambda a(t)b(t)$, and increases in the reproduction process with a positive term $\sigma b(t)$.

By setting the left sides of eqs. (1.1) to 0 and then solving the equations, we obtain two absorbing stationary states: (1) $\hat{a} = 0$, $\hat{b} = 0$; (2) $\hat{a} = 0$, $\hat{b} \to \infty$; and one non-zero stationary state (3) $a^* = \frac{\sigma}{\lambda}$, $b^* = \frac{\mu}{\lambda}$, i.e., when the initial values of $a(0)$ and $b(0)$ happen to be one of these three sets, they would maintain their values unchanged. For non-zero initial population

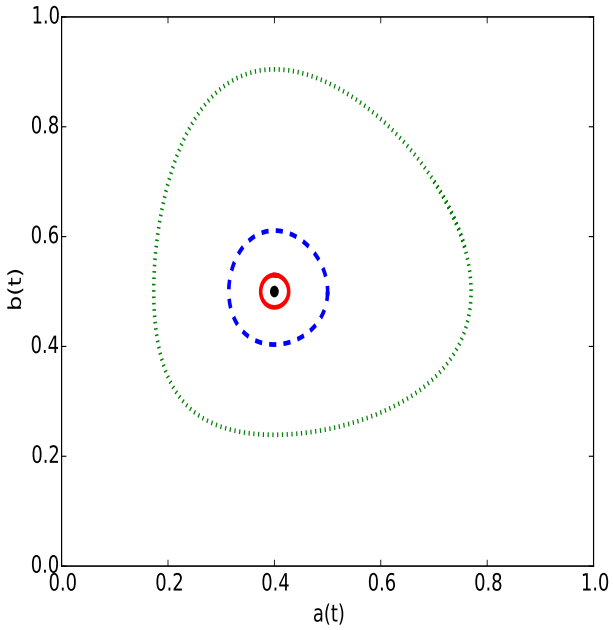

Figure 1.1: Numerical solution of mean-field rate equations (1.1) with reaction rates $\lambda = 1.0$, $\mu = 0.5$, and $\sigma = 0.4$. Its non-zero solution is $(a^*, b^*) = (0.4, 0.5)$ represented by a black dot. The other three curves display the neutral circle solutions when initial densities are $(0.4, 0.53)$ (red solid), $(0.5, 0.5)$ (blue dash), and $(0.7, 0.7)$ (green dot).

densities other than (a^*, b^*), $a(t)$ and $b(t)$ would form neutral circles as demonstrated by the following calculation. First calculate the ratio of the two equations in eqs. (1.1)

$$\frac{da}{db} = \frac{\lambda ab - \mu a}{-\lambda ab + \sigma b}\,.$$

This equation can be rewritten as

$$-\lambda da + \sigma \frac{da}{a} - \lambda db + \mu \frac{db}{b} = 0\,.$$

The first integral of the above equation gives a conserved quantity

$$K(t) = -\lambda(a(t) + b(t)) + \sigma \ln a(t) + \mu \ln b(t) = K(0)\,.$$

The conservation of $K(t)$ indicates that the solutions of the deterministic Lotka–Volterra rate equations form closed orbits, i.e., $a(t)$ and $b(t)$ oscillate periodically and return to their initial values after each period. Fig. 1.1 shows the numerical solutions of eqs. (1.1) when setting $\lambda = 1.0$, $\mu = 0.5$, and $\sigma = 0.4$. Its only non-zero stationary solution is $(0.4, 0.5)$ indicated by a black dot in the graph. Closed orbits form when we try three different non-zero initial

states here: $(0.4, 0.53)$ (red solid curve), $(0.5, 0.5)$ (blue dashed curve), and $(0.7, 0.7)$ (green dotted curve). Thus the temporal evolution of the population densities is only determined by the initial conditions. There is an analytical solution for the oscillation frequency when the oscillation orbit is close to the non-zero stationary state: $a(t) = \delta a + a^*$, and $b(t) = \delta b + b^*$, where δa, δb are small compared with a^* and b^*. Eqs. (1.1) can be rewritten as:

$$\begin{aligned} \delta\dot{a} &= \lambda(a^* + \delta a)(b^* + \delta b) - \mu(a^* + \delta a)\,, \\ \delta\dot{b} &= -\lambda(a^* + \delta a)(b^* + \delta b) + \sigma(b^* + \delta b)\,. \end{aligned}$$

To linear order in δa, δb, these can be further simplified as

$$\begin{aligned} \delta\dot{a} &= \lambda a^* \delta b\,, \\ \delta\dot{b} &= -\lambda b^* \delta a\,. \end{aligned}$$

The combination of these two equations returns second-order derivatives of δa and δb:

$$\begin{aligned} \delta\ddot{a} &= -\sigma\mu\delta a\,, \\ \delta\ddot{b} &= -\sigma\mu\delta b\,. \end{aligned}$$

The oscillation frequency of both $a(t)$ and $b(t)$ is $\sqrt{\sigma\mu}$.

The deterministic Lotka–Volterra model makes a lot of assumptions or simplifications about the ecosystem: Only two species are present in the model. All particles are well mixed in an infinite-dimensional system without spatial or temporal correlations. The prey maintains a constant reproduction rate, without considering the availability of food, water, habitat, etc. Only one individual is involved in the reproduction process. One new predator particle is generated whenever a prey is consumed. There is no limit on the total number of prey consumed by the predators. Temporal and environmental variation of the system is totally ignored. Particles from the same species are homogeneous in sharing the same reaction rates, and newly generated individuals are just cloned from their parent particles. These simplifications are ecologically unrealistic, thus attracting many criticisms.

1.2 Non-equilibrium statistical physics and ecological background

The motivation of solving problems in both ecology and non-equilibrium statistical physics drives us to study the LV model and its variants. Our research is partially motivated by the goal of solving ecological problems such as understanding the emergence and stability of biodiversity in ecology [3, 4]. To make it easy to understand the problems, one can imagine an isolated system of all kinds of animals interacting with each other. Herbivorous species, like sheep, do not directly rely on other animals for food resources. Instead they could

survive and reproduce under suitable environmental conditions, including water, heat, living habitat, etc. Carnivores, like wolf, prey on other species as the only method of food supply. Interactions between herbivores and carnivores represent a predator-prey relationship which is very important in maintaining the balance of ecosystems. Wolves prevent sheep from diverging in population or exceeding the environmental capacity; sheep provide wolves with food. If the wolf species accidentally goes extinct, there is no way for it to reappear. If wolves eat up all sheep, they would die out as well owing to lack of food. In natural ecosystems, wolves of course do not understand the art of eating only a 'right' amount of sheep and saving the remaining for the future. We study simple mathematical models computationally and analytically in hope of capturing the underlying mechanism which help maintain a balance between sheep and wolves so that both species coexist stably. In our simulations, the coexistence regions are measured by carefully tuning the reaction rates. To account for the spatial degree of freedom of ecological systems, we implement the LV model on a two-dimensional square lattice as a relatively simple method [5–18]. A recent review of stochastic population dynamics in spatially extended predator-prey systems can be found in reference [19]. Fig.1.2 shows the distribution of particles located on square lattice sites, with their colors indicating different species. Spatial correlation is introduced by the restriction that particles are only allowed to react with their neighbors to account for the finite range of movement or territories of real animals. Since the sequence of the three reactions and the participating particles are totally random, temporal stochasticity also exists and dramatically influences the dynamical properties of the system. These spatial and temporal correlations drive the system's behavior away from the deterministic model. Once either the predator or the prey species vanishes, their recovery from it is impossible according to the stochastic reaction process, thus breaking time reversal symmetry. Detailed balance [21], which is necessarily required for a system to reside in thermal equilibrium states, is broken as well because the reactions are irreversible. For example, a predator particle is replaced by an empty lattice site in its death process; however, an empty lattice site does not spontaneously change back to a predator particle. As a result, the two absorbing states described in chapter 1.1 are the only stationary states of the system if it is finite. Non-equilibrium statistical physicists study population dynamics for two reasons: First, it is comparatively easy to utilize Monte Carlo simulations to study the corresponding lattice models, especially when powerful computational resources are available; second, there are a lot of interesting far-from-equilibrium phenomena to be better understood in these systems. This thesis is going to cover some of the major topics of non-equilibrium statistical physics we have studied such as temporal evolution of order parameters, an active-to-absorbing phase transition, universality, boundary effects, and noise-induced pattern formation.

In part 2, we find the predator population density follows an exponential decay from its initial value when the system resides in the two-species stable state, but a power-law decay in the critical region of the phase transition point. By making microscopic changes in the model, i.e., tuning the reaction rates, we observe a macroscopic change that a two-species coexistence state with the densities of both species positive and constant is replaced by an absorbing state wherein the predator species goes extinct. Part 2 mainly focuses on the critical properties

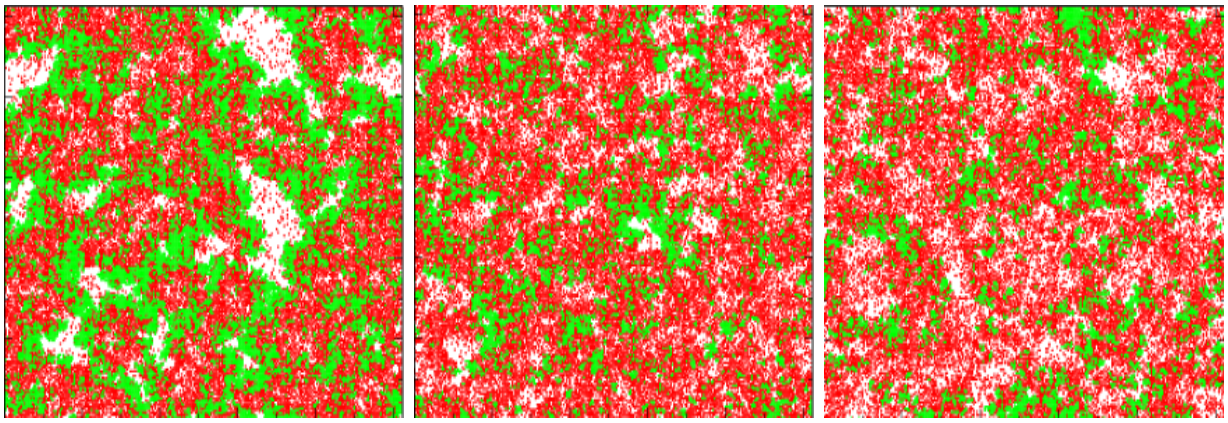

Figure 1.2: Copied from paper [20] Fig.1. Snapshots of the spatial particle distribution for a single Monte Carlo simulation run of a stochastic Lotka–Volterra model on a 256×256 square lattice with periodic boundary conditions, successively from left to right at $t = 500$ Monte Carlo steps (MCS), $t = 1000$ MCS, and $t = 2000$ MCS, with reaction probabilities (see text) $\mu = 0.025$, $\lambda = 0.25$, and $\sigma = 1.0$; only at most one particle per lattice site is allowed: sites occupied by predators are indicated in red, prey in green, while empty sites are shown white.

including: critical slowing-down, breaking of time-translation invariance, dynamic scaling, and critical aging. Despite their difference in details, some models may belong to a single universality class that share the same critical exponents. Continuous active-to-absorbing state transitions are usually governed by the universal scaling properties of the directed percolation (DP) universality class [21–23]. We measured the critical exponents of the lattice LV model and found them close to the DP values within the error bars. One valuable technique of protecting endangered ecosystems is to find effective ways to provide warnings before a species vanishes. Part 2 describes our effort in demonstrating dynamic critical properties such as aging as warning signals of predator extinction.

One expects the population dynamics to be dramatically changed by spatial variation, for example at the boundary between a river and land. In chapter 3, we introduce a spatially inhomogeneous system and then study its boundary effects. We study population densities, relaxation time, and correlation length at the boundary between two domains in this spatially inhomogeneous system.

An ecosystem is very unlikely to stay temporally unchanged due to several reasons: first, most weather elements such as temperature and moisture change seasonally with some stochasticity; second, animals evolve with time and some noticeable changes occur within as fast as tens of generations; third, outer species could invade a system and bring qualitative changes. In chapter 4, inspired by Darwinian evolution, we allow particles to evolve their predation efficiency, death rate, and reproduction rate so that a newly generated particle is never exactly cloned from its parent particle. To understand the stability of a system undergoing

the 'invasion' of an outcomer, we add in a new predator species and try various reaction rules that help make three-species coexistence possible. Environmental oscillations are also simulated by periodically switching the parameters.

Even though this thesis mainly focuses on computational methods, it is necessary to mention important experimental efforts in ecology since our research originates in these experiments more or less. There were few choices of experimental techniques besides long-time observation in the very early stage of studying population dynamics [25]. Ecologists have some controls over the system by finding an almost isolated environment, for example an island, and doing some simple experiments such as introducing new species [26]. Our work of studying the competition of two relative predator species in chapter 4 is inspired by these experiments. Recently, genetic engineering techniques make it possible to make an ecosystem of species interacting with desired rules [27]. In chapter 5, E. coli is engineered to be a predator species and a prey species, which are then put in a single system for the purpose of observing their competition.

Due to spatio-temporal correlations, particles behave in a collective way, and thus form dynamical spatial patterns such as clusters, waves, activity fronts, spirals, etc. Chapter 5 explains a biological experiment of two competing E. coli species, wherein a 'kill' zone of the prey E. coli forms and several large prey colonies grow inside the zone compared with the other prey colonies. We design a LV-like model to help understand the formation of this special pattern. Another very important research field not covered in this thesis is using bosonic creation and annihilation operators to map the master equations to Liouville operator formulations, and then borrowing mathematical tools from quantum field theory to analytically study the stochastic lattice models. For example, one can map the Lotka–Volterra model in the vicinity of the predator extinction threshold to Reggeon field theory, which explains the reason why the LV model at the active-to-absorbing phase transition point belongs to the DP universality class [18, 24].

1.3 Models studied in this thesis

Table 1.1 lists the models studied in each of the following parts of this thesis and their corresponding research foci. The second part of this thesis studies the non-equilibrium relaxation in a stochastic two-species Lotka–Volterra model on a two-dimensional square lattice with periodic boundary conditions. Setting the prey carrying capacity finite casts a phase transition from an active state with both species coexisting to an absorbing state with only prey remaining. We are mostly interested in the non-equilibrium relaxation of the system in the vicinity of the phase transition point. The following critical behaviors are observed: a power law dependence of the relaxation time on the predation rate, algebraic decay of the predator density at the extinction critical point, and dynamic scaling of the two-time autocorrelation functions at the phase transition point. Within the statistical errors, the

Chapter 2 [20]	a stochastic lattice LV model, critical slowing-down, aging, early warning signals of predator extinction
Chapter 3 [28]	a spatially inhomogeneous lattice LV model, boundary effects
Chapter 4 [29]	a three-species predator-prey model, coexistence, 'Darwinian' evolution, direct competition
Chapter 5 [30]	a biological experiment with two E. coli strains, and a corresponding lattice simulation model

Table 1.1: This table summarizes the main contents of this thesis: models studied in each part and their corresponding research foci.

numerically measured critical experiments agree with the established values of the directed percolation (DP) universality class, which demonstrates that the stochastic lattice LV model at the phase transition point belongs to the DP class. This part of our work is already published as reference [20].

Real ecological environments spatially consist of different domains including forest, desert, river, ocean, etc. The local ecology is roughly homogeneous within these domains, compared with the big changes on their boundaries. Interfaces are formed between neighboring patches. In order to investigate boundary effects, the third part of this dissertation studies a spatially inhomogeneous version of the lattice Lotka—Volterra model. We first split the system into two patches: One half of the system attains an absorbing state wherein only the prey survives, while the other half resides in a stable coexistence state where both species remain active. The predator population density displays a marked enhancement at the boundary domain because there is abundant prey available on the absorbing side. There is a net predator flow from the active side to the absorbing side, resulting in the minimum of predator correlation length at the boundary. We do not see prominent influence of the existence of two distinct domains on the frequency of the population oscillations. When we successively divide the system into subdomains in a checkerboard pattern and assign two different reaction rates to neighboring patches, the boundary effects become less prominent. When the size of the subdomains gets decreased to the scale of the correlation length, the mean population densities of the whole system attain values close to those in a disordered system wherein reaction rates are randomly drawn from a bimodal distribution. This part of our work is already published as reference [28].

The two-species model is still too simplified compared with natural ecosystems where multiple species coexist in a single system. With the purpose of rendering the model closer to the real world and studying the problem of two relative species competing for the same food, the fourth part of this thesis performs computational experiments on a predator-prey community consisting of two predator species and one prey species. Each predator individual is assigned reaction rates to which evolution is introduced. Competing for limited source (prey) drives the predators' efficiency optimized to high values. This natural selection strongly impacts

the population dynamics and evolutionary dynamics. We find it necessary to include both evolution and direct competition to stabilize a three-species coexistence state. This part of our work is submitted for application as reference [29].

In the last part, we collaborate with an experimental biological team who studies the evolution of a microecology from a killer-prey relationship to coexistence using two different non-motile Escherichia coli strains with one species being the killer and the other one the prey. Spatiotemporal patterns of the cells' distribution are observed: The killers are located at the center of the disk; a 'kill zone' of prey forms immediately surrounding the killer, beyond which the prey population gradually increases outward; several prey colonies grow in the 'kill zone' and their sizes are larger than the ones further away from the center. We design a lattice killer-prey competition model with an absolute circular boundary. This model qualitatively reproduces the spatiotemporal patterns observed in the actual experiment, thus helping us understand the underlying dynamics of the E. coli system. This work is already accepted for publication as a part of reference [30].

Chapter 2

Non-equilibrium relaxation in a stochastic lattice Lotka–Volterra model

This chapter was essentially copied from our publication:

Chen S, Täuber U C, 2016, "Non-equilibrium relaxation in a stochastic lattice Lotka–Volterra model," Physical Biology, 13, 025005, "Copyright (2016) by IOP Publishing Ltd "

I contributed all the contents of this paper under Prof. Täuber's supervision.

2.1 Introduction

There is growing interest in quantitatively understanding biodiversity in ecology [3, 4] and population dynamics [26,31,32]. The motivations for this very active research field range from seeking a fundamental and comprehensive understanding of noise-induced pattern formation and phase transitions in far-from-equilibrium systems to potential practical applications in protecting endangered species in threatened ecosystems.

Unfortunately, the full complexity of interacting species in coupled ecosystems in nature cannot yet be reliably modeled with the required faithful incorporation of demographic fluctuations and internal stochasticity induced by the involved reproduction and predation reactions. One therefore typically resorts to detailed investigations of idealized, simplified models that however are intended to capture the important system ingredients and ensuing characteristic properties. The Lotka–Volterra predator-prey model [1, 2] has served as such a simple but intriguing and powerful paradigm to study the emerging coexistence of just two species, predators and prey, as a first step to grasp the initially counter-intuitive appearance of biodiversity among competing species. In the model's original formulation, the authors just analyzed the associated coupled mean-field rate equations, whose solution remarkably entails a stable active coexistence state in the form of a neutral cycle: the densities of both populations hence display periodic non-linear oscillations.

Yet this classical deterministic Lotka–Volterra model has been aptly criticized for its non-realistic feature of the oscillations being fully determined by the system's initial state, and for the lack of robustness of the marginally stable neutral cycle against model perturbations [26]. The importance of stochasticity as well as spatio-temporal correlations, both entirely neglected in the mean-field approximation, was subsequently recognized in a series of numerical simulation studies of several stochastic spatially extended lattice Lotka–Volterra model variants [5–18, 33, 34]. Even in the absence of spatial degrees of freedom, stochastic Lotka–Volterra models display long-lived but ultimately decaying random population oscillations rather than strictly periodic temporal evolution; these can be understood as resonantly amplified demographic fluctuations [17]. Sufficiently large spatially extended predator-prey systems with efficient predation are similarly characterized by large initial erratic population oscillations. Ultimately, a quasi-stationary state (in the limit of large particle numbers) is reached, where both population densities remain non-zero [7–16, 18]. The exceedingly long transients towards this asymptotic predator-prey coexistence state are characterized by strong spatio-temporal correlations associated with the spontaneous formation of spreading activity fronts, depicted in Fig. 1.2, which induce marked renormalizations of the oscillation parameters as compared to the mean-field predictions [16, 18, 24].

To model finite population carrying capacities caused by limited resources, one may restrict the local particle density or lattice site occupation number [9, 10, 15, 16, 18]. For the Lotka–Volterra model, this in turn introduces a new absorbing state, where the predator population goes extinct, while the prey proliferate through the entire system. By tuning the reaction

rates as control parameters, one thus encounters a continuous active-to-absorbing state non-equilibrium phase transition [5, 10–12, 15, 18, 34]. In addition, near the predator extinction threshold, population oscillations cease, and both predator and prey concentrations directly relax exponentially to their quasi-stationary values [18]; c.f. Fig. 2.1.

Note that the existence of an absorbing state for the predator population, which cannot ever recover from extinction under the system's stochastic dynamics, explicitly breaks the detailed balance conditions required for systems to effectively reside in a thermal equilibrium state. Generically, one expects continuous active-to-absorbing state transitions to be governed by the universal scaling properties of the directed percolation universality class (see, e.g., the overviews in Refs. [21–23]). This is in accord with the numerical data obtained in lattice Lotka–Volterra models; moreover, via representing the corresponding stochastic master equation through an equivalent Doi-Peliti pseudo-Hamiltonian and associated coherent-state functional integral, one can explicitly map the Lotka–Volterra model near the predator extinction threshold to Reggeon field theory that describes the directed percolation universality class [18, 24].

Induced by severe environmental changes in nature, certain ecosystems may collapse and at least some of its species face the danger of extinction. In order to monitor viability of populations and maintain ecological diversity, it is of great importance to identify appropriate statistical indicators that signify impending population collapse and may thus serve as early warning signals. In our simulations, we simply perform sudden predation rate switches to mimic fast environmental changes. If such a rate quench leads near the predator species extinction threshold, we observe the characteristic critical slowing-down and aging features expected at continuous phase transitions [21–23]. We demonstrate how either of these two characteristic dynamical signatures, but specifically the emergence of aging scaling, might be utilized as advanced warning signals for species extinction [35].

2.2 Model description and simulation protocol

We study a spatially extended stochastic Lotka–Volterra model by means of Monte Carlo simulations performed on a two-dimensional square lattice with 1024×1024 sites, subject to periodic boundary conditions; we largely follow the procedures described in Refs. [15, 16, 18]. In this work, we impose locally limited carrying capacities for each species through implementing lattice site occupation restrictions: The number of particles per lattice site can only be either 0 or 1; i.e., each lattice site can either be empty, occupied by a 'predator' A, or occupied by a 'prey' B particle. The individual particles in the system undergo the following stochastic reaction processes:

$$A \xrightarrow{\widetilde{\mu}} \emptyset\,, \quad A + B \xrightarrow{\widetilde{\lambda}} A + A\,, \quad B \xrightarrow{\widetilde{\sigma}} B + B\,. \tag{2.1}$$

The predators A thus spontaneously die with decay rate $\widetilde{\mu} > 0$. Upon encounter, they may

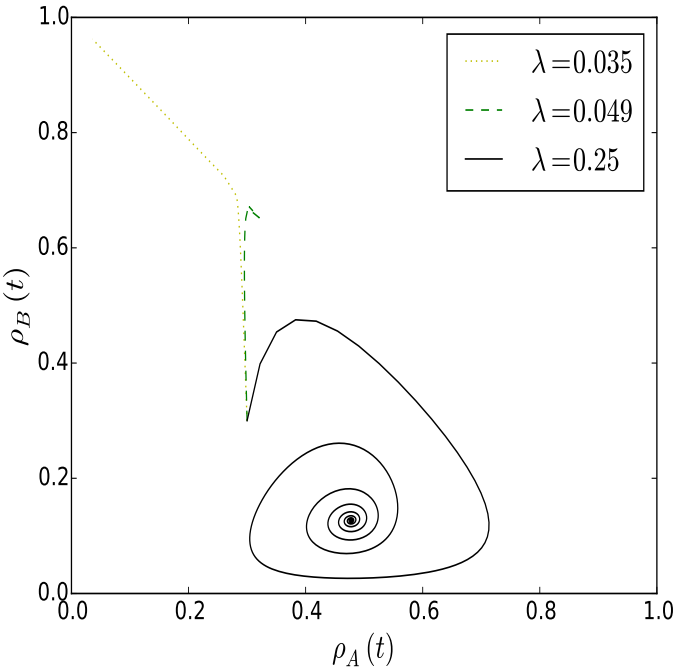

Figure 2.1: Adapted from paper [20] Fig.2. Monte Carlo simulation trajectories for a stochastic Lotka–Volterra model on a 1024×1024 square lattice with periodic boundary conditions and restricted site occupancy (at most one particle allowed on each lattice site) shown in the predator $\rho_A(t)$ versus prey density $\rho_B(t)$ phase plane ($\rho_A + \rho_B \leq 1$) with initial values $\rho_A(0) = 0.3 = \rho_B(0)$, fixed reaction probabilities $\mu = 0.025$, $\sigma = 1.0$, and different predation efficiencies: (i) $\lambda = 0.035$ (yellow dot): predator extinction phase; (ii) $\lambda = 0.049$ (green dash): direct exponential relaxation to the quasi-stationary state just above the extinction threshold in the predator-prey coexistence phase; (iii) $\lambda = 0.250$ (black solid): the trajectories spiral into a stable fixed point, signifying damped oscillations deep in the coexistence phase.

also consume a prey particle B located on a lattice site adjacent to theirs, and simultaneously reproduce with 'predation' rate $\widetilde{\lambda} > 0$. Hence the B particle on the nearest-neighbor site to the predator becomes replaced by another A particle. We remark that in a more realistic description, predation and predator offspring production should naturally be treated as separate stochastic processes. While such an explicit separation induces very different dynamical behavior on a mean-field rate equation level, it turns out that in dimensions $d < 4$ the corresponding stochastic spatially extended system displays qualitatively the very same features as the simplified reaction scheme (2.1) [15].

Prey in turn may reproduce with birth rate $\widetilde{\sigma} > 0$, with the offspring particles placed on one of their parent's nearest-neighbor sites. Note that we do not include nearest-neighbor hopping processes here. Instead, diffusive particle spreading is effectively generated through the reproduction processes that involve placement of the offspring onto adjacent lattice sites;

earlier work has ascertained that incorporating hopping processes (with rate $\widetilde{D}$) independent of particle production yields no qualitative changes [18], except for extremely fast diffusion $\widetilde{D} \gg \widetilde{\mu}, \widetilde{\lambda}, \widetilde{\sigma}$, which leads to effective homogenization and consequent suppression of spatial correlations. In our present study, we will hold the rates $\widetilde{\mu}$ and $\widetilde{\sigma}$ fixed while varying $\widetilde{\lambda}$ as our control parameter.

In general, the detailed Monte Carlo algorithm for the stochastic lattice Lotka–Volterra model proceeds as follows [18]:

- Select an occupied lattice site at random and generate a random number r uniformly distributed in the range $[0, 1]$ to perform either of the following four possible reactions (with probabilities D, μ, λ, and σ in the range $[0, 1]$):
- If $r < 1/4$, select one of the four sites adjacent to this occupant, and move the occupant there with probability D, provided the selected neighboring site is empty (nearest-neighbor hopping).
- If $1/4 \leq r < 1/2$ and if the occupant is an A particle, then with probability μ the site will become empty (predator death, $A \to \emptyset$).
- If $1/2 \leq r < 3/4$ and if the occupant is an A particle, choose a neighboring site at random; if that selected neighboring site holds a B particle, then with probability λ it becomes replaced with an A particle (predation reaction, $A + B \to A + A$).
- If $3/4 \leq r < 1$ and if the occupant is a B particle, randomly select a neighboring site; if that site is empty, then with probability σ a new B particle is placed on this neighboring site (prey offspring production, $B \to B + B$).

We use a float number t to represent the 'time' of the simulation process. Its initial value is 0 and it is added by the inverse of the total number of the particles present in the system when the above simulation process is performed once. One Monte Carlo Step (MCS) is considered completed when the integer part of time t increases by 1. To clarify our algorithm, we discuss a simple example: If r is generated to be 0.1, the first case applies, whence we need to perform nearest-neighbor hopping with probability D. Since for simplicity we set $D = 0$ in our simulation, we just skip this step and proceed to generate a new random number r. We remark that different versions of similar simulation algorithms can naturally be implemented wherein the microscopic reaction processes and their ordering are varied. However, macroscopic long-time simulation results should not qualitatively differ for such variations, only the effective reaction rates $\widetilde{\mu}$, $\widetilde{\lambda}$, $\widetilde{\sigma}$ in (2.1), and the diffusivity $\widetilde{D}$ that result from the microscopic probabilities μ, λ, σ, and D, and the overall time scale will need to be rescaled accordingly.

Figures 1.2 and 2.1 show the results of typical Monte Carlo simulation runs in two-dimensional stochastic lattice Lotka–Volterra models with periodic boundary conditions and site occupations restricted to at most a single predator (A) or prey (B) particle; thus both their local

and mean densities are restricted to the range $\rho_A + \rho_B \leq 1$. Here, $\rho_{A/B}(t)$ is defined as the total predator (prey) number at time t divided by the number of lattice sites $(1024)^2$. The snapshots at various simulation times in Fig. 1.2 visualize the early spreading activity fronts in the two-species coexistence phase, i.e., prey (green) invading empty (white) regions followed by predators (red), which induce the initial large-amplitude population oscillations. At longer run times, the prey here localize into fluctuating clusters, and the net population densities reach their quasi-stationary values. In the prey vs. predator density phase plot depicted in Fig. 2.1, the associated trajectory (iii) is a spiral converging to the asymptotic density values. Upon approaching the predator extinction threshold (holding μ and σ fixed, at lower values of λ), the population oscillations cease and the trajectory (ii) relaxes directly to the quasi-stationary coexistence state. Finally, below the extinction threshold (i), the predator population dies out, and the prey particles eventually fill the entire lattice.

2.3 Results

2.3.1 Relaxation dynamics within the coexistence phase

To set the stage, we first consider the time evolution of our stochastic Lotka–Volterra system on a two-dimensional lattice starting from a random initial configuration with the rate parameters set such that the model resides within the active coexistence state: the mean densities for both predator and prey species will thus remain positive and asymptotically reach constant values. Fig. 2.2(a) shows the time evolution of the mean population densities $\rho_A(t)$ and $\rho_B(t)$, averaged over the entire lattice. Fig. 2.2(a) shows the mean densities both for single simulation as well as data that result from averaging over 200 independent Monte Carlo runs. As is apparent in Fig. 1.2, already in moderately large lattices there emerge almost independent spatially separated population patches. The system is thus effectively self-averaging; as a consequence, the mean data from multiple runs essentially coincide with those from single ones. The reaction rates in the scheme (2.1) constitute the only control parameters in our system. Thus, if we fix the probabilities σ and μ, the predation probability λ fully determines the final state. For generating the data in Fig. 2.2, we used constant reaction probabilities $\mu = 0.025$, $\lambda = 0.25$, and $\sigma = 1.0$. The particles of both species are initially distributed randomly on the lattice with equal densities $\rho_A(0) = 0.3 = \rho_B(0)$.

In the early-time regime, the population densities are non-stationary and oscillate with an exponentially decreasing amplitude $\sim e^{-\zeta t} = e^{-t/t_c}$. We may utilize the damping rate ζ or decay time $t_c = 1/\zeta$ to quantitatively describe the relaxation process towards the quasi-steady state. Since ζ is identical for both species, we just obtain this relaxation rate from the predator density decay via measuring the half-peak width of the absolute value of the Fourier transform of the time signal, $f_A(\omega) = \left| \int \rho_A(t)\, e^{i\omega t}\, dt \right|$. Alternatively, one might employ a direct fit in the time domain to damped oscillations. However, such a procedure is usually less accurate, as the early-time regime tends to be assigned too much weight in determining the

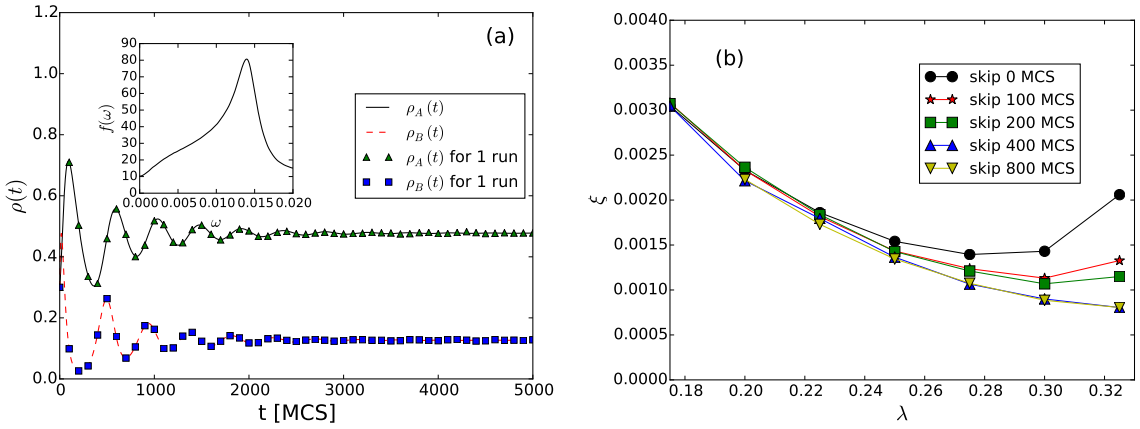

Figure 2.2: Adapted from paper [20] Fig.3. Monte Carlo simulation data for a stochastic Lotka–Volterra model on a 1024×1024 square lattice with periodic boundary conditions (single runs shown in triangles and squares; the solid and dashed curves are from data averaged over 200 independent simulation runs): (a) Temporal evolution of the mean predator density $\rho_A(t)$ (full black lines and green triangles) and the mean prey density $\rho_B(t)$ (dashed red line and blue squares) for fixed reaction probabilities $\mu = 0.025$, $\lambda = 0.25$, and $\sigma = 1.0$, with initial densities $\rho_A(0) = 0.3 = \rho_B(0)$. The inset shows the absolute value of the Fourier transform $f_A(\omega)$ of $\rho_A(t)$ (full black curve). (b) Measured damping rate ζ in MCS^{-1}, as obtained from the peak half-width of $f_A(\omega)$, as function of the predation rate λ, when respectively $\Delta t = 0$, 100, 200, 400, and 800 (top to bottom) initial MCS are skipped in the time series $\rho_A(t)$ as the Fourier transform is performed.

fit parameters. Using the temporal Fourier transform and deducing the damping rate from the peak width in frequency space constitutes a numerically superior method. For example, for the predator density $\rho_A(t)$ shown in Fig. 2.2(a), the Fourier transform displayed in the inset yields $t_c \approx 650$ MCS. Indeed, by $t = 3000$ MCS $\approx 5\, t_c$, the system has clearly reached its quasi-stationary state.

In the following, we aim to ascertain that the stochastic lattice Lotka–Volterra model loses any memory of its initial configuration once it has evolved for a duration $t > t_c$. We set the initial configuration at $t = 0$ to be a random spatial distribution of particles with densities $\rho_A(0) = 0.3 = \rho_B(0)$, and hold $\mu = 0.025$ and $\sigma = 1.0$ fixed. We then record the relaxation kinetics for various values of λ, all in the interval $[0.175, 0.325]$ to ensure that the final states reside deep within the species coexistence region, and measure the associated damping rates ζ. The black dotted line in Fig. 2.2(b) plots the resulting function $\zeta(\lambda)$; the relaxation rate is indeed predominantly determined just by the reaction rates, but also influenced by the system's initial state. The initial configuration effects can however be removed in a straightforward manner as follows: In the evaluation of the Fourier transform $f_A(\omega)$, we skip a certain initial MCS interval Δt and just use the remaining data for $\rho_A(t)$ rather than the

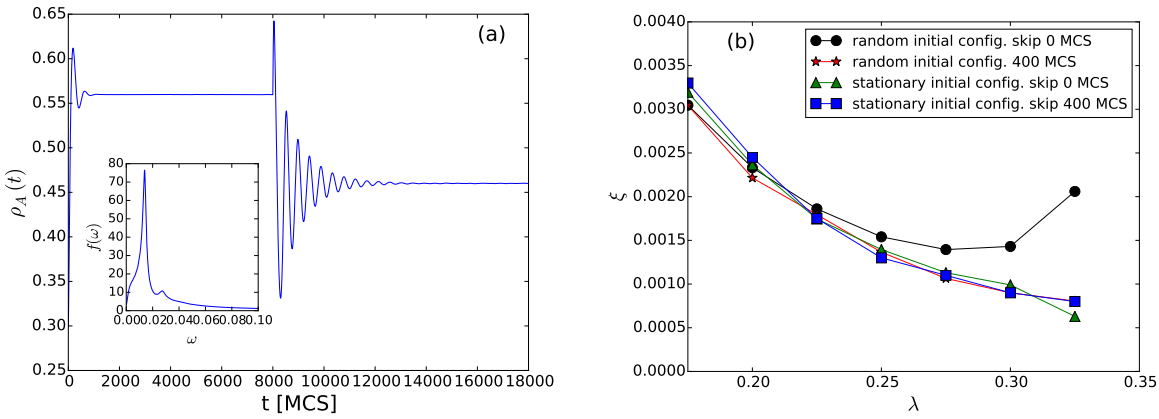

Figure 2.3: Adapted from paper [20] Fig.4. Monte Carlo simulation data for the predation rate quench scenario within the predator-prey coexistence phase on a 1024×1024 square lattice with periodic boundary conditions (data averaged over 200 independent simulation runs): (a) The main plot shows the temporal evolution of the mean predator density $\rho_A(t)$ for $\mu = 0.025$, $\sigma = 1.0$, $\rho_{A/B}(0) = 0.3$. At $t_1 = 8000$ MCS, the predation probability is suddenly switched from $\lambda_1 = 0.125$ to $\lambda_2 = 0.275$. The inset displays the absolute value of the Fourier transform $f_A(\omega)$ of the time series after the quench ($t > t_1$). (b) Measured damping rate $\zeta(\lambda)$ when the system starts from a random initial condition with skipped initial time interval duration $\Delta t = 0$ (black dots) or 400 MCS (red stars; same data as in Fig. 2.2(b)), and following a quench from a quasi-steady state, where $\Delta t = 0$ (green triangles) and $\Delta t = 400$ MCS (blue squares).

entire time sequence. If in fact the initial configuration only affects the system up to time $t \approx t_c$, the thereby obtained values of the function $\zeta(\lambda)$ should become independent of the length of the discarded initial time interval Δt once $\Delta t > t_c(\lambda)$.

In Fig. 2.2(b), we display the functions $\zeta(\lambda)$ obtained for various skipped initial time interval lengths Δt, ranging from 0 to 800 MCS. For large values of the predation probability λ, and ensuing long relaxation times $t_c(\lambda) = 1/\zeta(\lambda)$, a marked dependence on Δt is apparent. Yet for the entire λ range under investigation, the two curves for $\Delta t = 400$ MCS and 800 MCS overlap (and we have checked this holds also for other values of $\Delta t > 400$ MCS). Consequently, any dependencies on the initial configurations in the function $\zeta(\lambda)$ have been removed once $\Delta t > 400$ MCS. This already gives a rough estimate for the typical relaxation rate, $\zeta \approx 0.0025$ MCS^{-1}, which indeed nicely matches the actual values seen in Fig. 2.2(b).

Next we check and confirm the above conclusions by considering a set of completely different initial configurations: Starting again from a random particle distribution with initial particle densities $\rho_A(0) = 0.3 = \rho_B(0)$, we first let the system relax to its quasi-steady state at prescribed reaction probabilities $\mu = 0.025$, $\sigma = 1.0$, and $\lambda_1 = 0.125$. Then we suddenly switch the predation probability to a new value λ_2. As a consequence, the system is driven

away from the close to stationary, spatially highly correlated configurations that are characterized by well-formed domains of predators and prey, and relaxes towards a new stable quasi-steady state. Fig. 2.3(a) illustrates such a 'quench' scenario: At $t_1 = 8000$ MCS, the predation probability is instantaneously changed from the initial value $\lambda_1 = 0.125$ to $\lambda_2 = 0.275$; it is apparent that the predation rate switch once again induces large transient population oscillations. We measure the ensuing relaxation rate $\zeta(\lambda)$ as function of the post-quench predation probability $\lambda = \lambda_2$ following the procedures outlined above, and with λ_2 in the interval $[0.175, 0.325]$. In Fig. 2.3(b) we plot the result, if in the computation of the Fourier transform $f_A(\omega)$ an initial time interval of duration $\Delta t = 400$ MCS is skipped (blue squares). For comparison, we also show the data for $\Delta t = 0$ (green triangles) and replot the corresponding graphs for $\Delta t = 0$ (black dots) and $\Delta t = 400$ MCS (red stars) obtained for spatially random initial configurations. Both functions $\zeta(\lambda)$ with $\Delta t = 400$ MCS overlap with the one for $\Delta t = 0$ initiated in the quasi-steady state: Once $\Delta t > t_c(\lambda)$, the system's initial states (here, spatially random or correlated) have no noticeable influence on the functional dependence of the relaxation rate on λ.

2.3.2 Relaxation kinetics following critical quenches

In the stochastic lattice Lotka–Volterra model with limited local carrying capacity, there exists an active-to-absorbing phase transition, namely an extinction threshold for the predator population, as illustrated in Fig. 2.1 and Fig. 2.4. Here, our Monte Carlo simulation runs were initiated with randomly placed predator and prey particles with densities $\rho_A(0) = 0.3 = \rho_B(0)$ and reaction probabilities $\mu = 0.025$, $\sigma = 1.0$, and $\lambda_1 = 0.250$. After $t_1 = 8000$ MCS, when the system has clearly reached its quasi-steady state, we suddenly switch the predation probability from λ_1 to much lower values λ_2 in the range $[0.03, 0.05]$, which reside in the vicinity of the extinction critical point. The curves in Fig. 2.4 show the ensuing time evolution for the mean predator density $\rho_A(t)$. For small λ_2, all predator particles disappear, and eventually only the prey species survives, in contrast to the active two-species coexistence phase at larger λ_2 values, where both species persist with finite, stable mean population densities. In this subsection, we investigate in detail the non-equilibrium relaxation properties and ensuing dynamic scaling behavior following the quench from a quasi-steady coexistence state to the critical point.

Near the active-to-absorbing phase transition, in our two-dimensional stochastic Lotka–Volterra model located at $\lambda_c = 0.0416 \pm 0.0001$ for fixed $\mu = 0.025$ and $\sigma = 1.0$, one should anticipate the standard critical dynamics phenomenology for continuous phase transitions [21, 22]: Fluctuations become prominent, and increasingly large spatial regions behave cooperatively, as indicated by a diverging correlation length $\xi(\tau) \sim |\tau|^{-\nu}$, where $\tau = (\lambda/\lambda_c) - 1$. Consequently, the characteristic relaxation time should scale as

$$t_c(\tau) \sim \xi(\tau)^z \sim |\tau|^{-z\,\nu} \,, \tag{2.2}$$

implying a drastic critical slowing-down of the associated dynamical processes. Thus, expo-

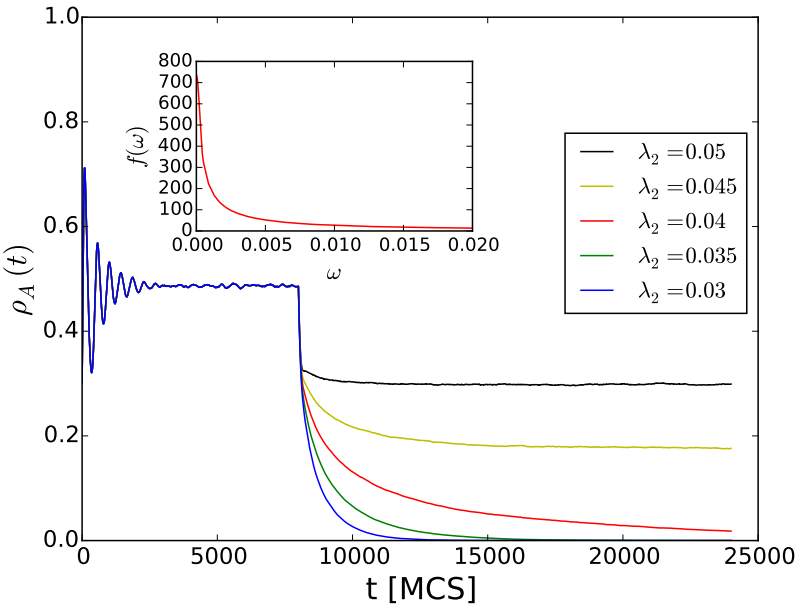

Figure 2.4: Adapted from paper [20] Fig.5. Monte Carlo simulation data (single runs) for the mean predator density $\rho_A(t)$ with $\rho_{A/B}(0) = 0.3$ on a 1024×1024 square lattice with periodic boundary conditions: The initial reaction probabilities are set to $\mu = 0.025$, $\sigma = 1.0$, and $\lambda_1 = 0.250$; at $t_1 = 8000$ MCS the system is quenched into the vicinity of the critical predator extinction point via switching the predation probability to $\lambda_2 = 0.050$, 0.045, 0.040, 0.035, and 0.030 (top to bottom). The inset shows the absolute value $f_A(\omega)$ of the Fourier transform of $\rho_A(t)$ for $\lambda_2 = 0.040$ after the quench.

nential relaxation with time becomes replaced by much slower algebraic decay of the predator population density precisely at its extinction threshold λ_c,

$$\tau = 0 : \ \rho_A(t) \sim t^{-\alpha} \ . \tag{2.3}$$

The values of the three independent critical scaling exponents ν, z, and α characterize certain dynamical universality classes. Generically, one expects active-to-absorbing phase transitions to be governed by the critical exponents of directed percolation (DP) [21, 22]; the middle column in Table 2.1 lists the established numerical literature values (from Refs. [36, 37]) for α and the product $z\,\nu$ in two dimensions. Indeed, standard field-theoretic procedures allow a mapping of the near-critical stochastic spatial Lotka–Volterra system to Reggeon field theory [18, 24], which represents the effective field theory for critical directed percolation [21, 38].

In order to analyze the dynamic critical scaling behavior at the predator population extinction threshold, we follow the protocol outlined above and shown in Fig. 2.4, and first let the system relax to its quasi-steady state with a large predation probability $\lambda_1 = 0.250$. After 8000 MCS, we quench the system to its critical point by switching this probability

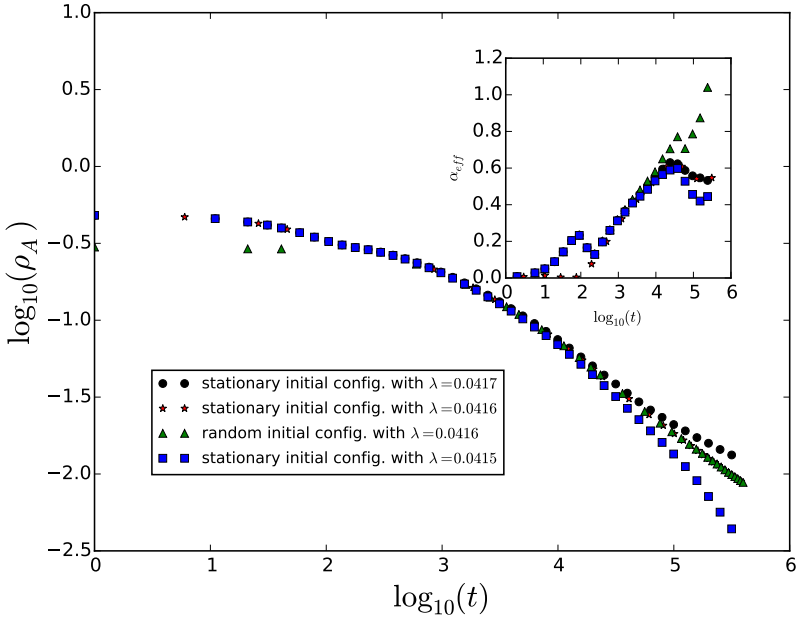

Figure 2.5: Adapted from paper [20] Fig.6. Double-logarithmic plot of the mean predator density decay $\rho_A(t)$ at the critical extinction threshold $\lambda_c = 0.0416$ for fixed $\mu = 0.025$ and $\sigma = 1.0$, for both quasi-stationary (red stars) and random (green triangles) initial configurations (data averaged over 2000 independent simulation runs). For comparison, the predator density decay data are shown also for $\lambda = 0.0417$ (black dots, active coexistence phase) and $\lambda = 0.0415$ (blue squares, absorbing predator extinction phase). The graphs in the inset show the local negative slopes of the curves in the main panel (using intervals of size 0.05), i.e., the time-dependent effective critical decay exponent $\alpha_{\text{eff}}(t)$.

$d = 2$	SLLVM	DP sim.	DP exp.
α	0.540(7)	0.4505(10) [36]	0.48(5) [39]
$z\,\nu$	1.208(167)	1.2950(60) [37]	1.29(11) [39]
Λ_c/z	2.37(19)	2.8(3) [41]	2.5(1) [39]
b	0.879(5)	0.901(2) [41]	0.9(1) [39]

Table 2.1: Monte Carlo simulation results for the critical exponents near the predator extinction threshold in the stochastic lattice Lotka–Volterra model (SLLVM) on a square lattice. For comparison, the table also lists the accepted literature scaling exponents for the directed percolation (DP) universality class [36,37] as well as experimental values measured in turbulent liquid crystals (MBBA) [39]. The critical aging scaling exponents as obtained in our simulations along with earlier numerical results for the contact process [41] and experimental data [39] are included as well. The numbers in brackets indicate the estimated uncertainty in the last digits.

instantaneously to $\lambda_c = 0.0416$. In order to acquire decent statistics, we perform 2000 independent Monte Carlo simulation runs and then average our results. Fig. 2.5 shows a double-logarithmic plot of the decay of the mean predator density $\rho_A(t)$ following the quench (red stars); the inset displays the measured local slope of this graph (taken with intervals of size 0.05), which can be interpreted as a time-dependent effective critical decay exponent $\alpha_{\rm eff}(t) = -d \log \rho_A(t)/d \log t$. A clean power law decay is thus reached when the slope stays constant, which in our data happens only quite late, at $t > 10^5$ MCS. An asymptotically constant slope is observed as long as the value of λ_2 is sufficiently close to the critical point λ_c. Our simulation data (in the rather short time interval with constant $\alpha_{\rm eff}$) yield the critical decay exponent value $\alpha = 0.54 \pm 0.007$; we note that the accepted directed percolation universality class value is $\alpha \approx 0.4505$, which has been obtained by performing activity spreading simulations [36], see also Ref. [18]. For comparison, we also display the data for quenches to $\lambda = 0.0417$ (black dots) and $\lambda = 0.0415$ (blue squares): In the former case, the predator density approaches a finite value as the system is still, albeit barely, in the active two-species coexistence phase, while for the lower predation rate the absorbing state is reached, with the predator population going extinct.

We wish to ascertain the independence of the asymptotic critical exponent $\alpha = \alpha_{\rm eff}(t \to \infty)$ from the starting configurations in our simulations. To this end, we directly initialize our stochastic lattice Lotka–Volterra system with reaction probabilities $\mu = 0.025$, $\sigma = 1.0$, and $\lambda = \lambda_c = 0.0416$. The resulting Monte Carlo data, averaged over again 2000 independent runs, are also shown in Fig. 2.5 (green triangles). It is apparent that for the selected parameter values, the initial conditions become irrelevant for $t > 1000$ MCS, whereafter our results for random and correlated quasi-steady state initial conditions perfectly overlap.

As visible in Fig. 2.4, the stochastic spatial Lotka–Volterra system immediately senses the

predation rate change and the predator density decreases rapidly after the quench; for a very brief time period (about 200 MCS), this decay is in fact independent of the new predation probability λ_2. Subsequently, the relaxation curves are quite sensitive to the selected value of λ_2. We measure the ensuing relaxation times $t_c(\lambda_2)$ through evaluating the temporal Fourier transform, while skipping an initial time interval of duration $\Delta t = 200$ MCS right after the quench in accord with the previous observation, averaging over 500 independent Monte Carlo simulation runs. Fig. 2.6 depicts our numerically determined relaxation time data for t_c as a function of λ_2 in the vicinity of the critical predator extinction threshold λ_c. Note in the left inset that since we only consider a finite time interval (at most 128000 MCS) after the quench for the computation of $f_A(\omega)$, our thus measured relaxation times do not diverge, but display a peak as function of λ_2 that becomes both more pronounced and sharper as the duration of the Monte Carlo simulation is increased. Indeed, we can estimate the critical value λ_c from the peak position of the data curve for the longest simulations runs.

Since the left part of the graph turns out considerably smoother than the right part, we perform a power law fit only to the corresponding data subset ($\tau < 0$). As shown in the main panel of Fig. 2.6, this yields the critical exponent product $z\,\nu = 1.208 \pm 0.167$; within our statistical error bars this is in reasonable agreement with the two-dimensional directed percolation literature values $\nu \approx 0.7333$ and $z = 1.7660$ [22], i.e., $z\,\nu \approx 1.295$ [37]. The right inset displays the local time-dependent effective exponent $(z\,\nu)_{\rm eff}(t) = -d \log t_c(\tau)/d \log|\tau|$ for the longest simulation runs; the data appear not settled at a constant value yet, but indeed rather tend towards the slightly larger asymptotic DP value. Even with our longest Monte Carlo simulation runs, we have at best just barely reached the asymptotic scaling regime, and thus cannot very precisely determine the associated critical exponents for quasi-stationary observables.

A remarkable experiment with yeast cells has recently demonstrated a drastic increase in the relaxation time of the dynamics for a biological system near its population extinction threshold [35]. The authors therefore propose to utilize critical slowing-down as an indicator to provide advanced warning of an impending catastrophic population collapse. However, as we have demonstrated in our simulations, c.f. Figs. 2.5 and 2.6, the unique and universal power law features in the population density decay and divergence of the relaxation time are asymptotic phenomena and emerge only rather late, in our system after $t \approx 10^5$ MCS. Such a long required time period to unambiguously confirm an ecological system's proximity to an irreversible tipping point may preclude timely interventions to save the endangered ecosystem. As we shall see in the following, the appearance of physical aging features in appropriate two-time observables may serve as more advantageous warning signals for population collapse, as they provide both earlier and often more accurate indications for critical behavior (see, e.g., Ref. [40]).

As a consequence of the drastic slowing-down of relaxation processes, near-critical systems hardly ever reach stationarity. During an extended transient period, time translation invariance is broken, and the initial configuration strongly influences the system: both these features characterize the phenomenon of physical aging [23]. In the vicinity of critical points

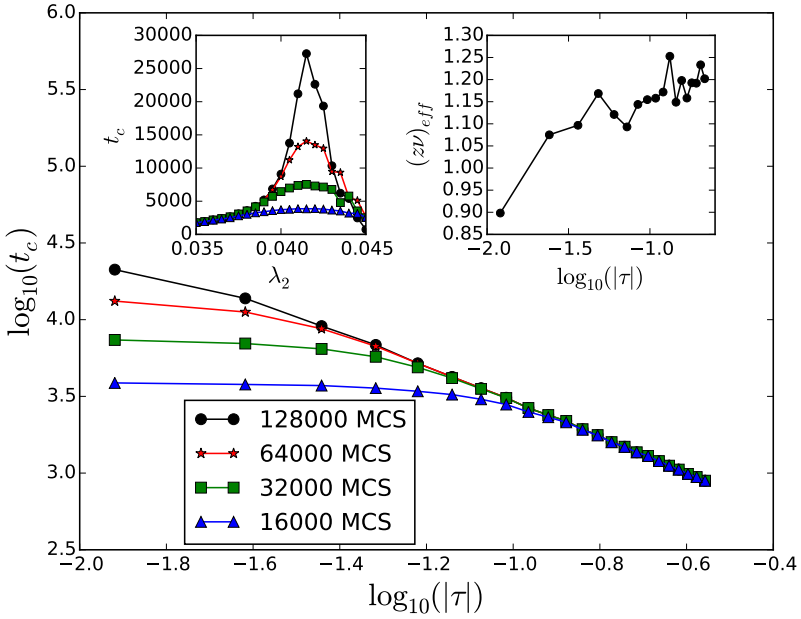

Figure 2.6: Adapted from paper [20] Fig.7. Characteristic relaxation time t_c for the near-critical stochastic Lotka–Volterra model on a 1024×1024 square lattice. The left inset shows the relaxation time $t_c(\lambda_2)$ when the system is quenched from a quasi-stationary state at $\lambda_1 = 0.25$ to smaller values λ_2 in the vicinity of the predator extinction threshold $\lambda_c = 0.0416$. The different curves indicate the resulting relaxation time estimates when respectively 128000, 64000, 32000, and 16000 MCS (top to bottom) were performed after the quench (all data averaged over 500 independent simulation runs). The main panel displays the same data in double-logarithmic form. For $|\tau| = |(\lambda_2/\lambda_c) - 1| > 0.1$, the different graphs overlap, collapsing onto a straight line with slope $-z\,\nu = -1.208 \pm 0.167$. The right inset shows the associated local slope or effective exponent $(z\,\nu)_{\rm eff}(t)$.

as well as in a variety of other instances where algebraic growth and decay laws are prominent, the non-equilibrium aging kinetics is moreover governed by dynamical scaling laws. In our context, aging scaling is conveniently probed in the two-time particle density autocorrelation function

$$C(t,s) = \langle n_i(t)\, n_i(s)\rangle - \langle n_i(t)\rangle\, \langle n_i(s)\rangle \ , \tag{2.4}$$

where $n_i(t) = 0$ or 1 indicates the occupation number (here, for the predators A) on lattice site i at time t. The cumulant (2.4) thus measures local temporal correlations as function of the two time instants s and $t > s$; we shall refer to t and s as the observation and waiting time, respectively.

In a stationary dynamical regime, reached for both $t, s > t_c$, time translation invariance should hold, implying that $C(t,s)$ becomes a function of the evolved time difference $t - s$ only. In the transient aging window, characterized by double time scale separation $t_c \gg t, s, t - s \gg t_{\rm mic}$, where $t_{\rm mic}$ represents typical microscopic time scales, one often encounters a simple aging scenario described by the dynamical scaling form

$$C(t,s) = s^{-b}\, f_c(t/s)\,, \quad f_c(y) \sim y^{-\Lambda_c/z} \tag{2.5}$$

with the aging scaling exponent b, and a scaling function f_c that asymptotic obeys a power law decay in the long-time limit, governed by the ratio of the autocorrelation exponent Λ_c and dynamic critical exponent z [23]. Near continuous phase transitions both in and far from thermal equilibrium, the simple aging dynamical scaling form (2.5) can be derived by means of renormalization group methods [21,38]. For directed percolation, the aging exponents are related to the quasi-stationary critical exponents through the scaling relations (in d space dimensions) [23]

$$b = 2\,\alpha \ , \quad \Lambda_c/z = 1 + \alpha + d/z \ . \tag{2.6}$$

In perhaps the simplest lattice realization of the directed percolation universality class, the contact process, numerical simulations have confirmed the simple aging scaling form (2.5), with scaling exponents $b = 0.901 \pm 0.002$ and $\Lambda_c/z = 2.8 \pm 0.3$ in two dimensions, see Table 2.1 [41]. If universality holds near active-to-absorbing phase transitions, we should observe the same scaling properties at the predator extinction threshold in our stochastic lattice Lotka–Volterra model.

In our Monte Carlo simulations, the predator density autocorrelation function $C(t,s)$ is obtained in a straightforward manner by monitoring the occupations of the lattice sites with A particles following the previously discussed predation probability quench scenario to its critical value λ_c after the system had first reached a quasi-stationary state. If time translation invariance applies, the ensuing curves of $C(t,s)$ plotted against $t - s$ should overlap for different values of the waiting time s. Indeed, this is clearly seen in the inset of Fig. 2.7(a) for the expected exponentially fast relaxation of the predator density autocorrelation function following a sudden quench from $\lambda_1 = 0.250$ to $\lambda_2 = 0.125$, whence the system remains within the two-species coexistence phase. In stark contrast, as becomes apparent in Fig. 2.7(a), time translation invariance is manifestly broken at the critical point.

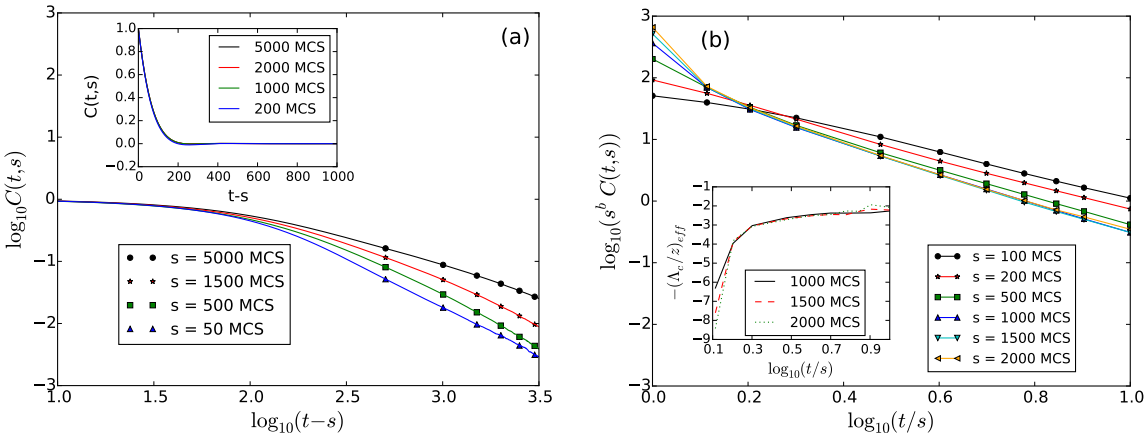

Figure 2.7: Adapted from paper [20] Fig.8. (a) Double-logarithmic plot of the predator density autocorrelation function $C(t, s)$ as a function of the time difference $t - s$ for various waiting times $s = 50, 500, 1500, 5000$ MCS (left to right) at the predator extinction critical point $\lambda_c = 0.0416$; the data are averaged over 100 independent simulation runs for each value of s. The inset shows that in contrast $C(t, s)$ decays exponentially fast for $\lambda_2 = 0.125$, i.e., a quench within the coexistence phase, and demonstrates that time translation invariance holds in this situation (data averaged over 400 simulation runs for the waiting times $s = 5000, 2000, 1000,$ and 200 (top to bottom). (b) Simple aging dynamical scaling analysis: $s^b\, C(t, s)$ is graphed versus the time ratio t/s, for 1000 independent simulation runs for each waiting time s. The straight-slope section of the curves with large waiting times $s \geq 1000$ MCS yields $\Lambda_c/z = 2.37 \pm 0.19$, and the aging scaling exponent is determined to be $b = 0.879 \pm 0.005$. The inset displays the local effective exponent $-(\Lambda_c/z)_{\rm eff}(t)$.

In Fig. 2.7(b), we plot our data for the critical density autocorrelations, now averaged over 1000 simulation runs, in the form of $s^b\, C(t,s)$ versus the time ratio t/s, for a set of waiting times 100 MCS $\leq s \leq$ 2000 MCS, in order to test for the simple aging dynamical scaling scenario (2.5). The aging exponent b is determined by attempting to collapse the data for the three large waiting times $s \geq 1000$ MCS onto a single master curve. With the choice $b = 0.879 \pm 0.005$, the predator density autocorrelation function displays simple aging scaling for $s = 1000$, 1500, and 2000 MCS. However, for small $s \leq 500$ MCS, the curves cannot be properly rescaled and collapsed. Depending on how many data points in the t/s plot are used, one obtains slightly different values for b; their standard deviation gives our estimated errors. Within these error bars, the directed percolation scaling relation $b = 2\,\alpha$ is just marginally fulfilled. We also remark that since our estimate for the location of the critical point λ_c is inevitably measured only with limited accuracy, and we cannot meaningfully extend our finite-system simulation runs for arbitrarily long time periods, we also do not observe aging scaling anymore for $s \gg 2000$ MCS; to extend the aging analysis to larger waiting times would require both a more accurate measurement of λ_c and larger simulation domains.

Finally, the exponent ratio Λ_c/z may be estimated from the slope of the master curve in Fig. 2.7(b) resulting from the data collapse at large waiting times; see also the inset that shows the associated effective exponent. We find $\Lambda_c/z = 2.37 \pm 0.19$, which within the estimated error bars is in fair agreement with the value 2.8 ± 0.3 measured for the contact process in $d = 2$ dimensions [41], and in accord with the scaling relation (2.6). To ascertain that the critical aging exponents do not depend on the initial configurations, we have repeated the above procedures for Monte Carlo simulations initiated with randomly distributed particles at the critical predation probability λ_c rather than starting with the spatially correlated initial configurations prepared in quasi-steady states. We have confirmed that we thereby obtain identical values for b and Λ_c/z, as listed in the first column of Table 2.1. Within our error bars these are in accord with the two-dimensional values obtained for the contact process [41] and in experiments on turbulent liquid crystals [39].

Fig. 2.7(b) demonstrates that convincing critical aging scaling collapse is achieved for $t/s \geq 5$, or $t \approx 10^4$ MCS even for the longest waiting time $s = 2000$ MCS under consideration here. Note that aging scaling thus appears by about a factor of 10 earlier in the system's temporal evolution than the critical power laws describing the quasi-stationary predator density decay and the divergence of the characteristic relaxation time. Just as critical slowing-down, the emergence of physical aging and certainly the associated dynamical scaling is an indicator of the ecosystem's proximity to population extinction. Critical aging scaling hence provides a complementary warning signal for impending collapse, yet becomes visible markedly earlier in the system's time evolution.

We end our discussion of non-equilibrium relaxation processes in spatially extended stochastic Lotka–Volterra models by briefly addressing the sole remaining quench scenario, which takes the system from the active two-species coexistence state to the absorbing phase wherein the predator population goes extinct. Outside the critical parameter region, the characteris-

tic relaxation time t_c is finite; i.e., the mean predator density will decay to zero exponentially fast, as local predator clusters become increasingly dilute, while the prey gradually fill the entire system. In the absorbing state, population density fluctuations eventually cease, whence no interesting dynamical features remain.

2.4 Conclusions

To conclude this part, we have investigated non-equilibrium relaxation features in a stochastic Lotka–Volterra Model on a two-dimensional lattice via detailed Monte Carlo simulations. If the prey carrying capacity is limited, i.e., in the presence of site restrictions (and for sufficiently large system size), there appears a predator extinction threshold that separates an inactive phase wherein the prey proliferate and the predators die out, from an active phase where both species coexist and compete. In a first set of numerical experiments, we observe the system's relaxation either from a random initial configuration or between two quasi-stationary states within the active coexistence phase via suddenly changing the predation rate. As expected, we find that the initial state generically only influences the subsequent oscillatory dynamics for the duration of about one characteristic relaxation time, implying that the system exponentially quickly loses any memory of the initial configuration.

Our main focus has thus been the analysis of critical quenches and the ensuing dynamical scaling behavior. Following a quench of the predation rate to its critical value for the predator species extinction threshold, we have measured the dynamic scaling exponents for the diverging relaxation time and the algebraic decay of the predator density. Within our systematic and statistical errors, we obtained the expected values for the directed percolation universality class that generically characterizes active-to-absorbing phase transitions. In addition, we have studied the critical aging properties of this system: Reflecting critical slowing-down, the characteristic relaxation time diverges at the extinction threshold; as a consequence, time translation invariance is broken, and physical aging governed by universal scaling features emerges. Our measured aging scaling exponents are close to those found previously for the contact process, which is perhaps the simplest lattice realization of the directed percolation universality class. We remark that at least to our knowledge, this present study constitutes only the second investigation of aging scaling at an active-to-absorbing phase transition, and hence provides a crucial test of universality for non-equilibrium critical phenomena.

We also emphasize that universal aging scaling sets in considerably earlier during the system's time evolution than asymptotic quasi-stationary power laws emerge, and in addition often yields more accurate exponent estimates [40]. In comparison with detecting critical slowing-down, this critical aging effect might thus serve as a preferable and more reliable early warning signal for impending population collapse.

Chapter 3

Boundary effects on population dynamics in stochastic lattice Lotka–Volterra models

This chapter was essentially copied from our publication:

Heiba B, Chen S, Täuber U C, 2018, "Boundary effects on population dynamics in stochastic lattice Lotka–Volterra models," Physica A, 491, 582-590, "Copyright (2017) by Elsevier B.V."

Bassel Heiba was an undergraduate student working under my guidance. He collected the original data by doing Monte Carlo simulations. I analyzed his data, and then drew all the graphs. We worked together to finish this paper under Prof. Täuber's supervision.

3.1 Introduction

Due to its wide range of applications and relative simplicity, variants of the Lotka–Volterra predator-prey competition model represent paradigmatic systems to study the emergence of biodiversity in ecology, noise-induced pattern formation in population dynamics and (bio-) chemical reactions, and phase transitions in far-from-equilibrium systems. In the classical deterministic Lotka–Volterra model [1,2], two coupled mean-field rate equations describe the population dynamics of a two-species predator-prey system, whose solutions display periodic non-linear oscillations fully determined by the system's initial state. Yet the original mean-field Lotka–Volterra rate equations do not incorporate demographic fluctuations and internal noise induced by the stochastic reproduction and predation reactions in coupled ecosystems encountered in nature.

In a series of numerical simulation studies [5–16, 18, 20, 33, 34], the population dynamics of several stochastic spatially extended lattice Lotka–Volterra model variants was found to substantially differ from the mean-field rate equation predictions due to stochasticity and the emergence of strong spatio-temporal correlations: Both predator and prey populations oscillate erraticly, and do not return to their initial densities; the oscillations are moreover damped and asymptotically reach a quasi-stationary state with both population densities finite and constant [7]– [20]. In a non-spatial setting, these persistent non-linear oscillations can be understood through resonantly amplified demographic fluctuations [17].

Local carrying capacity restrictions, representing limited resources in nature, can be implemented in lattice simulations by constraining the number of particles on each site [9, 10, 15, 16, 18]. These local occupation number restrictions cause the emergence of a predator extinction threshold and an absorbing phase, wherein the predator species ultimately disappears while the prey proliferate through the entire system. Upon tuning the reaction rates, one thus encounters a continuous active-to-absorbing state non-equilibrium phase transition whose universal features are governed by the directed percolation universality class [5, 10–12, 15, 18, 20, 34].

Biologically more relevant models should include spatial rate variability to account for environmental disorder. The population dynamics in a patch surrounded by a hostile foe [42–44] is well represented by Fisher's model [45], which includes diffusive spreading as well as a reaction term capturing interactions between individuals and with the environment. For the stochastic Lotka–Volterra model, the influence of environmental rate variability on the population densities, transient oscillations, spatial correlations, and invasion fronts was investigated by assigning random reaction rates to different lattice sites [46,47]. Spatial variability in the predation rate results in more localized activity patches, a remarkable increase in the asymptotic population densities, and accelerated front propagation. These studies assumed full environmental disorder, as there was no correlation at all between the reaction rates on neighboring sites.

In a more realistic setting, the system should consist of several domains with the environment fairly uniform within each patch, but differing markedly between the domains, e.g., representing different topographies or vegetation states. In our simulations, we split the system into several patches and assign different reaction rates to neighboring regions. By tuning the rate parameters, we can force some domains to be in an absorbing state, where the predators go extinct, or alternatively in an active state for which both species coexist at non-zero densities. One would expect the influence of the boundary between the active and absorbing regions to only extend over a distance on the scale of the characteristic correlation length in the system. In this work, we study the local population densities, correlation length, as well as the local oscillation frequency and attenuation, as functions of the distance from the domain boundary. As we successively divide the system further in a checkerboard pattern so that each patch decreases in size, the population dynamics features quantitatively tend towards those of a randomly disordered model with reaction rates assigned to the lattice sites from a bimodal distribution.

3.2 Model description and background

We use Monte Carlo simulations for the stochastic Lotka–Volterra model based on the reactions (2.1) performed on a two-dimensional square lattice with 512×512 sites and periodic boundary conditions to fully account for emerging spatial structures and internal reaction noise. We note that we have also performed simulations on twodimensional square lattices with 256×256 and 128×128 sites; aside from overall noisier data, as one would expect, we obtain no noticeable quantitative differences. Given that the correlation lengths ξ measured below are much smaller than these system sizes, this is not surprising. Due to our limited computational resources, we have not attempted runs on even larger systems. In the following, all listed Monte Carlo data and extracted quantitative results refer to 512×512 square lattices. Also, for the reaction processes, we only consider the four nearest-neighbor sites, and have not extended interactions to larger distances. In our model, we implement occupation number limitations or finite local carrying capacities; i.e., the number of particles on any lattice site is restricted to be either 0, if the site is empty, or 1, if it is occupied by a predator or a prey individual. We shall examine the population densities of each species, given by their total particle number divided by the number of lattice sites, and aim to quantify the ensuing oscillations and through characteristic observables that include their frequency and attenuation, as well as typical population cluster sizes as determined by their spatial correlation length.

The simulation algorithm, which is slightly different from that in section 2.2, proceeds as follows: For each iteration, an occupied site is randomly selected and then one of its four adjacent sites is picked at random. If the two selected sites contain a predator and a prey particle, a random number $x_1 \in [0, 1]$ is generated; if $x_1 < \lambda$, the prey individual is removed and a newly generated predator takes its place. Similarly, if the occupant is a predator, a

random number $x_2 \in [0,1]$ is generated, and the particle is removed if $x_2 < \mu$. Yet if the initially selected occupant is a prey particle and the chosen neighbor site empty, a random number $x_3 \in [0,1]$ is generated; if $x_3 < \sigma$ a new prey individual is added to this site.

The variables that can be tuned in our simulations are: the system size L, the initial predator density $\rho_A(0)$, the initial prey density $\rho_B(0)$, the predator death rate μ, the prey reproduction rate σ, the predation rate λ, and the number of Monte Carlo steps. We chose the linear system size $L = 512$. Naturally one must avoid starting the simulations from one of the absorbing states. For any non-zero initial predator and prey density, the population numbers and particle distribution at the outset of the simulation runs influence the system merely for a limited time, and the final (quasi-)stationary state of the system is only determined by the three reaction rates [20]. In our simulations, the rates μ and σ are kept constant for simplicity, while λ is considered to be the only relevant control parameter. The dynamical properties are generically determined by the ratio of the reaction rates; the subsequent results apply also for different sets of μ and σ with appropriately altered predation rate λ. Since we only have two species, predators and prey, $0 \leq \rho_A + \rho_B \leq 1$ due to the site occupation restrictions. For each parameter set we perform 1000 independent simulation runs and use the average of these repeats in the data analysis to reduce statistical errors.

In the case of very low predation rates λ, the predators will gradually starve to death, and the remaining prey will finally occupy the whole system. On the other hand, when λ is large, there is a finite probability (in any finite lattice) that all prey individuals would be devoured; subsequently the predators would die out as well because of starvation. In fact, the absorbing extinction state is the only truly stable state in a finite population with the stochastic dynamics (2.1). However, in sufficiently large systems, quasi-stable states in which both species survive with relatively constant population densities during the entire simulation duration are indeed observed in certain regions of parameter space. In the simulations, we select the non-linear predation reaction rate λ as the only control parameter with the reaction probabilities $\mu = 0.125$ and $\sigma = 1.0$ held fixed. We chose the initial population densities as $\rho_A(0) = 0.3 = \rho_B(0)$ with the particles randomly distributed among the lattice sites. The trajectories of the prey population density $\rho_B(t)$ versus that of the predators $\rho_A(t)$ for different values of λ are very similar to those in Fig. 2.1: With $\lambda = 0.1$, the predators have low predation efficiency and thus gradually go extinct; the system then reaches an absorbing state with only prey particles remaining and ultimately filling the entire lattice ($\rho_B \to 1$). If we increase the value of λ to 0.18, just above the predator extinction threshold, the system relaxes exponentially to a quasi-stationary state with non-zero densities for both species. For $\lambda = 0.4$, the system resides deep in this coexistence phase and the simulation trajectory spirals into a stable fixed point, indicating damped oscillatory kinetics. According to our investigations, we estimate the critical predation rate of the predator extinction phase transition point at $\lambda_c = 0.12 \pm 0.01$.

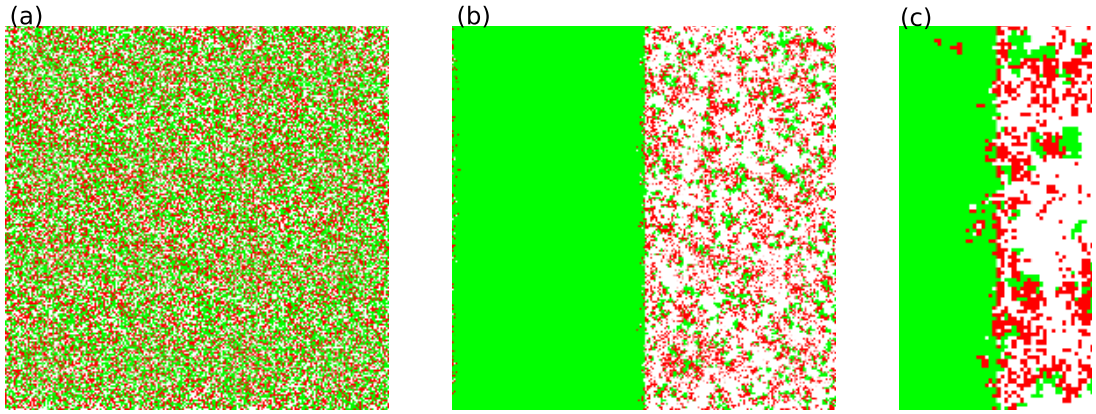

Figure 3.1: Adapted from paper [28] Fig.2. Snapshots of the spatial particle distribution on a 512×512 lattice (with periodic boundary conditions) that is split into equally large predator extinction (left) and species coexistence (right) regions: prey are indicated in green, predators in red, white spaces in white. (a) Random initial distribution with densities $\rho_A = 0.3 = \rho_B$; (b) state of the system after 1000 MCS, when it has reached a quasi-stationary state with uniform rates $\mu = 0.125$ and $\sigma = 1.0$, while $\lambda_l = 0.1$ on columns $[0, 255]$, $\lambda_r = 0.8$ on columns $[256, 511]$.

3.3 Boundary effects at a coexistence / predator extinction interface

Natural environments vary in space and boundaries are formed between different regions, yielding often quite sharp interfaces, e.g., between river and land, desert and forest, etc. At the boundaries of such spatially inhomogeneous systems, interesting phenomena may arise. In order to study boundary effects on simple predator-prey population dynamics, we split our simulation domain into two equally large pieces with one half residing in the predator extinction state, and the other half in the two-species coexistence phase. We use a two-dimensional lattice with 512×512 sites with periodic boundary conditions, and index the columns with integers in the interval $[0, 511]$. Whereas the predator death and prey reproduction rates are uniformly set as $\mu = 0.125$ and $\sigma = 1.0$ on all sites, we assign $\lambda_l = 0.1 < \lambda_c$ on columns $[0, 255]$ to enforce predator extinction on the "left" side, and $\lambda_r = 0.8 > \lambda_c$ for the columns on the "right" half with indices $[256, 511]$, which is thus held in the predator-prey coexistence state. Fig. 3.1(a) depicts the initial random particle distribution with equal population densities $\rho_A = 0.3 = \rho_B$. After the system has evolved for 1000 MCS, a quasi-steady state is obtained as shown in Fig. 3.1(b). The predators are able to penetrate into the "left" absorbing region by less than 10 columns, and no predator individuals are encountered far away from the active-absorbing interface. On the right

half, we observe a predator-prey coexistence state with the prey particles forming clusters surrounded by predators and predation reactions occurring at their perimeters.

Since only the predator species is subject to the extinction transition into an absorbing state, while the prey can survive throughout the entire simulation domain, we concentrate on boundary effects affecting the predator population. We measure the column densities of predators $\rho_A(n)$, defined as the number of predators on column n divided by $L = 512$, and record their averages from 1000 independent simulation runs as a function of column index n. As shown in the inset of Fig. 3.2(a), $\rho_A(n)$ decreases to 0 deep inside the absorbing half of the system, and reaches a positive constant 0.195 ± 0.001 within the active region. The main graph focuses on the boundary region, where we observe a marked predator density peak right at the interface (column 256). The predator density enhancement at the boundary is obviously due to the net intrusion flow of species A from the active subdomain with high predation rate into the predator extinction region with abundant food in the form of the near uniformly spread prey population. We also ran simulations for other predation rate pairs such as $\lambda_l = 0.1$ and $\lambda_r = 0.2$ (still in the coexistence phase), and observed very similar behavior (except that the peak of ρ_A appeared on column 257 in that situation instead of at $n = 256$).

Fig. 3.2(b) shows the exponential decay of the predator column density $\rho_A(n)$ as function of the distance $|255 - n|$ from the boundary (located at $n = 255$) towards the "left", absorbing side. A simple linear regression gives the inverse characteristic decay length $|k| = 0.286$. However, on the "right" active half of the system, $\rho_A(n)$ neither fits exponential nor algebraic decay. Instead, ρ_A reaches the asymptotic constant value 0.195 ± 0.001 deep in the coexistence region through an apparent stretched exponential form $\rho_A(n) \sim e^{-c(n-256)^l} + 0.195$ with stretching exponent $l \approx 0.348$, as demonstrated in Fig. 3.2(c).

On the "right" semidomain set in the predator-prey coexistence phase, the particle reproduction processes induce clustering of individuals from each species. The cluster size may vary with the distance from the boundary. We utilize the correlation length ξ, obtained from the equal-time correlation function $C(x)$, to characterize the spatial extent of these clusters. For species $\alpha, \beta = A, B$, the (connected) correlation functions are defined as $C_{\alpha\beta}(x) = \langle n_\alpha(x)\, n_\beta(0)\rangle - \langle n_\alpha(x)\rangle \langle n_\beta(0)\rangle$, where $n_\alpha(x) = 0, 1$ denotes the local occupation number of species α at site x [16]. For $x = 0$ and $\alpha = \beta$, in a spatially homogeneous system it is simply given by the density $\langle n_A\rangle$: $C_{\alpha\alpha}(0) = \langle n_A\rangle(1 - \langle n_A\rangle)$. For $|x| > 0$, $\langle n_\alpha(x)\, n_\beta(0)\rangle$ is computed as follows: First choose a site, and then a second site at distance x away from the first one. $n_\alpha(x)\, n_\beta(0)$ equals 1 only if the first site is occupied by an individual of species β, and the second one by an particle of species α, otherwise the result is 0. One then averages over all sites.

Here, we compute the predator correlations $C_{AA}(x, n)$ on a given column n, i.e., we only take the mean in the above procedure over the $L = 512$ sites on that column. The main panel in Fig. 3.3(a) shows the predator correlation function $C_{AA}(x, n)$ on column $n = 274$ with $x \in [0, 9]$, where the correlations $C_{AA}(x)$ gradually decrease to zero. The inset presents the

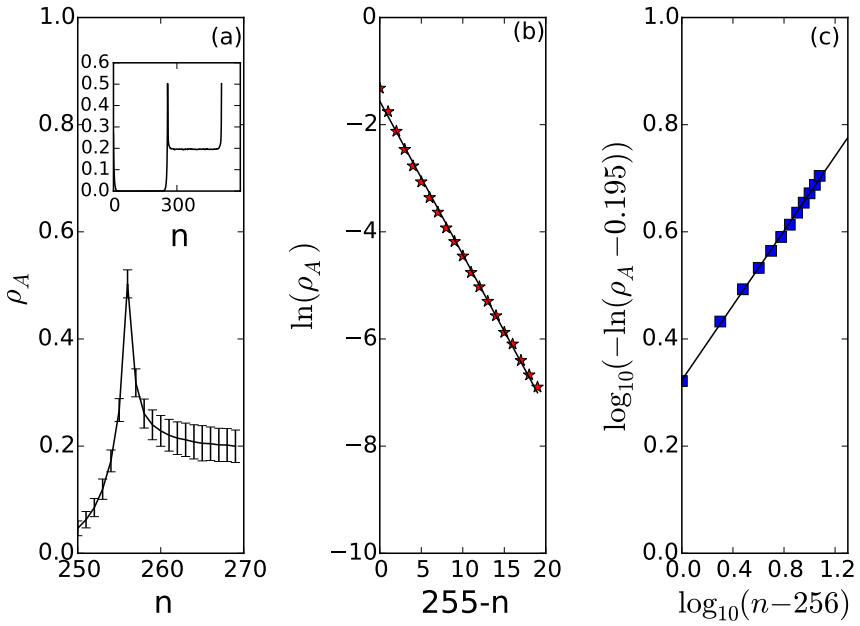

Figure 3.2: Adapted from paper [28] Fig.3. After the split system with rates $\mu = 0.125$, $\sigma = 1.0$ and $\lambda_l = 0.1$ on columns $[0, 255]$, $\lambda_r = 0.8$ on columns $[256, 511]$ evolves for 1000 MCS, it arrives at a quasi-stationary state: (a) the main plot shows the column densities of the predator population $\rho_A(n)$ as function of column index $n \in [251, 270]$, and the inset on all $L = 512$ columns (data averaged over 1000 independent runs); (b) exponential decay of $\rho_A(n)$ from the boundary (located at $n = 255$) into the absorbing region with $n \in [235, 255]$: The red stars depict our simulation results, while the black straight line represents a linear regression of the data with slope $k = -0.286$; (c) the column density ρ_A decays to a positive constant value 0.195 ± 0.001 deep in the right coexistence region. The blue squares display $\log_{10}(-\ln(\rho_A - 0.195))$ versus $\log_{10}(n - 256)$, while the black straight line with slope $l = 0.348$ is obtained from linear data regression.

same data in a logarithmic scale, demonstrating exponential decay according to $C(x, n) \sim e^{-x/\xi(n)}$. Since the statistical errors grow at large distances x, we only use the initial data points up to $x = 6$ for the analysis. Linear regression of $\ln(C_{AA}(x, n = 274))$ over $x \in [1, 6]$ gives $\xi(n = 274) \approx 3.2$, indicated as red square in Fig. 3.3(b). In the same manner, we obtain the characteristic correlation lengths $\xi(n)$ for each column n as shown in Fig. 3.3(b), starting at the interface at $n = 256$. We observe $\xi(n)$ to increase by about a factor of four within the first ten columns away from the boundary, and then saturate at the bulk value $\xi \approx 3.2$. Near the absorbing region, the predator clusters are thus much smaller, owing to the net flux of predators across the boundary into the extinction domain. These values of ξ are measured after the entire system has reached its (quasi-)steady state after 1000 MCS, and would not change for longer simulations run times. We note that the relationship between

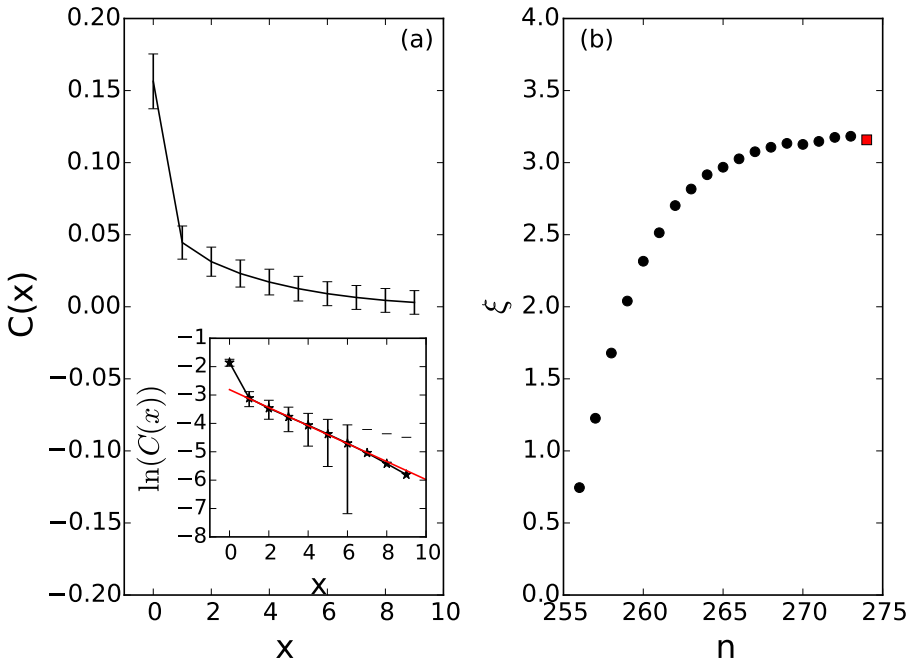

Figure 3.3: Adapted from paper [28] Fig.4. (a) Main panel: the predator correlation function $C_{AA}(x, n)$ on column $n = 274$ (data averaged over 1000 independent simulation runs). Inset: $\ln(C_{AA}(x, n))$; the red straight line indicates a simple linear regression of the data points with $x \in [1, 6]$, and yields the characteristic decay length $\xi(n = 274) \approx 3.2$. (b) Correlation length $\xi(n)$ versus column number n, with $\xi(n)$ defined as the negative reciprocal of the slope of $\ln(C_{AA}(x, n))$.

the correlation length ξ and the predation rate λ is manifestly not linear, i.e., a very large value of λ does not imply huge predator clusters. We surmise that the cluster size remains finite even in that scenario, and the predators would penetrate into the "left" absorbing region for a finite number of columns only. For sufficiently large domain size, the system should thus remain spatially inhomogeneous even for very high predation rates λ. Finally, the dependence of the typical cluster size $\xi(n)$ on column index n correlates inversely with the column density plotted in Fig. 3.2: High local density corresponds to small cluster size and vice versa. We note that the product $\rho_A(n)\,\xi(n)$ is however not simply constant across different columns; rather it is minimal near the boundary (at $n = 256$), then increases away from the interface, and ultimately reaches a fixed value within 10 columns inside the active region.

Spatially homogeneous stochastic Lotka–Volterra systems display damped population oscillations in the predator-prey coexistence phase after being initialized with random species distribution, see, for example, the (blue square) trajectory in Fig. 2.1. We next explore the boundary effects on these population oscillations near the active-absorbing interface. We

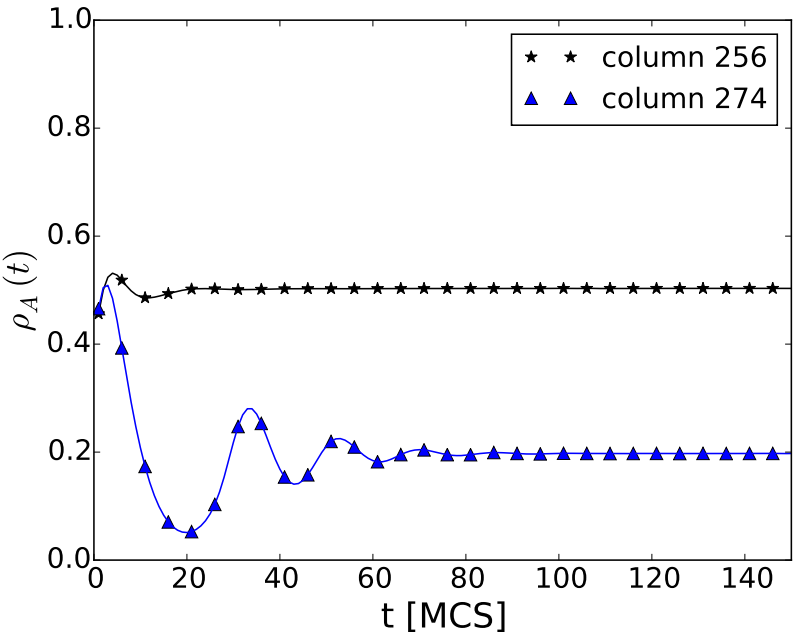

Figure 3.4: Adapted from paper [28] Fig.5. The temporal evolution of the average predator column densities $\rho_A(t, n)$ (averaged over 1000 independent runs) on columns $n = 256$ (black stars) and $n = 274$ (blue triangles), with initial predator density $\rho_A(0) = 0.3$ and rates $\mu = 0.125$, $\sigma = 1.0$, $\lambda_l = 0.1$ on columns $n \in [0, 255]$, and $\lambda_r = 0.8$ for $n \in [256, 511]$.

prepare the system with the same parameters as mentioned above so that its "left" half is in the absorbing state while the "right" side sustains species coexistence. The initial population densities are again set to $\rho_A(0) = 0.3 = \rho_B(0)$, with the particles randomly distributed on the lattice. We then measure the column predator densities as a function of time (MCS). Fig. 3.4 displays the temporal evolution of $\rho_A(t, n)$ on columns $n = 256$ and $n = 274$. We observe the oscillations on the column closest to the interface to be strongly damped, whereas deeper inside the active region the population oscillations are more persistent and subject to much weaker attenuation. Both column densities asymptotically reach the expected quasi-steady state values.

In order to determine the dependence of the local oscillation frequencies on the distance from the active-absorbing interface, we compute the Fourier transform amplitude $f_A(\omega, n) = |\int e^{-i\omega t}\, \rho_A(t, n)\, dt|$ of the column density time series data by means of the fast Fourier transform algorithm for $n \in [256, 274]$, as shown in Fig. 3.5(a). Assuming the approximate functional form $\rho_A(t, n) \sim e^{-t/t_c(n)} \cos(2\pi t/T(n))$, we may then identify the peak position of $f_A(\omega, n)$ with the characteristic oscillation frequency $2\pi/T(n)$, and the peak half-width at half maximum with the attenuation rate or inverse relaxation time $1/t_c(n)$. We find that the oscillation frequencies are constant except for the column at the boundary ($n = 256$), which shows a very slight reduction. We conclude that the presence of the extinction region

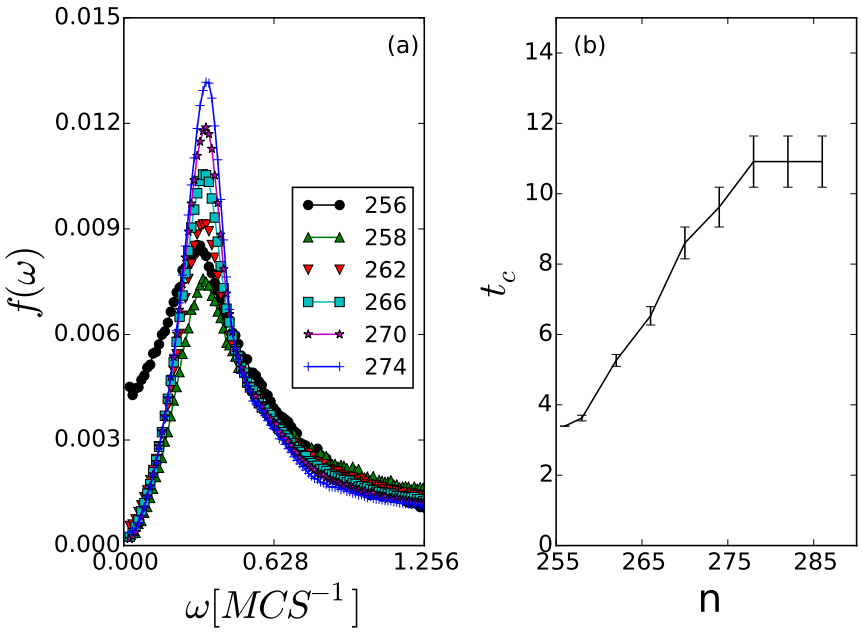

Figure 3.5: Adapted from paper [28] Fig.6. (a) Fourier transform amplitude $f_A(\omega, n)$ of the predator column density time evolution on columns $n = 256$ (black dots), 258 (green triangles up), 262 (red triangles down), 266 (cyan squares), 270 (magenta stars), and 274 (blue plus marks), with rates $\mu = 0.125$, $\sigma = 1.0$, and $\lambda_l = 0.1$ for $n \in [0, 255]$, $\lambda_r = 0.8$ for $n \in [256, 511]$; (b) measured characteristic decay time $t_c(n)$ on columns near the active-absorbing boundary, inferred from the peak widths in (a).

does not markedly affect the frequency of the population oscillations in the active regime. In contrast, the attenuation rate decreases by a factor of three within about 20 columns in the vicinity of the interface, as demonstrated in Fig. 3.5(b). Beyond $n \approx 278$ in the coexistence region, the relaxation time assumes its constant bulk value.

3.4 Checkerboard division of the system

To further explore boundary (and finite-size) effects in spatially inhomogeneous Lotka–Volterra systems, we proceed by successively dividing the simulation domain into subdomains in a checkerboard pattern, setting the predation rate to two distinct values in neighboring patches, and thus preparing them alternatingly in either the active coexistence or absorbing predator extinction states. Fig. 3.6(a) shows a case when the system is split into four subregions with $\sigma = 1.0$ and $\mu = 0.125$, and with two distinct values for the predation rate $\lambda = 0.1$ and 0.8 assigned to alternating patches of the 2×2 checkerboard structure. Note that the low predation rate value posits the corresponding patches in the predator extinction

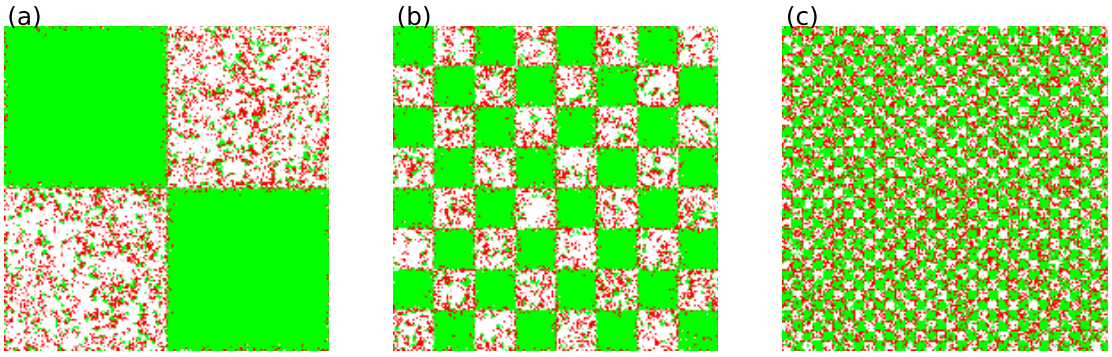

Figure 3.6: Copied from paper [28] Fig.7. Snapshots of the distribution of predator (red) and prey (green) particles after the system has evolved for 1000 MCS with rates $\mu = 0.125$, $\sigma = 1.0$, and λ switched alternatingly between the values 0.1 (predator extinction) and 0.8 (species coexistence) on neighboring subdomains, as the full 512×512 system is periodically divided into successively smaller square patches with lengths 256 (a), 64 (b), and 16 (c), respectively. The square subdomains dominantly colored in green reside in the extinction state ($\lambda = 0.1$), whereas predator-prey coexistence pertains to the other patches ($\lambda = 0.8$).

state, whereas the subdomains with the high predation rate reside in the species coexistence phase. Figures 3.6(b) and (c) depict the situations when the total simulation domain with 512×512 sites is respectively split into 8×8 and 32×32 square patches: If for a given box λ is set to 0.1, then the adjacent square subdomains above, below, to its right, and to its left are given a value $\lambda = 0.8$.

1000 simulations were performed for each setting, and the averages over these independent runs were used to analyze the data. We also generated and inspected simulation videos: snapshots are depicted in Fig. 3.6. As we split the system into successively smaller and more pieces in the checkerboard-patterned fashion with λ switching between 0.1 and 0.8 on neighboring subregions, we find the boundaries to have less of an impact on the population densities. We observe that in this sequence the prey density decreases on the patches with lower predation rate 0.1, but stays roughly the same on the subdomains where $\lambda = 0.8$. The predator density in contrast increases in both the active and absorbing regions as the subdivision proceeds. We have also confirmed that these changes in the total population densities naturally become less significant if the two different predation rate values are chosen closer to each other.

In Fig. 3.7, we plot the total (summed over all subdomains) predator and prey population densities ρ in the simulation domain split into $N \times N$ checkerboard patches, as functions of $\log_{10} N$. Here, $N = 1$ corresponds to the situation studied in chapter 3.3, where the system was divided into two rectangular subdomains. The other values of $N =$

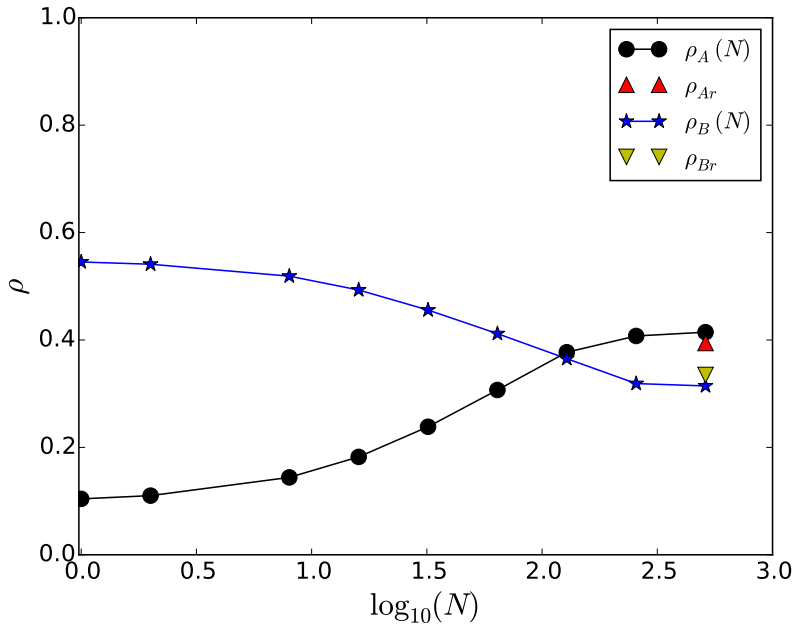

Figure 3.7: Adapted from paper [28] Fig.8. Total population densities for predators (black dots) and prey (blue stars) versus number of checkerboard-patterned subdivisions N of the simulation domain, after the system has evolved for 1000 MCS and reached a quasi-stationary state, with reaction rates $\mu = 0.125$, $\sigma = 1.0$, and λ alternatingly switched between 0.1 and 0.8. For comparison, the graph also shows the total quasi-steady state population densities for predators (red triangle up) and prey (yellow triangle down) in a system with randomly assigned predation, drawn with equal probability from a bimodal distribution with values $\lambda = 0.1$ and 0.8.

$512, 256, 128, 64, 32, 16, 8, 2$ refer to checkerboard square patches with lengths $512/N$. The mean population density ρ shown for each data point represents an average of 1000 independent simulation runs; the associated statistical error was very small, with a standard deviation of order 10^{-3}. As apparent in the data, the overall population predator density ρ_A monotonically increases with growing number N of subdivisions, while the prey density ρ_B decreases.

We also performed the analogous sequence of measurements for other pairs of predation rate values. For instance, with checkerboard subdomains with $\lambda = 0.1$ and 0.2 (also just within the species coexistence range), the population density changes with increasing N are less pronounced than in Fig. 3.7, and ρ_A, ρ_B acquire maximum and minimum values at $N = 256$ rather than 512. The origin of this slight shift can be traced to the fact that the predator correlation length is of order one lattice constant at the boundary of the $\lambda = 0.1/0.8$ system, but extends over about two sites for the 0.1/0.2 case.

For comparison, we also measured the overall population predator and prey densities in a Lotka–Volterra system with quenched spatial disorder in the predation rates, where either of the two values $\lambda = 0.1$ and 0.8 are assigned at random to each lattice site with equal probability. The resulting net population density values are also shown in Fig. 3.7; they are close, but not identical to those obtained for the $N = 512$ system, for which these two predation rates are alternatingly assigned to the lattice sites in a periodic regular manner. We would expect the population densities in these two distinct systems to reach equal values if the associated correlation lengths at the boundaries were large compared to the lattice constant, which is however not the case here.

3.5 Conclusions

In this part, we have focused on studying boundary effects in a stochastic Lotka–Volterra predator-prey competition model on a two-dimensional lattice, by means of detailed Monte Carlo simulations. We first considered a system split into two equally large parts with distinct non-linear predation rates, such that one domain is set to be in the predator extinction state, while the other one resides in the two-species coexistence phase. We have primarily addressed the influence of such an absorbing-active separation on both populations' density oscillations as function of the distance from the boundary.

We find a remarkable peak in the column density oscillation amplitude of the predator population, as shown in Fig. 3.2(a), which reflects its net steady influx towards the absorbing region. Correspondingly, the predator correlation length that characterizes the typical cluster size reaches a minimum value at the boundary, see Fig. 3.3(b). The population oscillation frequency there shows only small deviations from its bulk value, while the attenuation rate is locally strongly enhanced, see Fig. 3.5(b), inducing overdamped relaxation kinetics. Overall, the ecosystem remains stable.

Furthermore, upon splitting the system successively into more pieces in a checkerboard fashion, the observed boundary effects become less significant, and as demonstrated in Fig. 3.7, the overall population densities acquire values that are close to those in a disordered system with randomly assigned predation rates drawn from a bimodal distribution.

Chapter 4

Evolutionary dynamics and competition stabilize three-species predator-prey communities

This chapter was essentially copied from a preprint submitted to Ecol. Complex.:

Chen S, Dobramysl U, Täuber U C, 2017, "Evolutionary dynamics and competition stabilize three-species predator-prey communities," submitted to Ecological Complexity [arXiv:1711.05208]

Ulrich Dobramysl contributed Fig. 4.5(b) and Fig. 4.8, and I did all the other work under Prof. Täuber's supervision.

4.1 Introduction

Ever since Darwin first introduced his theory that interspecific competition positively contributes to ecological character displacement and adaptive divergence [48], debates abounded about its importance in biodiversity. Character displacement is considered to occur when a phenotypical feature of the animal [25], which could be morphological, ecological, behavioral, or physiological, beak size for example, is shifted in a statistically significant manner due to the introduction of a competitor [49, 50]. One example of ecological character displacement is that the body size of an island lizard species becomes reduced on average upon the arrival of a second, competing lizard kind [26]. Early observational and experimental studies of wild animals provided support for Darwinian evolutionary theory [25, 51]. One famous observation related to finches, whose beak size would change in generations because of competition [51]. However, recent studies using modern genetic analysis techniques do not find genetic changes to the same extent as the phenotypic break change, thereby casting doubt on Darwin's observational studies [52, 53]. Another concern with experiments on birds or other animal species is that they may live for decades, rendering this sort of study too time-consuming. Evolutionary theory is based on the assumption that interspecific competition occurs mostly between closely related species because they share similar food resources, thus characters exploiting new resources are preferred. Ecologists perform experiments with wild animals by introducing a second competing species and recording their observable characters including the body size, beak length, and others [26, 53]. Unfortunately, direct control over natural ecosystems is usually quite limited; for example, ecological character displacement with wild animals cannot be shut down at will in natural habitats. However, this is easily doable in carefully designed computer simulations.

Game theory has a long history in the study of biological problems [54]. Among all the mathematical models of studying biodiversity in ecology, the Lotka–Volterra (LV) [1, 2] predator-prey model may rank as possibly the simplest one. Only one predator and one prey species are assumed to exist in the system. Individuals from each species are regarded as simple particles with their reaction rates set uniformly and spatially homogeneous. They display three kinds of behaviors which are influenced by pre-determined reaction rates: prey particles may reproduce, predator particles can spontaneously die, and predators may remove a prey particle and simultaneously reproduce. This simple LV model kinetics may straightforwardly be implemented on a regular lattice (usually square in two or cubic in three dimensions) to simulate situations in nature, where stochasticity as well as spatio-temporal correlations play an important role [5–16, 18, 20, 33, 34]. It is observed in such spatial stochastic LV model systems that predator and prey species may coexist in a quasi-stable steady state where both populations reach non-zero densities that remain constant in time; here, the population density is defined as the particle number in one species divided by the total number of lattice sites. Considering that the original LV model contains only two species, we here aim to modify it to study a multi-species system. We note that there are other, distinct well-studied three-species models, including the rock-paper-scissors model [19, 55], which is

designed to study cyclic competitions, and a food-chain-like three-species model [56], as well as more general networks of competing species [19], all of which contain species that operate both as a predator and a prey. In this paper we mainly focus on predator-prey competitions, where any given species plays only one of those ecological roles.

Compared with the original LV model, we introduce one more predator into the system so that there are two predator species competing for the same prey. We find that even in a spatially extended and stochastic setting, the 'weaker' of the two predator species will die out fast if all reaction rates are fixed. Afterwards the remaining two species form a standard LV system and approach stable steady-state densities. Next we further modify the model by introducing evolutionary adaptation [47]. We also add a positive lower bound to the predator death rates in order to avoid 'immortal' particles. Finally, we incorporate additional direct competition between predator individuals. Stable multiple-species coexistence states are then observed in certain parameter regions, demonstrating that adaptive 'evolution' in combination with direct competition between the predator species facilitate ecosystem stability. Our work thus yields insight into the interplay between evolutionary processes and inter-species competition and their respective roles to maintain biodiversity.

4.2 Stochastic lattice Lotka–Volterra model with fixed reaction rates

4.2.1 Model description

We spatially extend the LV model by implementing it on a two-dimensional square lattice with linear system size $L = 512$. It is assumed that there are three species in the system: two predator species A, B, and a single prey species C. Our model ignores the detailed features and characters of real organisms, and instead uses simple 'particles' to represent the individuals of each species. These particles are all located on lattice sites in a two-dimensional space with periodic boundary conditions (i.e., on a torus) to minimize boundary effects. Site exclusion is imposed to simulate the natural situation that the local population carrying capacity is finite: Each lattice site can hold at most one particle, i.e., is either occupied by one 'predator' A or B, occupied by one 'prey' C, or remains empty. This simple model partly captures the population dynamics of a real ecological system because the particles can predate, reproduce, and spontaneously die out; these processes represent the three main reactions directly affecting population number changes. There is no specific hopping process during the simulation so that a particle will never spontaneously migrate to other sites. However, effective diffusion is brought in by locating the offspring particles on the neighbor sites of the parent particles in the reproduction process [15,20]. The Monte Carlo simulation algorithm in this chapter is similar to the one described in section 2.2. The stochastic

reactions between neighboring particles are described as follows:

$$\begin{aligned} A \xrightarrow{\mu_A} \emptyset\,, \quad B \xrightarrow{\mu_B} \emptyset\,, \\ A + C \xrightarrow{\lambda_A} A + A\,, \quad B + C \xrightarrow{\lambda_B} B + B\,, \\ C \xrightarrow{\sigma} C + C\,. \end{aligned} \tag{4.1}$$

The 'predator' A (or B) may spontaneously die with with decay rate $\mu_A\,(\mu_B) > 0$. The predators may consume a neighboring prey particle C, and simultaneously reproduce with 'predation' rate $\lambda_{A/B}$, which is to replace C with a new predator particle in the simulation. In nature, predation and predator offspring production are separate processes. But such an explicit separation would not introduce qualitative differences in a stochastic spatially extended system in dimensions $d < 4$ [15]. When a prey particle has an empty neighboring site, it can generate a new offspring prey individual there with birth rate $\sigma > 0$. Note that a separate prey death process $C \to 0$ can be trivially described by lowering the prey reproduction rate and is therefore not included. We assume asexual reproduction for all three species, i.e., only one parent particle is involved in the reproduction process. Each species consists of homogeneous particles with identical reaction rates. Predator species A and B may be considered as close relatives since they display similar behavior (decay, predation and reproduction, effective diffusion) and most importantly share the same mobile food source C. As for now we do not include evolution in the reproduction processes, all offspring particles are exactly cloned from their parents. We are now going to show that these two related predator species can never coexist.

4.2.2 Mean-field rate equations

The mean-field approximation ignores spatial and temporal correlations and fluctuations, and instead assumes the system to be spatially well-mixed. We define $a(t)$ and $b(t)$ as the predators' population densities and $c(t)$ as the prey density. Each predator population decreases exponentially with death rate μ, but increases with the predation rate λ and prey density $c(t)$. The prey population $c(t)$ increases exponentially with its reproduction rate σ, but decreases as a function of the predator population densities. The mean-field rate equations consequently read

$$\begin{aligned} \frac{da(t)}{dt} &= -\mu_A a(t) + \lambda_A a(t) c(t)\,, \\ \frac{db(t)}{dt} &= -\mu_B b(t) + \lambda_B b(t) c(t)\,, \\ \frac{dc(t)}{dt} &= \sigma c(t)\left[1 - \frac{a(t) + b(t) + c(t)}{K}\right] - \lambda_A a(t) c(t) - \lambda_B b(t) c(t)\,. \end{aligned} \tag{4.2}$$

$K > 0$ represents the finite prey carrying capacity. In order to obtain stationary densities, the left-side derivative terms are set to zero. The ensuing (trivial) extinction fixed points

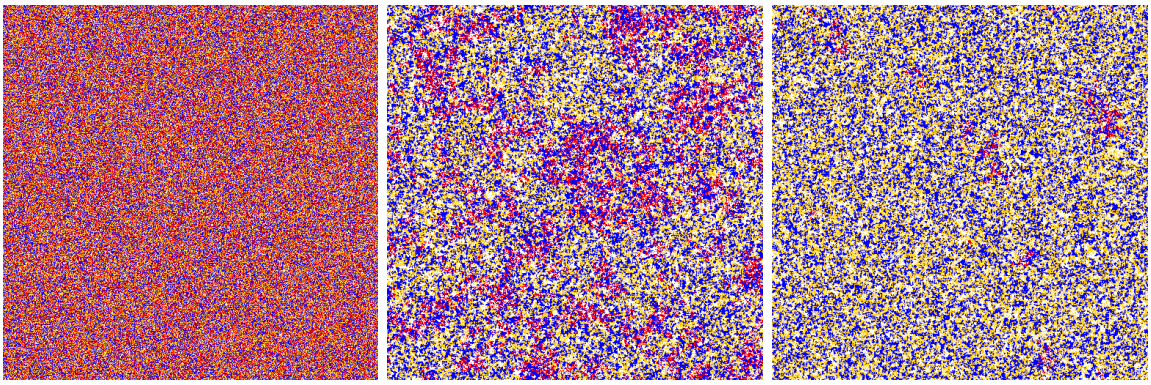

Figure 4.1: Adapted from paper [29] Fig.1. Snapshots of the spatial particle distribution for a single Monte Carlo simulation run of a stochastic predator-predator-prey Lotka–Volterra model on a 512×512 square lattice with periodic boundary conditions at (from left to right) $t = 0$ Monte Carlo Steps (MCS), $t = 10,000$ MCS, and $t = 50,000$ MCS, with predation rates $\lambda_A = 0.5$, $\lambda_B = 0.5$, predator death rates $\mu_A = 0.126$, $\mu_B = 0.125$, and prey reproduction rate $\sigma = 1.0$. Only at most one particle per lattice site is allowed. Predator particles A are indicated in red, predators B in yellow, and prey C in blue, while empty sites are shown in white.

are: (1) $a = b = c = 0$; (2) $a = b = 0$, $c = K$; (3) for $\mu_A < \lambda_A K$: $a = \frac{\sigma(\lambda_A K - \mu_A)}{\lambda_A(\lambda_A K + \sigma)}$, $b = 0$, $c = \mu_A/\lambda_A$; (4) for $\mu_B < \lambda_B K$: $a = 0$, $b = \frac{\sigma(\lambda_B K - \mu_B)}{\lambda_B(\lambda_B K + \sigma)}$, $c = \mu_B/\lambda_B$. When $\mu_A/\lambda_A \neq \mu_B/\lambda_B$, there exists no three-species coexistence state. Yet in the special situation $\mu_A/\lambda_A = \mu_B/\lambda_B$, another line of fixed points emerges: $(\frac{\sigma}{K} + \lambda_A)a + (\frac{\sigma}{K} + \lambda_B)b + \frac{\sigma}{K}c = \sigma$, $c = \mu_A/\lambda_A = \mu_B/\lambda_B$.

4.2.3 Lattice Monte Carlo simulation results

In the stochastic lattice simulations, population densities are defined as the particle numbers for each species divided by the total number of lattice sites (512×512). We prepare the system so that the starting population densities of all three species are the same, here set to around 0.3, i.e., 78643 particles for each species, and the particles are initially randomly distributed on the lattice. The system begins to leave this initial state as soon as the reactions start and the ultimate stationary state is only determined by the reaction rates, independent of the system's initialization. We can test the simulation program by setting the parameters as $\lambda_A = \lambda_B = 0.5$ and $\mu_A = \mu_B = 0.125$. Since species A and B are now exactly the same, they coexist with an equal population density in the final stable state, as indeed observed in the simulations. We increase the value of μ_A by 0.001 so that predator species A is more likely to die than B. Fig. 4.1 shows the spatial distribution of the particles at 0, $10,000$, and $50,000$ Monte Carlo Steps (MCS, from left to right), indicating sites occupied by A particles in red, B in yellow, C in blue, and empty sites in white. As a consequence of the reaction scheme (4.1), specifically the clonal offspring production, surviving particles in effect remain

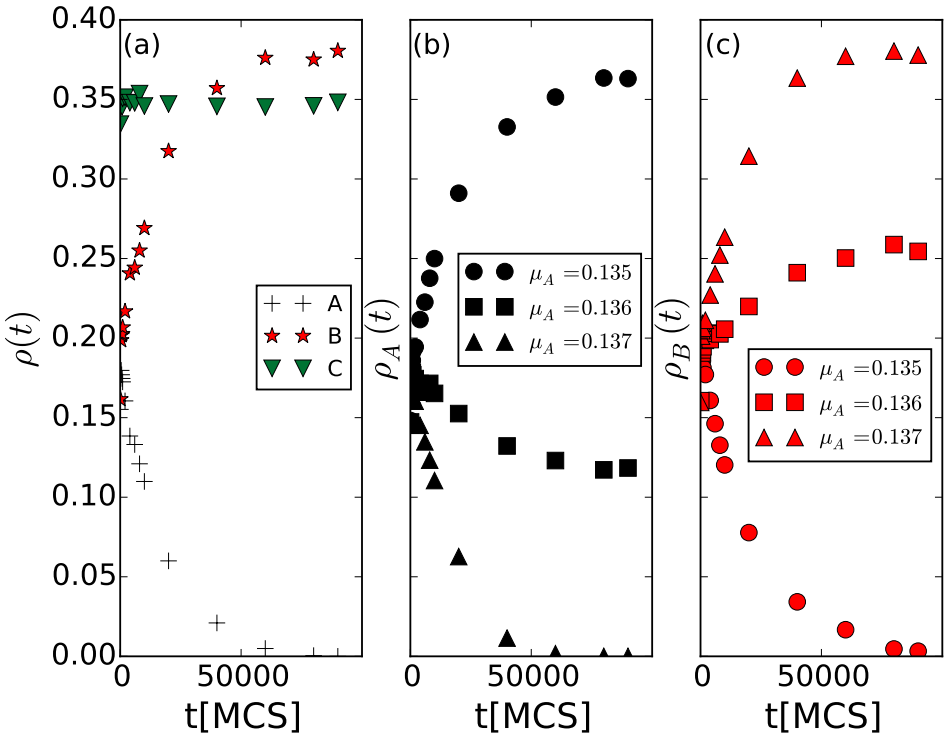

Figure 4.2: Adapted from paper [29] Fig.2. The two predator species cannot coexist in Monte Carlo simulations of the two-predator-one-prey model with fixed reaction rates. (a) Time evolution of the population densities with fixed reaction rates: predation rates $\lambda_A = 0.5$, $\lambda_B = 0.5$, predator death rates $\mu_A = 0.126$, $\mu_B = 0.125$, and prey reproduction rate $\sigma = 1.0$; (b,c) temporal evolution of the population densities $\rho_A(t)$ and $\rho_B(t)$ with fixed $\lambda_A = 0.55$, $\lambda_B = 0.5$, $\mu_B = 0.125$, and μ_A varying from 0.135, 0.136, to 0.137. The curves in (b) and (c) sharing the same markers are from the same (single) simulation runs.

close to other individuals of the same species and thus form clusters. After initiating the simulation runs, one typically observes these clusters to emerge quite quickly; as shown in Fig. 4.1, due to the tiny difference between the death rates $\mu_A - \mu_B > 0$, the 'weaker' predator species A gradually decreases its population number and ultimately goes extinct. Similar behavior is commonly observed also with other sets of parameters: For populations with equal predation rates, only the predator species endowed with a lower spontaneous death rate will survive. Fig. 4.2(a) records the temporal evolution of the three species' population densities. After about $60,000$ MCS, predator species A has reached extinction, while the other two populations eventually approach non-zero constant densities. With larger values of μ_A such as 0.127 or 0.13, species A dies out within a shorter time interval; the extinction time increases with diminishing death rate difference $|\mu_A - \mu_B|$.

In Figs. 4.2(b) and (c), we set $\lambda_A = 0.55$, $\lambda_B = 0.5$, $\mu_B = 0.125$, and various values of $\mu_A > 0.13$. The larger rate λ_A gives species A an advantage over B in the predation process, while the bigger rate μ_A enhances the likelihood of death for A as compared to B. Upon increasing μ_A from 0.135 to 0.137, we observe a phase transition from species B dying out to A going extinct in this situation with competing predation and survival advantages. When μ_A thus exceeds a certain critical value (in this example near 0.136), the disadvantages of high death rates cannot balance the gains due to a more favorable predation efficiency; hence predator species A goes extinct. In general, whenever the reaction rates for predator species A and B are not exactly the same, either A or B will ultimately die out, while the other species remains in the system, coexisting with the prey C. This corresponds to actual biological systems where two kinds of animals share terrain and compete for the same food. Since there is no character displacement occurring within one generation, the weaker species' population will gradually decrease. This trend cannot be turned around unless the organisms improve their capabilities or acquire new skills to gain access to other food sources; either change tends to be accompanied by character displacements [57–60].

In order to quantitatively investigate the characteristic time for the weaker predator species to vanish, we now analyze the relation between the relaxation time t_c of the weaker predator species (A here) and the difference of death rates $|\mu_A - \mu_B|$ under the condition that $\lambda_A = \lambda_B$. Fig. 4.2(a) indicates that prey density (green triangles) reaches its stationary value much faster than the predator populations. When $|\mu_A - \mu_B|$ becomes close to zero, the system returns to a two-species model, wherein the relaxation time of the prey species C is finite. However, the relaxation time of either predator species would diverge because it takes longer for the stronger species to remove the weaker one when they become very similar in their death probabilities. Upon rewriting eqs. (4.2) for $\lambda_A = \lambda_B$ by replacing the prey density $c(t)$ with its stationary value μ_B/λ_B, we obtain a linearized equation for the weaker predator density: $\frac{da(t)}{dt} = -|\mu_A - \mu_B|a(t)$, describing exponential relaxation with decay time $t_c = 1/|\mu_A - \mu_B|$.

We further explore the relation between the decay rate of the weak species population density and the reaction rates through Monte Carlo simulations. Fig. 4.3(a) shows an example of the weaker predator A population density decay for fixed reaction rates $\lambda_A = 0.5$, $\lambda_B = 0.5$, $\mu_A = 0.126$, $\mu_B = 0.125$, and $\sigma = 1.0$, and in the inset also the corresponding Fourier amplitude $f(\omega) = |\int e^{-i\omega t}\, \rho_A(t)\, dt|$ that is calculated by means of the fast Fourier transform algorithm. Assuming an exponential decay of the population density according to $\rho_A(t) \sim e^{-t/t_c}$, we identify the peak half-width at half maximum with the inverse relaxation time $1/t_c$. For other values of $\mu_A > 0.125$, the measured relaxation times t_c for the predator species A are plotted in Fig. 4.3(b). We also ran simulations for various parameter values $\mu_A < 0.125$, for which the predator population B would decrease toward extinction instead of A, and measured the corresponding relaxation time for $\rho_B(t)$, plotted in Fig. 4.3(b) as well. The two curves overlap in the main panel of Fig. 4.3(b), confirming that t_c is indeed a function of $|\mu_A - \mu_B|$ only. The inset of Fig. 4.3(b) demonstrates a power law relationship $t_c \sim |\mu_A - \mu_B|^{-z\nu}$ between the relaxation time and the reaction rate difference, with exponent $z\nu \approx 1.23 \pm 0.01$ as inferred

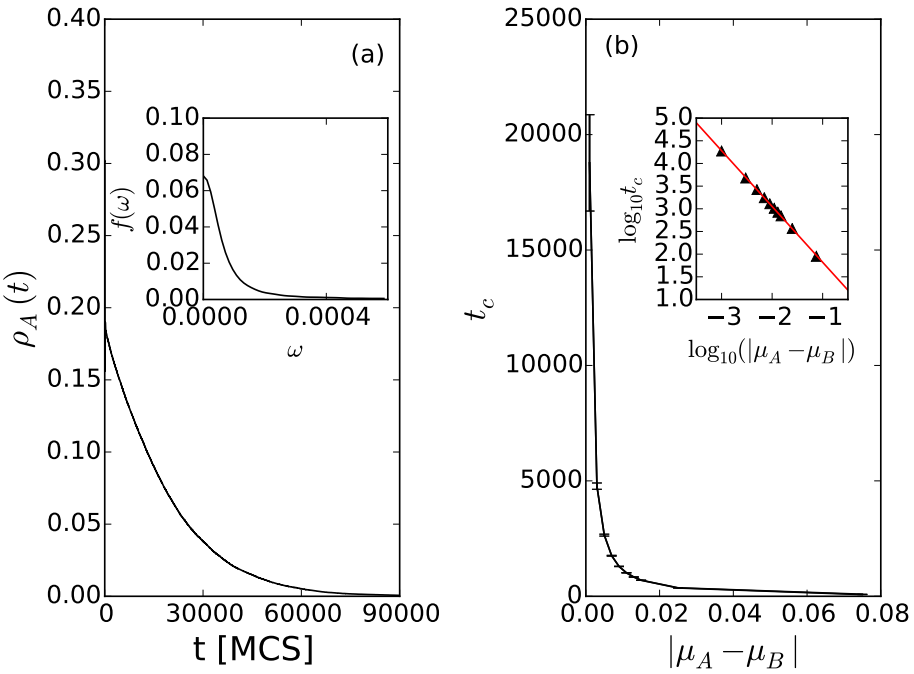

Figure 4.3: Adapted from paper [29] Fig.3. Characteristic decay time of the weaker predator species measured in Monte Carlo simulations of the two-predator-one-prey model with fixed reaction rates. (a) Main panel: temporal evolution of the predator population density $\rho_A(t)$ with predation rates $\lambda_A = 0.5$, $\lambda_B = 0.5$, predator death rates $\mu_A = 0.126$, $\mu_B = 0.125$, and prey reproduction rate $\sigma = 1.0$. Inset: Fourier transform amplitude $f(\omega)$ of the predator density time series $\rho_A(t)$. (b) Main panel: characteristic decay time t_c as obtained from the peak width of $f(\omega)$, versus the death rate difference $|\mu_A - \mu_B|$, with all other reaction rates fixed as in (a). Inset: the black triangles show the data points $\log_{10} t_c$ versus $\log_{10}(|\mu_A - \mu_B|)$, while the red straight line with slope -1.23 ± 0.01 is inferred from linear regression.

from the slope in the double-logarithmic graph via simple linear regression. This value is to be compared with the corresponding exponent $z\nu \approx 1.295 \pm 0.006$ for the directed percolation (DP) universality class [37]. Directed percolation [61] represents a class of models that share identical values of their critical exponents at their phase transition points, and is expected to generically govern the critical properties at non-equilibrium phase transitions that separate active from inactive, absorbing states [21,22]. Our result indicates that the critical properties of the two-predator-one-prey model with fixed reaction rates at the extinction threshold of one predator species appear to also be described by the DP universality class.

As already shown in Fig. 4.1, individuals from each species form clusters in the process of the stochastically occurring reactions (4.2). The correlation lengths ξ, obtained from equal-time correlation functions $C(x)$, characterize the average sizes of these clusters. The definition of the correlation functions between the different species $\alpha, \beta = A, B, C$ is $C_{\alpha\beta}(x) =$

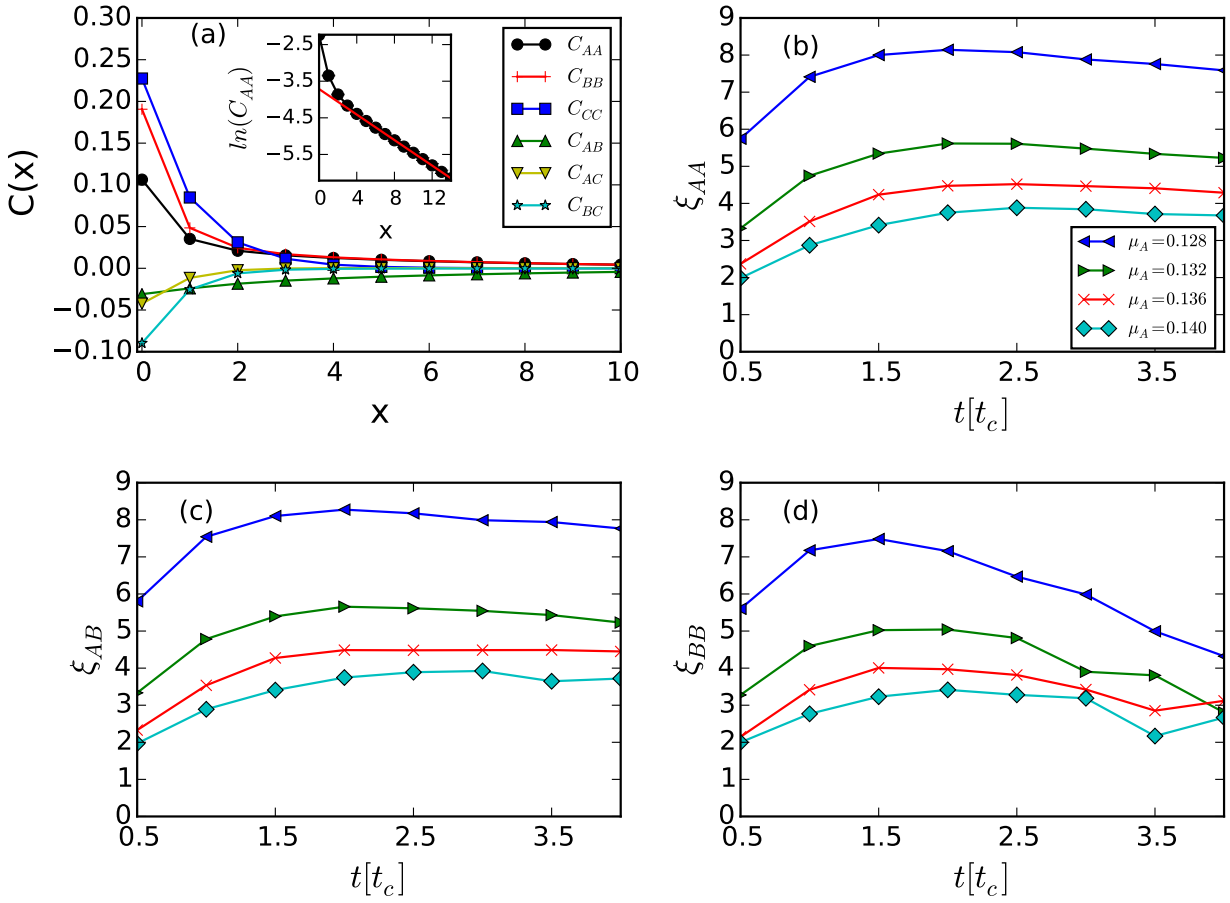

Figure 4.4: Adapted from paper [29] Fig.4. Time evolution for correlation lengths during Monte Carlo simulations of the two-predator-one-prey model with fixed reaction rates. (a) Main panel: correlation functions $C(x)$ after the system has evolved for one half of the relaxation time $0.5t_c \approx 2386$ MCS, with reaction rates $\lambda_A = 0.5$, $\lambda_B = 0.5$, $\mu_A = 0.128$, $\mu_B = 0.125$, and $\sigma = 1.0$. Inset: $\ln(C_{AA})$ with a simple linear regression of the data points with $x \in [4, 14]$ (red straight line) that yields the characteristic correlation decay length $\xi_{AA} \approx 5.8$. (b,c,d) Measured correlation lengths ξ_{AA}, ξ_{AB}, and ξ_{BB} as function of the system evolution time t relative to t_c, with reaction rates as in (a) except $\mu_A = 0.128$ (blue triangles left), 0.132 (green triangles right), 0.136 (red crosses), and 0.140 (cyan diamonds).

$\langle n_\alpha(x)n_\beta(0)\rangle - \langle n_\alpha(x)\rangle\langle n_\beta(0)\rangle$, where $n_\alpha(x) = 0, 1$ denotes the local occupation number of species α at site x. First choosing a lattice site, and then a second site at distance x away, we note that the product $n_\alpha(x)n_\beta(0) = 1$ only if a particle of species β is located on the first site, and a particle of species α on the second site; otherwise the product equals 0. We then average over all sites to obtain $\langle n_\alpha(x)n_\beta(0)\rangle$. $\langle n_\alpha(x)\rangle$ represents the average population density of species α.

In our Monte Carlo simulations we find that although the system has not yet reached stationarity at $0.5\,t_c$, its correlation functions do not vary appreciably during the subsequent time evolution. This is demonstrated in Figs. 4.4(b-d) which show the measured correlation lengths from $0.5\,t_c$ to $3.75\,t_c$, during which time interval the system approaches its quasi-stationary state. The main panel in Fig. 4.4(a) shows the measured correlation functions after the system has evolved for $0.5\,t_c \approx 2386$ MCS, with predator A death rate $\mu_A = 0.128$. Individuals from the same species are evidently spatially correlated, as indicated by the positive values of $C_{\alpha\alpha}$. Particles from different species, on the other hand, display anti-correlations. The inset demonstrates exponential decay: $C_{AA}(x) \sim e^{-|x|/\xi_{AA}}$, where ξ_{AA} is obtained from linear regression of $ln(C_{AA}(x))$. In the same manner, we calculate the correlation length ξ_{AA}, ξ_{BB}, and ξ_{AB} for every $0.5\,t_c$ the system evolves, for different species A death rates $\mu_A = 0.128$, 0.132, 0.136, and 0.140, respectively. Fig. 4.4(b) shows that predator A clusters increase in size by about two lattice constants within $1.5\,t_c$ after the reactions begin, and then stay almost constant. In the meantime, the total population number of species A decreases exponentially as displayed in Fig. 4.3, which indicates that the number of predator A clusters decreases quite fast. Fig. 4.4(c) does not show prominent changes for the values of $\xi_{AB}(t)$ as the reaction time t increases, demonstrating that species A and B maintain a roughly constant distance throughout the simulation. In contrast, Fig. 4.4(d) depicts a significant temporal evolution of $\xi_{BB}(t)$: the values of ξ_{BB} are initially close to those of ξ_{AA}, because of the coevolution of both predator species A and B; after several decay times t_c, however, there are few predator A particles left in the system. The four curves for ξ_{BB} would asymptotically converge after species A has gone fully extinct.

To summarize this chapter, the two indirectly competing predator species cannot coexist in the lattice three-species model with fixed reaction rates. The characteristic time for the weaker predator species to go extinct diverges as its reaction rates approach those of the stronger species. We do not observe large fluctuations of the correlation lengths during the system's time evolution, indicating that spatial structures remain quite stable throughout the Monte Carlo simulation.

4.3 Introducing character displacement

4.3.1 Model description

The Lotka–Volterra model simply treats the individuals in each population as particles endowed with uniform birth, death, and predation rates. This does not reflect a natural environment where organisms from the same species may still vary in predation efficiency and death or reproduction rates because of their size, strength, age, affliction with disease, etc. In order to describe individually varying efficacies, we introduce a new character $\eta \in [0, 1]$, which plays the role of an effective trait that encapsulates the effects of phenotypic changes and behavior on the predation / evasion capabilities, assigned to each individual particle [47]. When a predator A_i (or B_j) and a prey C_k occupy neighboring lattice sites, we set the probability $(\eta_{Ai} + \eta_{Ck})/2$ [or $(\eta_{Bj} + \eta_{Ck})/2$] for C_k to be replaced by an offspring predator A_z (or B_z). The indices i, j, k, and z here indicate specific particles from the predator populations A or B, the prey population C, and the newly created predator offspring in either the A or B population, respectively. In order to confine all reaction probabilities in the range $[0, 1]$, the efficiency η_{Az} (or η_{Bz}) of this new particle is generated from a truncated Gaussian distribution that is centered at its parent particle efficiency η_{Ai} (or η_{Bj}) and restricted to the interval $[0, 1]$, with a certain prescribed distribution width (standard deviation) $\omega_{\eta A}$ (or $\omega_{\eta B}$). When a parent prey individual C_i gives birth to a new offspring particle C_z, the efficiency η_{Cz} is generated through a similar scheme with a given width $\omega_{\eta C}$. Thus any offspring's efficiency entails inheriting its parent's efficacy but with some random mutational adaptation or differentiation. The distribution width ω models the potential range of the evolutionary trait change: for larger ω, an offspring's efficiency is more likely to differ from its parent particle. Note that the width parameters ω here are unique for particles from the same species, but may certainly vary between different species. In previous work, we studied a two-species system (one predator and one prey) with such demographic variability [47, 62]. In that case, the system arrived at a final steady state with stable stationary positive species abundances. On a much faster time scale than the species density relaxation, their respective efficiency η distributions optimized in this evolutionary dynamics, namely: the predators' efficacies rather quickly settled at a distribution centered at values near 1, while the prey efficiencies tended to small values close to 0. This represents a coevolution process wherein the predator population on average gains skill in predation, while simultaneously the prey become more efficient in evasion so as to avoid being killed.

4.3.2 Quasi-species mean-field equations and numerical solution

We aim to construct a mean-field description in terms of quasi-subspecies that are characterized by their predation efficacies η. To this end, we discretize the continuous interval of possible efficiencies $0 \leq \eta \leq 1$ into N bins, with the bin midpoint values $\eta_i = (i + 1/2)/N$,

$i = 0, \ldots, N-1$. We then consider a predator (or prey) particle with an efficacy value in the range $\eta_i - 1/2 \leq \eta \leq \eta_i + 1/2$ to belong to the predator (or prey) subspecies i. The probability that an individual of species A with predation efficiency η_1 produces offspring with efficiency η_2 is assigned by means of a reproduction probability function $f(\eta_1, \eta_2)$. In the binned version, we may use the discretized form $f_{ij} = f(\eta_i, \eta_j)$. Similarly, we have a reproduction probability function g_{ij} for predator species B and h_{ij} for the prey C. Finally, we assign the arithmetic mean $\lambda_{ik} = (\eta_i + \eta_k)/2$ to set the effective predation interaction rate of predator i with prey k [47, 62].

These prescriptions allow us to construct the following coupled mean-field rate equations for the temporal evolution of the subspecies populations:

$$\begin{aligned}
\frac{\partial a_i(t)}{\partial t} &= -\mu a_i(t) + \sum_{jk} \lambda_{kj} f_{ki} a_k(t) c_j(t) \,, \\
\frac{\partial b_i(t)}{\partial t} &= -\mu b_i(t) + \sum_{jk} \lambda_{kj} g_{ki} b_k(t) c_j(t) \,, \\
\frac{\partial c_i(t)}{\partial t} &= \sigma \sum_k h_{ki} c_k(t) \left(1 - \frac{\sum_z [a_z(t) + b_z(t) + c_z(t)]}{K} \right) \\
&\quad - \sum_j \lambda_{ji} a_j(t) c_i(t) - \sum_j \lambda_{ji} b_j(t) c_i(t) \,.
\end{aligned} \tag{4.3}$$

Steady-state solutions are determined by setting the time derivatives to zero, $\partial a_i(t)/\partial t = \partial b_i(t)/\partial t = \partial c_i(t)/\partial t = 0$. Therefore, the steady-state particle counts can always be found by numerically solving the coupled implicit equations

$$\begin{aligned}
\mu a_i &= \sum_{jk} \lambda_{kj} f_{ki} a_k c_j \,, \\
\mu b_i &= \sum_{jk} \lambda_{kj} g_{ki} b_k c_j \,, \\
\sigma \sum_k h_{ki} c_k(t) \left(1 - \frac{\sum_z [a_z(t) + b_z(t) + c_z(t)]}{K} \right) &= \sum_j \lambda_{ji} a_j c_i + \sum_j \lambda_{ji} b_j c_i \,.
\end{aligned} \tag{4.4}$$

In the special case of a uniform inheritance distribution for all three species, $f_{ij} = g_{ij} = h_{ij} = 1/N$, the above equations can be rewritten as

$$\begin{aligned}
\mu(a_i + b_i) &= \frac{1}{N} \sum_{jk} \lambda_{kj} (a_k + b_k) c_j \,, \\
\frac{1}{N} \sigma \sum_k c_k \left(1 - \frac{\sum_z [a_z(t) + b_z(t) + c_z(t)]}{K} \right) &= \sum_j \lambda_{ji} (a_j + b_j) c_i \,,
\end{aligned} \tag{4.5}$$

whose non-zero solutions are

$$\begin{aligned}
&(i) \quad a_i = 0, \quad \frac{b_i}{\sum_j b_j} = \frac{1}{N}\,, \quad \frac{c_i}{\sum_j c_j} = \frac{2}{N \ln 3} \frac{1}{1+2\eta_i}\,; \\
&(ii) \quad b_i = 0, \quad \frac{a_i}{\sum_j a_j} = \frac{1}{N}\,, \quad \frac{c_i}{\sum_j c_j} = \frac{2}{N \ln 3} \frac{1}{1+2\eta_i}\,; \\
&(iii) \quad \frac{a_i + b_i}{\sum_j (a_j + b_j)} = \frac{1}{N}\,, \quad \frac{c_i}{\sum_j c_j} = \frac{2}{N \ln 3} \frac{1}{1+2\eta_i}\,.
\end{aligned} \tag{4.6}$$

We could not obtain the full time-dependent solutions to the mean-field equations in closed form. We therefore employed an explicit fourth-order Runge–Kutta scheme to numerically solve eqs. (4.3), using a time step of $\Delta t = 0.1$, the initial condition $a_i(t = 0) = b_i(t = 0) = c_i(t = 0) = 1/(3N)$ for $i = 1, ..., N$, a number of subspecies $N = 100$, and the carrying capacity $K = 1$. An example for the resulting time evolution of the predator B density is shown in Fig. 4.5(b); its caption provides the remaining parameter values.

4.3.3 Lattice simulation

We now proceed to Monte Carlo simulations for this system on a two-dimensional square lattice, and first study the case where trait evolution is solely introduced to the predation efficiencies η. In these simulation, the values of μ and σ are held fixed, as is the nonzero distribution width ω, so that an offspring's efficiency usually differs from its parent particle. In accord with the numerical solutions for the mean-field equations (4.3), we find that the three-species system (predators A and B, prey C) is generically unstable and will evolve into a final two-species steady state, where one of the predator species goes extinct, depending only on the value of ω (given that μ and σ are fixed).

At the beginning of the simulation runs, the initial population densities, which are the particle numbers of each species divided by the lattice site number, are assigned the same value 0.3 for all the three species. The particles are randomly distributed on the lattice sites. We have checked that the initial conditions do not influence the final state by varying the initial population densities and efficiencies. We fix the predator death rate to $\mu = 0.125$ for both species A and B, and set the prey reproduction rate as $\sigma = 1.0$. The predation efficacies for all particles are initialized at $\eta = 0.5$. We have varied the values of the distribution width ω and observed the final (quasi-)steady states. For the purpose of simplification, we fix $\omega_{\eta A} = \omega_{\sigma C} = 0.1$, and compare the final states when various values of $\omega_{\eta B}$ are assigned.

Fig. 4.5(a) shows the population density $\rho_B(t)$ of predator species B with the listed values for $\omega_{\eta B}$. Each curve depicts a single simulation run. When $\omega_{\eta B} > 0.1$, the $\rho_B(t)$ quickly tends to zero; following the extinction of the B species, the system reduces to a stable A-C two-species predator-prey ecology. When $\omega_{\eta B} = 0.1$, there is no difference between species A and B, so both populations survive with identical final population density; for $\omega_{\eta B} = 0.01, 0.05$, predator species A finally dies out and the system is reduced to a B-C two-species system; we

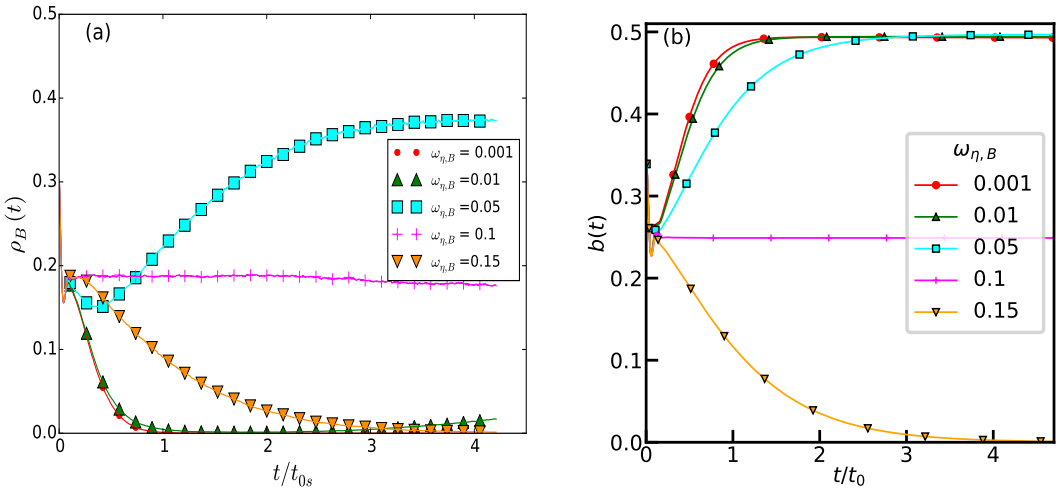

Figure 4.5: Copied from paper [29] Fig.5. (a) Stochastic lattice simulation of the two-predator-one-prey model with "Darwinian" evolution only introduced to predation efficiency η. Population density $\rho_B(t)$ with various values of efficiency distribution width $\omega_{\eta B} = 0.001$ (red dot), 0.01 (green triangle up), 0.05 (blue square), 0.1 (pink plus), 0.15 (orange triangle down) while all the other reaction rates are fixed as $\mu = 0.125$, $\sigma = 1.0$ and $\omega_{\eta A} = \omega_{\eta C} = 0.1$. Time t is rescaled with the relaxation time $t_{0s} = 1900$ MCS of the blue-square curve ($\omega_{\eta B} = 0.05$). (b) Numerical solution of the mean-field eqs. (4.3) with $b(t) = \frac{1}{N}\sum_i b_i(t)$ denoting the average subspecies density. The parameters are set at the same values as for the lattice simulations. Time t is normalized with the relaxation time $t_0 = 204.32$ of the $\omega_{\eta B} = 0.05$ curve. Note that the limited carrying capacity in both lattice simulations and the mean-field model introduces damping which suppresses the characteristic LV oscillations.

remark that the curve for $\omega_{\eta B} = 0.01$ (green triangles up) decreases first and then increases again at very late time points which is only partially shown in the graph. For $\omega_{\eta B} = 0.001$ and even smaller, $\rho_B(t)$ goes to zero quickly, ultimately leaving an A-C two-species system. We tried another 100 independent runs and obtained the same results: for $\omega_{\eta B} \neq \omega_{\eta A}$, one of the predator species will vanish and the remaining one coexists with the prey C. When $\omega_{\eta B}$ is smaller than $\omega_{\eta A}$ but not too close to zero, predator species B prevails, while A goes extinct. For $\omega_{\eta B} = 0$, there is of course no evolution for these predators at all, thus species A will eventually outlast B. Thus there exists a critical value ω_{Bc} for the predation efficacy distribution width $\omega_{\eta B}$, at which the probability of either predator species A or B to win the 'survival game' is 50%. When $\omega_{Bc} < \omega_{\eta B} < \omega_{\eta A}$, B has an advantage over A, i.e., the survival probability of B is larger than 50%; conversely, for $\omega_{Bc} > \omega_{\eta B}$, species A outcompetes B. This means that the evolutionary 'speed' is important in a finite system, and is determined by the species plasticity ω.

Fig. 4.5(b) shows the numerical solution of the associated mean-field model defined by

eqs. (4.3). In contrast to the lattice simulations, small $\omega_{\eta B}$ do not yield extinction of species B; this supports the notion that the reentrant phase transition from B to A survival at very small values of $\omega_{\eta B}$ is probably a finite-size effect, as discussed below. Because of the non-zero carrying capacity, oscillations of population densities are largely suppressed in both Monte Carlo simulations and the mean-field model. Spatio-temporal correlations in the stochastic lattice system rescale the reaction rates, and induce a slight difference between the steady-state population densities in Figs. 4.5(a) and (b) even though the microscopic rate parameters are set to identical values. For example, for $\omega_{\eta B} = 0.1$, the quasi-stationary population density of predator species B is ≈ 0.19 (pink plus symbols) in the lattice model, but reaches 0.25 in the numerical solution of the mean-field rate equations. Time t is measured in units of Monte Carlo Steps (MCS) in the simulation; there is no method to directly convert this (discrete) Monte Carlo time to the continuous time in the mean-field model. For the purpose of comparing the decay of population densities, we therefore normalize time t by the associated relaxation times $t_{0s} = 1900$ MCS in the simulations and $t_0 = 204.32$ in the numerical mean-field solution; both are calculated by performing a Fourier transform of the time-dependent prey densities $\rho_B(t)$ and $b(t)$ for $\omega_{\eta B} = 0.05$ (blue squares).

Our method to estimate ω_{Bc} was to scan the value space of $\omega_{\eta B} \in [0, 1]$, and perform 1000 independent simulation runs for each value until we found the location in this interval where the survival probability for either A or B predator species was 50%. With the simulations on a 512×512 system and all the parameters set as mentioned above, ω_{Bc} was measured to be close to 0.008. We repeated these measurements for various linear system sizes L in the range $[128, 2048]$. Fig. 4.6(a) shows ω_{Bc} as a function of $1/L$, indicating that ω_{Bc} decreases with a divergent rate as the system is enlarged. Because of limited computational resources, we were unable to extend these results to even larger systems. According to the double-logarithmic analysis shown in Fig. 4.6(b), we presume that ω_{Bc} would fit a power law $\omega_{Bc} \sim L^{-\theta}$ with exponent $\theta = 0.2$. This analysis suggests that $\omega_{Bc} = 0$ in an infinitely large system, and that the reentrant transition from B survival to A survival in the range $\omega_{\eta B} \in [0, \omega_{\eta A}]$ is likely a finite-size effect. We furthermore conclude that in the three-species system (two predators and a single prey) the predator species with a smaller value of the efficiency distribution width ω always outlives the other one. A smaller ω means that the offspring's efficiency is more centralized at its parent's efficacy; mutations and adaptations have smaller effects. Evolution may thus optimize the overall population efficiency to higher values and render this predator species stronger than the other one with larger ω, which is subject to more, probably deleterious, mutations. These results were all obtained from the measurements with $\omega_{\eta A} = 0.1$. However, other values of $\omega_{\eta A}$ including 0.2, 0.3, and 0.4 were tested as well, and similar results observed.

Our numerical observation that two predator species cannot coexist raises the challenge to explain multi-species coexistence in a system where two related predator species compete for the same food resource. Notice that 'Darwinian' evolution was only applied to the predation efficiency in our model. However, natural selection could also cause lower predator death rates and increased prey reproduction rates so that their survival chances would be

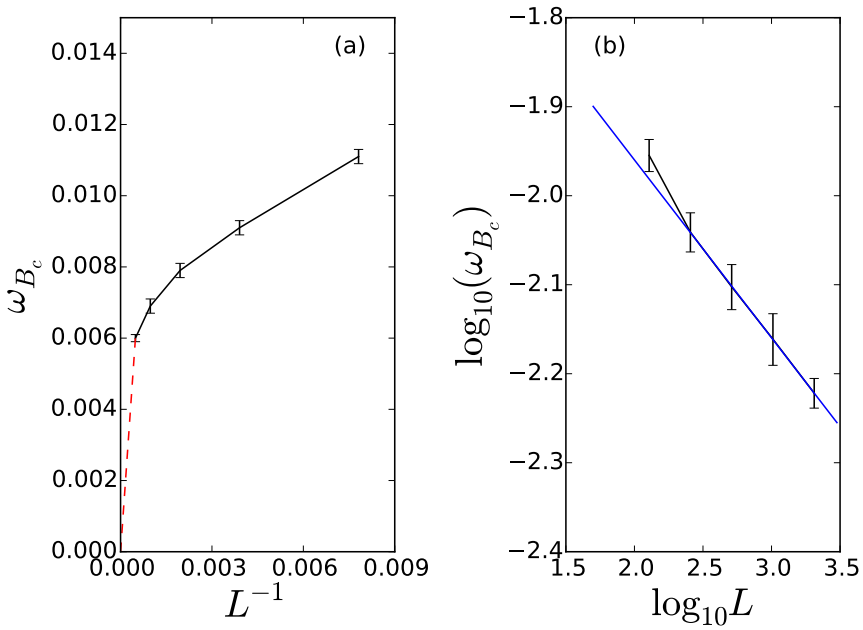

Figure 4.6: Adapted from paper [29] Fig.6. (a) Stochastic lattice simulation of the two-predator-one-prey model with "Darwinian" evolution only introduced to predation efficiency η: Critical distribution width ω_{Bc} as a function of 1/L, where L is the linear system size, with predator death rate $\mu = 0.125$, prey reproduction rate $\sigma = 1.0$, and $\omega_{\eta A} = 0.1$. The data are obtained with $L \in [128, 256, 512, 1024, 2048]$. (b) Double-logarithmic plot of the critical width ω_{Bc} as a function of system size L; the blue straight line is a simple linear regression of the 4 points with $L \in [256, 512, 1024, 2048]$ and the slope is -0.2. The point with $L = 128$ does not fall on the straight line because of additional finite-size effects.

enhanced in the natural selection competition. One ecological example are island lizards that benefit from decreased body size because large individuals will attract attacks from their competitors [26]. In the following, we adjust our model so that the other two reaction rates μ and σ do not stay fixed anymore, but instead evolve by following the same mechanism as previously implemented for the predation efficacies η. The death rate of an offspring predator particle is hence generated from a truncated Gaussian distribution centered at its parent's value, with positive standard deviations $\omega_{\mu A}$ and $\omega_{\mu B}$ for species A and B, respectively. The (truncated) Gaussian distribution width for the prey reproduction rate is likewise set to a non-zero value ω_σ.

In the simulations, the initial population densities for all three species are set at 0.3 with the particles randomly distributed on the lattice. The reaction rates and efficiencies for these first-generation individuals were chosen as $\eta_{A0} = \eta_{B0} = \eta_{C0} = 0.5$, $\mu_{A0} = \mu_{B0} = 0.125$, and $\sigma_0 = 1.0$. With this same initial set, we ran simulations with different values of the Gaussian distribution widths ω. Fig. 4.7 displays the temporal evolution of the three species'

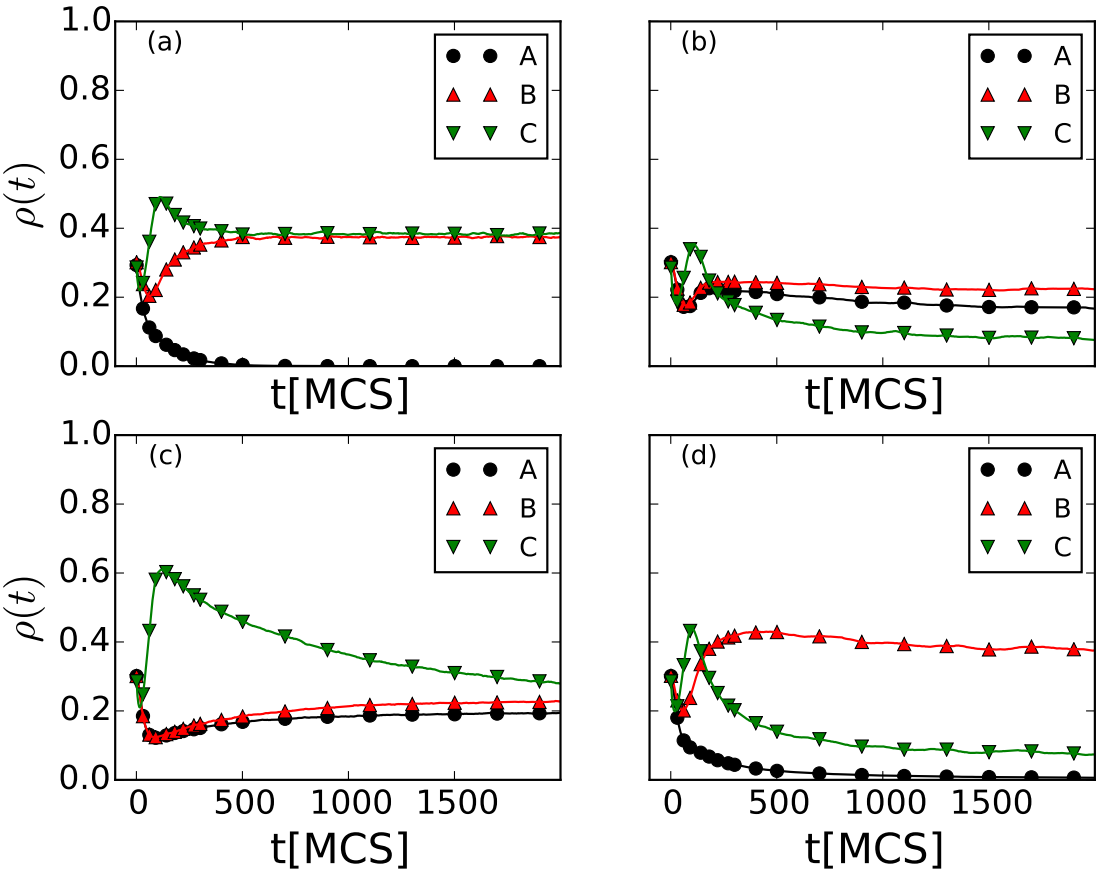

Figure 4.7: Adapted from paper [29] Fig.7. Population densities $\rho(t)$ from Monte Carlo simulations with "Darwinian" evolution introduced to both the predation efficiency η and predator death rate μ, while the prey reproduction rate is fixed at $\sigma = 1.0$. The species are indicated as blue dots for A, red squares for B and green triangles for C. The final states are A dying out; coexistence; coexistence; and B dying out from graph (a) to (d) with $\omega_{\eta A} = 0.11$, $\omega_{\mu A} = 0.3$, $\omega_{\mu B} = 0.125$ in (a), $\omega_{\eta A} = 0.08$, $\omega_{\mu A} = 0.1$, $\omega_{\mu B} = 0.09$ in (b), $\omega_{\eta A} = 0.08$, $\omega_{\mu A} = 0.4$, $\omega_{\mu B} = 0.39$ in (c) and $\omega_{\eta A} = 0.08$, $\omega_{\mu A} = 0.4$, $\omega_{\mu B} = 0.09$ in (d), while $\omega_{\eta B} = 0.1$, $\omega_{\eta C} = 0.1$, $\omega_{\sigma C} = 0$ for all four plots.

population densities with four sets of given widths ω: In Fig. 4.7(a), $\omega_{\eta A} = 0.11$, $\omega_{\eta B} = 0.1$, $\omega_{\eta C} = 0.1$, $\omega_{\mu A} = 0.3$, $\omega_{\mu B} = 0.125$, and $\omega_{\sigma C} = 0$. Since a smaller width ω gives advantages to the corresponding species, $\omega_{\eta B} < \omega_{\eta A}$ and $\omega_{\mu B} < \omega_{\mu A}$ render predators B stronger than A in general. As the graph shows, species A dies out quickly and finally only B and C remain in the system. In all four cases, the prey C stay active and do not become extinct.

However, it is not common that a species is stronger than others in every aspect, so we next set ω so that A has advantages over B in predation, i.e., $\omega_{\eta A} < \omega_{\eta B}$, but is disadvantaged through broader-distributed death rates $\omega_{\mu A} > \omega_{\mu B}$. In Fig. 4.7(b), $\omega_{\eta A} = 0.08$, $\omega_{\eta B} = 0.1$, $\omega_{\eta C} = 0.1$, $\omega_{\mu A} = 0.1$, $\omega_{\mu B} = 0.09$, and $\omega_{\sigma C} = 0$; in Fig. 4.7(c), $\omega_{\eta A} = 0.08$, $\omega_{\eta B} = 0.1$, $\omega_{\eta C} = 0.1$, $\omega_{\mu A} = 0.4$, $\omega_{\mu B} = 0.39$, and $\omega_{\sigma C} = 0$. In either case, none of the three species becomes extinct, and three-species coexistence will persist at least for 10 000 MCS. Monitoring the system's activity, we see that the system remains in a dynamic state with a large amount of reactions happening. When we repeat the measurements with other independent runs, similar results are observed, and we find the slow decay of the population densities to be rather insensitive to the specific values of the widths ω. As long as we implement a smaller width ω for the A predation efficiency than for the B species, but a larger one for its death rates, or vice versa, three-species coexistence emerges. Of course, when the values of the standard deviations ω differ too much between the two predator species, one of them may still approach extinction fast. One example is shown in Fig. 4.7(d), where $\omega_{\eta A} = 0.08$, $\omega_{\eta B} = 0.1$, $\omega_{\eta C} = 0.1$, $\omega_{\mu A} = 0.4$, $\omega_{\mu B} = 0.09$, and $\omega_{\sigma C} = 0$; since $\omega_{\mu A}$ is about five times larger than $\omega_{\mu B}$ here, the predation advantage of species A cannot balance its death rate disadvantage, and consequently species A is driven to extinction quickly. Yet the coexistence of all three competing species in Figs. 4.7(b) and (c) does not persist forever, and at least one species will die out eventually, after an extremely long time. Within an intermediate time period, which still amounts to thousands of generations, they can be regarded as quasi-stable because the decay is very slow. This may support the idea that in real ecosystems perhaps no truly stable multiple-species coexistence exists, and instead the competing species are in fact under slow decay which is not noticeable within much shorter time intervals. In Figs. 4.7(a) and (d), the predator A population densities decay exponentially with relaxation times of order 100 MCS, while the corresponding curves in (b) and (c) approximately follow algebraic functions (power law decay).

However, we note that in the above model implementation the range of predator death rates μ was the entire interval $[0, 1]$, which gives some individuals a very low chance to decay. Hence these particles will stay in the system for a long time, which accounts for the long-lived transient two-predator coexistence regime. To verify this assumption, we set a positive lower bound on the predators' death rates, preventing the presence of near-immortal individuals. We chose the value of the lower bound to be 0.001, with the death rates μ for either predator species generated in the predation and reproduction processes having to exceed this value. Indeed, we observed no stable three-species coexistence state, i.e., one of the predator species was invariably driven to extinction, independent of the values of the widths ω, provided they were not exactly the same for the two predator species. To conclude, upon introducing

a lower bound for their death rates, the two predator species cannot coexist despite their dynamical evolutionary optimization.

4.4 Effects of direct competition between predator species

4.4.1 Inclusion of direct predator competition and mean-field analysis

We proceed to include explicit direct competition between both predator species in our model. The efficiencies of predator particles are most likely to be different since they are randomly generated from truncated Gaussian distributions. When a strong A individual (i.e., with a large predation efficacy η) meets a weaker B particle on an adjacent lattice site, or vice versa, we now allow predation between both predators to occur. Direct competition is common within predator species in nature. For example, a strong lizard may attack and even kill a small lizard to occupy its habitat. A lion may kill a wolf, but an adult wolf might kill an infant lion. Even though cannibalism occurs in nature as well, we here only consider direct competition and predation between different predator species. In our model, direct competition between the predator species is implemented as follows: For a pair of predators A_i and B_j located on neighboring lattice sites and endowed with respective predation efficiencies η_{Ai} and $\eta_{Bj} < \eta_{Ai}$, particle B_j is replaced by a new A particle A_z with probability $\eta_{Ai} - \eta_{Bj}$; conversely, if $\eta_{Ai} < \eta_{Bj}$, there is a probability $\eta_{Bj} - \eta_{Ai}$ that A_i is replaced by a new particle B_z.

We first write down and analyze the mean-field rate equations for the simpler case when the predator species compete directly without evolution, i.e., all reaction rates are uniform and constant. We assume that A is the stronger predator with $\lambda_A > \lambda_B$, hence only the reaction $A + B \to A + A$ is allowed to take place with rate $\lambda_A - \lambda_B$, but not its complement, supplementing the original reaction scheme listed in (4.1). The associated mean-field rate equations read

$$\begin{aligned}
\frac{da(t)}{dt} &= -\mu_A a(t) + \lambda_A a(t)c(t) + (\lambda_A - \lambda_B)a(t)b(t)\,, \\
\frac{db(t)}{dt} &= -\mu_B b(t) + \lambda_B b(t)c(t) - (\lambda_A - \lambda_B)a(t)b(t)\,, \\
\frac{dc(t)}{dt} &= \sigma c(t)\left[1 - \frac{a(t)+b(t)+c(t)}{K}\right] - \lambda_A a(t)c(t) - \lambda_B b(t)c(t)\,,
\end{aligned} \tag{4.7}$$

with the non-zero stationary solutions

$$\begin{aligned}
(i) \quad & a = 0\,, \quad b = \frac{\sigma(K\lambda_B - \mu_B)}{\lambda_B(\sigma + K\lambda_B)}\,, \quad c = \frac{\mu_B}{\lambda_B}\,, \\
(ii) \quad & a = \frac{\sigma(K\lambda_A - \mu_A)}{\lambda_A(\sigma + K\lambda_A)}\,, \quad b = 0\,, \quad c = \frac{\mu_A}{\lambda_A}\,, \\
(iii) \quad & a + b + c = \frac{\mu_A - \mu_B}{\lambda_A - \lambda_B}\,, \quad \text{when} \quad a(0) + b(0) + c(0) = \frac{\mu_A - \mu_B}{\lambda_A - \lambda_B}\,.
\end{aligned} \tag{4.8}$$

Within this mean-field theory, three-species coexistence states exist only when the total initial population density is set to $a(0) + b(0) + c(0) = \frac{\mu_A - \mu_B}{\lambda_A - \lambda_B}$. In our lattice simulations, however, we could not observe any three-species coexistence state even when we carefully tuned one reaction rate with all others held fixed.

Next we reinstate 'Darwinian' evolution for this extended model with direct competition between the predator species. We utilize the function $\hat{\lambda}_{ij} = |\eta_i - \eta_j|$ to define the reaction rate between predators A and B. For the case that the predator death rate μ is fixed for both species A and B, the ensuing quasi-subspecies mean-field equations are

$$\begin{aligned}
\frac{\partial a_i(t)}{\partial t} &= -\mu a_i(t) + \sum_{jk} \lambda_{kj} f_{ki} a_k(t) c_j(t) + \sum_{j<k} \hat{\lambda}_{kj} f_{ki} a_k(t) b_j(t) \\
&\quad - \sum_{j>i} \hat{\lambda}_{ij} a_i(t) b_j(t)\,, \\
\frac{\partial b_i(t)}{\partial t} &= -\mu b_i(t) + \sum_{jk} \lambda_{kj} g_{ki} b_k(t) c_j(t) + \sum_{j<k} \hat{\lambda}_{kj} g_{ki} b_k(t) a_j(t) \\
&\quad - \sum_{j>i} \hat{\lambda}_{ji} b_i(t) a_j(t) \\
\frac{\partial c_i(t)}{\partial t} &= \sigma \sum_j h_{ji} c_j(t) \left(1 - \frac{\sum_z [a_z(t) + b_z(t) + c_z(t)]}{K} \right) \\
&\quad - \sum_j \lambda_{ji} [a_j(t) + b_j(t)] c_i(t)\,.
\end{aligned} \tag{4.9}$$

Since a closed set of solutions for eqs. (4.9) is very difficult to obtain, we resort to numerical integration. As before, we rely on an explicit fourth-order Runge–Kutta scheme with time step $\Delta t = 0.1$, initial conditions $a_i(t = 0) = b_i(t = 0) = c_i(t = 0) = 1/N$, number of subspecies $N = 100$, and carrying capacity $K = 3$. Four examples for such numerical solutions of the quasi-subspecies mean-field equations are shown in Fig. 4.8, and will be discussed in the following subsection.

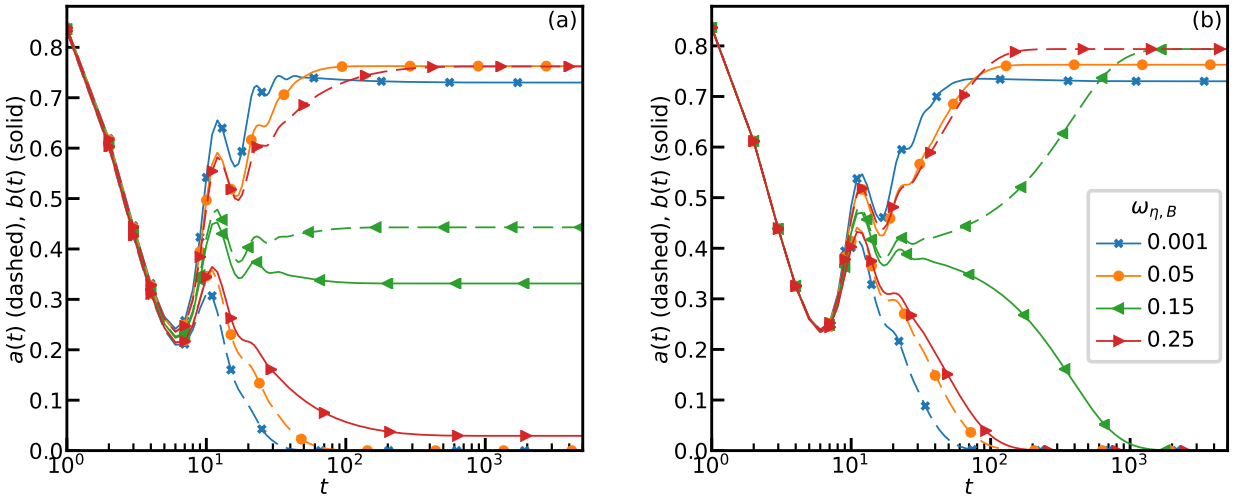

Figure 4.8: Copied from paper [29] Fig.8. Numerical solutions to eqs. (4.9) of the two-predator subspecies densities $a(t) = \frac{1}{N}\sum_i a_i(t)$ (dashed lines) and $b(t) = \frac{1}{N}\sum_i b_i(t)$ (solid lines) for different $\omega_{\eta,B}$ and the parameters $\omega_{\eta,A} = 0.14$, $\omega_{\eta,C} = \infty$, $\sigma = 1$, and $\mu = 0.5$. (a) Population densities in the presence of predator-predator competition and (b) in the absence of competition. Note that coexistence is only possible in the presence of direct predator-predator competition.

4.4.2 The quasi-stable three-species coexistence region

For the three-species system with two predators A, B and prey C, we now introduce 'Darwinian' evolution to both the predator death rates μ and the predation efficiencies η. In addition, we implement direct competition between the predators A and B. We set the lower bound of the death rates μ to 0.001 for both predator species. The simulations are performed on a 512×512 square lattice with periodic boundary conditions. Initially, individuals from all three species are randomly distributed in the system with equal densities 0.3. Their initial efficiencies are chosen as $\eta_A = 0.5 = \eta_B$ and $\eta_C = 0$. Since there is no evolution of the prey efficiency, η_C will stay zero throughout the simulation. The distribution widths for the predation efficiencies are fixed to $\omega_{\eta A} = 0.1$ and $\omega_{\eta B} = 0.15$, giving species A an advantage over B in the non-linear predation process. We select the width of the death rate distribution of species B as $\omega_{\mu B} = 0.1$. If $\omega_{\mu A}$ is also chosen to be 0.1, the B population density would decay exponentially. $\omega_{\mu A} > \omega_{\mu B} = 0.1$ is required to balance species A's predation adaptation advantage so that stable coexistence is possible. Fig. 4.9 shows the population densities resulting from our individual-based Monte Carlo simulations as a function of time, for different values $\omega_{\mu A} = 0.132$, 0.140, and 0.160. These graphs indicate the existence of phase transitions from species B extinction in Fig. 4.9(a) to predator A-B coexistence in Fig. 4.9(b), and finally to A extinction in Fig. 4.9(c)). In Fig. 4.9(a), species A is on average more efficient than B in predation, but has higher death rates. Predator species B is in general the weaker one, and hence goes extinct after about 100 000 MCS.

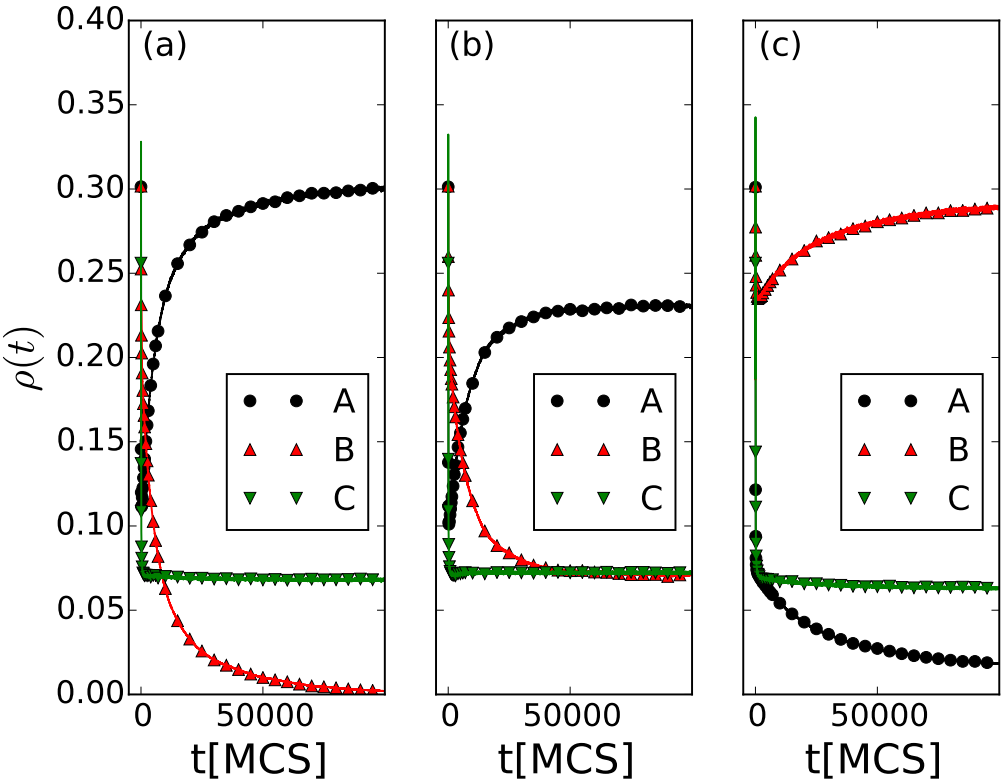

Figure 4.9: Adapted from paper [29] Fig.9. Data obtained from Monte Carlo simulations with direct competition between predator species, as well as evolutionary dynamics introduced: Temporal record of population densities with $\omega_{\eta A} = 0.1$, $\omega_{\eta B} = 0.15$, $\omega_{\mu B} = 0.1$ and $\omega_{\mu A} = 0.132, 0.140, 0.160$ from left to right with species indicated as A in black dots, B in red triangles up, and C green triangles down.

Fig. 4.9(b) shows a (quasi-)stable coexistence state with neither predator species dying out within our simulation time. In Fig. 4.9(c), $\omega_{\mu A}$ is set so high that A particles die much faster than B individuals, so that finally species A would vanish entirely.

Fig. 4.8(a) displays the time evolution for the solutions of the corresponding quasi-subspecies mean-field model (4.9) for four different values of the species B efficiency width $\omega_{\eta,B}$. In particular, it shows that there is a region of coexistence in which both predator species reach a finite steady-state density, supporting the Monte Carlo results from the stochastic lattice model. In contrast, numerical solutions of eqs. (4.9) with $\hat{\lambda}_{ij} = 0$, equivalent to eqs. (4.3), exhibit no three-species coexistence region; see Fig. 4.8(b).

At an active-to-absorbing phase transition threshold, one should anticipate the standard critical dynamics phenomenology for a continuous phase transition: exponential relaxation with time becomes replaced by much slower algebraic decay of the population density [21,22].

We determine the three-species coexistence range for our otherwise fixed parameter set to be in the range $\omega_{\mu A} \in [0.136, 0.159]$. Fig. 4.10(a) shows an exponential decay of the predator population A density with $\omega_{\mu A} = 0.2$, deep in the absorbing extinction phase. The system would attain B-C two-species coexistence within of the order 10^4 MCS. We also ran the Monte Carlo simulation with $\omega_{\mu A} = 0.1$, also inside an absorbing region, but now with species B going extinct, and observed exponential decay of $\rho_B(t)$. By changing the value of $\omega_{\mu A}$ to 0.136 as plotted in Fig. 4.10(b), $\rho_B(t) \sim t^{-\alpha_B}$ fits a power law decay with critical exponent $\alpha_B = 1.22$. Since it would take infinite time for ρ_B to reach zero while species A and C densities remain finite during the entire simulation time, the system at this point already resides at the threshold of three-species coexistence. Upon increasing $\omega_{\mu A}$ further, all three species densities would reach their asymptotic constant steady-state values within a finite time and then remain essentially constant (with small statistical fluctuations). At the other boundary of this three-species coexistence region, $\omega_{\mu A} = 0.159$, the decay of $\rho_A(t)$ also fits a power law as depicted in Fig. 4.10(c), and $\rho_B(t)$ would asymptotically reach a positive value. However, the critical power law exponent is in this case estimated to be $\alpha_A = 0.76$. We do not currently have an explanation for the distinct values observed for the decay exponents α_A and α_B, neither of which are in fact close to the corresponding directed-percolation value $\alpha = 0.45$ [36]. If we increase $\omega_{\mu A}$ even more, species A would die out quickly and the system subsequently reduce to a B-C two-species predator-prey coexistence state. We remark that the critical slowing-down of the population density at either of the two thresholds as well as the associated critical aging scaling may serve as a warning signal of species extinction [20, 35].

It is of interest to study the spatial properties of the particle distribution. We choose $\omega_{\mu A} = 0.147$ so that the system resides deep in the three-species coexistence region according to Fig. 4.10. The correlation functions are measured after the system has evolved for 10 000 MCS as shown in the main plot of Fig. 4.11. The results are similar to those in the previous sections in the sense that particles are positively correlated with the ones from the same species, but anti-correlated to individuals from other species. The correlation functions for both predator species are very similar: $C_{AA}(x)$ and $C_{BB}(x)$ overlap each other for $x \geq 5$, and C_{AC} and C_{BC} coincide for $x \geq 2$ lattice sites. The inset displays the measured characteristic correlation length as functions of simulation time, each of which varies on the scale of $\sim$ 0.1 during 70 000 MCS, indicating that the species clusters maintain nearly constant sizes and keep their respective distances almost unchanged throughout the simulations. The correlation lengths ξ_{AA} and ξ_{BB} are very close and differ only by less than 0.2 lattice sites. These data help to us to visualize the spatial distribution of the predators: The individuals of both A and B species arrange themselves in clusters with very similar sizes throughout the simulation, and their distances to prey clusters are almost the same as well. Hence predator species A and B are almost indistinguishable in their spatial distribution.

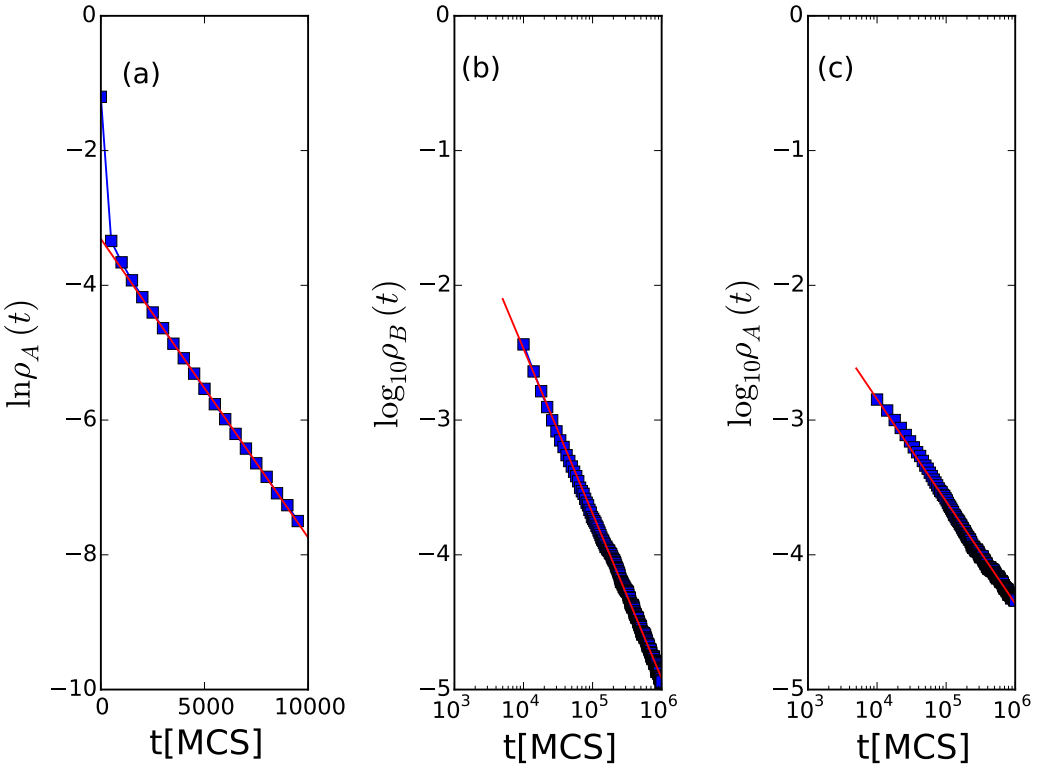

Figure 4.10: Adapted from paper [29] Fig.10. Monte Carlo simulations with direct predator competition: (a) Exponential decay of the population density $\rho_A(t)$ with $\omega_{\mu A} = 0.2$, $\omega_{\eta A} = 0.1$, $\omega_{\eta B} = 0.15$, and $\omega_{\mu B} = 0.1$, while the red straight is obtained from a linear regression of the data points for $x \geq 2000$, with slope -0.00044. (b) Algebraic decay of the species density of B with $\omega_{\mu A} = 0.136$ and the other parameters same as in (a); (c) Power-law decay of $\rho_A(t)$ when $\omega_{\mu A} = 0.159$. The blue squares are measured population densities from the simulations, while the red straight lines indicate simple linear regressions of the simulation data.

4.4.3 Monte Carlo simulation results in a zero-dimensional system

The above simulations were performed on a two-dimensional system by locating the particles on the sites of a square lattice. Randomly picked particles are allowed to react (predation, reproduction) with their nearest neighbors. Spatial as well as temporal correlations are thus incorporated in the reaction processes. In this subsection, we wish to compare our results with a system for which spatial correlations are absent, yet which still displays manifest temporal correlations. To simulate this situation, we remove the nearest-neighbor restriction and instead posit all particles in a 'zero-dimensional' space. In the resulting 'urn' model, the simulation algorithm entails to randomly pick two particles and let them react with a probability determined by their individual character values. We find that if all the particles

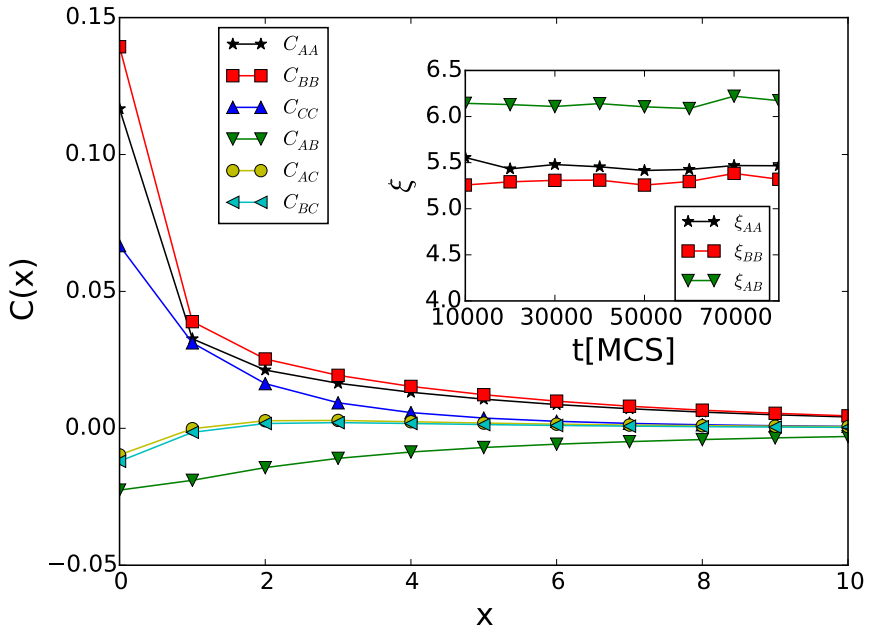

Figure 4.11: Adapted from paper [29] Fig.11. Monte Carlo simulations with direct predator competition: Main panel: Quasi-stationary correlation functions $C(x)$ after the system has evolved for 10 000 MCS with $\omega_{\mu A} = 0.147$, $\omega_{\eta A} = 0.1$, $\omega_{\eta B} = 0.15$, and $\omega_{\mu B} = 0.1$, when the system resides in the coexistence state. Inset: temporal evolution of the correlation length $\xi(t)$; all lengths are measured in units of the square lattice spacing.

from a single species are endowed with homogeneous properties, i.e., the reaction rates are fixed uniform as in section 4.2, no three-species coexistence state is ever observed. If evolution is added without direct competition between predator species as in section 4.3, the coexistence state does not exist neither. Our observation is again that coexistence occurs only when both evolution and direct competition are introduced. Qualitatively, therefore, we obtain the same scenarios as in the two-dimensional spatially extended system. The zero-dimensional system however turns out even more robust than the one on a two-dimensional lattice, in the sense that its three-species coexistence region is considerably more extended in parameter space. Fig. 4.12 displays a series of population density time evolutions from single zero-dimensional simulation runs with identical parameters as in Fig. 4.9. All graphs in Fig. 4.12 reside deeply in the three-species coexistence region, while Fig. 4.9(a) and (c) showed approaches to absorbing states with one of the predator species becoming extinct. With $\omega_{\eta A} = 0.1$, $\omega_{\eta B} = 0.15$, and $\omega_{\mu B} = 0.1$ fixed, three-species coexistence states in the zero-dimensional system are found in the region $\omega_{\mu A} \in (0, 1)$, which is to be compared with the much narrower interval $(0.136, 0.159)$ in the two-dimensional system, indicating that spatial extent tends to destabilize these systems.

This finding is in remarkable contrast to some already well-studied systems such as the three-

species cyclic competition model, wherein spatial extension and disorder crucially help to stabilize the system [46,63]. Even though we do not allow explicit nearest-neighbor 'hopping' of particles in the lattice simulation algorithm, there still emerges effective diffusion of prey particles followed by predators. Since predator individuals only have access to adjacent prey in the lattice model, the presence of one predator species would block their neighboring predators from their prey. Imagining a cluster of predator particles surrounded by the other predator species, they will be prevented from reaching their 'food' and consequently gradually die out. However, this phenomenon cannot occur in the zero-dimensional system where no spatial structure exists at all, and hence blockage is absent. In the previous subsection we already observed that the cluster size of predator species remains almost unchanged throughout the simulation process when the total population size of the weaker predator species gradually decreases to zero, indicating that clusters vanish in a sequential way. We also noticed that population densities reach their quasi-stationary values much faster in the non-spatial model, see Fig. 4.12, than on the two-dimensional lattice, Fig. 4.9. In the spatially extended system, particles form intra-species clusters, and reactions mainly occur at the boundaries between neighboring such clusters of distinct species, thus effectively reducing the total reaction speed. This limiting effect is absent in the zero-dimension model where all particles have equal chances to meet each other.

4.4.4 Character displacements

Biologists rely on direct observation of animals' characters such as beak size when studying trait displacement or evolution [25, 51–53, 57–60]. Interspecific competition and natural selection induces noticeable character changes within tens of generations so that the animals may alter their phenotype, and thus look different to their ancestors. On isolated islands, native lizards change the habitat use and move to elevated perches following invasion by a second lizard kind with larger body size. In response, the native subspecies may evolve bigger toepads [64]. When small lizards cannot compete against the larger ones, character displacement aids them to exploit new living habitats by means of developing larger toepads in this case, as a result of natural selection.

Interestingly, we arrive at similar observations in our model, where predation efficiencies η and death rates μ are allowed to be evolving features of the individuals. In Fig. 4.13, the predation efficiency η is initially uniformly set to 0.5 for all particles, and the death rate $\mu = 0.5$ for all predators (of either species). Subsequently, in the course of the simulations the values of any offspring's η and μ are selected from a truncated Gaussian distribution centered at their parents' characters with distribution width ω_η and ω_μ. When the system arrives at a final steady state, the values of η and μ too reach stationary distributions that are independent of the initial conditions. We already demonstrated above that smaller widths ω afford the corresponding predator species advantages over the other, as revealed by a larger and stable population density. In Fig. 4.13, we fix $\omega_{\eta A} = 0.15$, $\omega_{\eta B} = 0.1$, $\omega_{\mu B} = 0.1$, and choose values for $\omega_{\mu A} \in [0.144, 0.15, 0.156]$ (represented respectively by red squares, blue

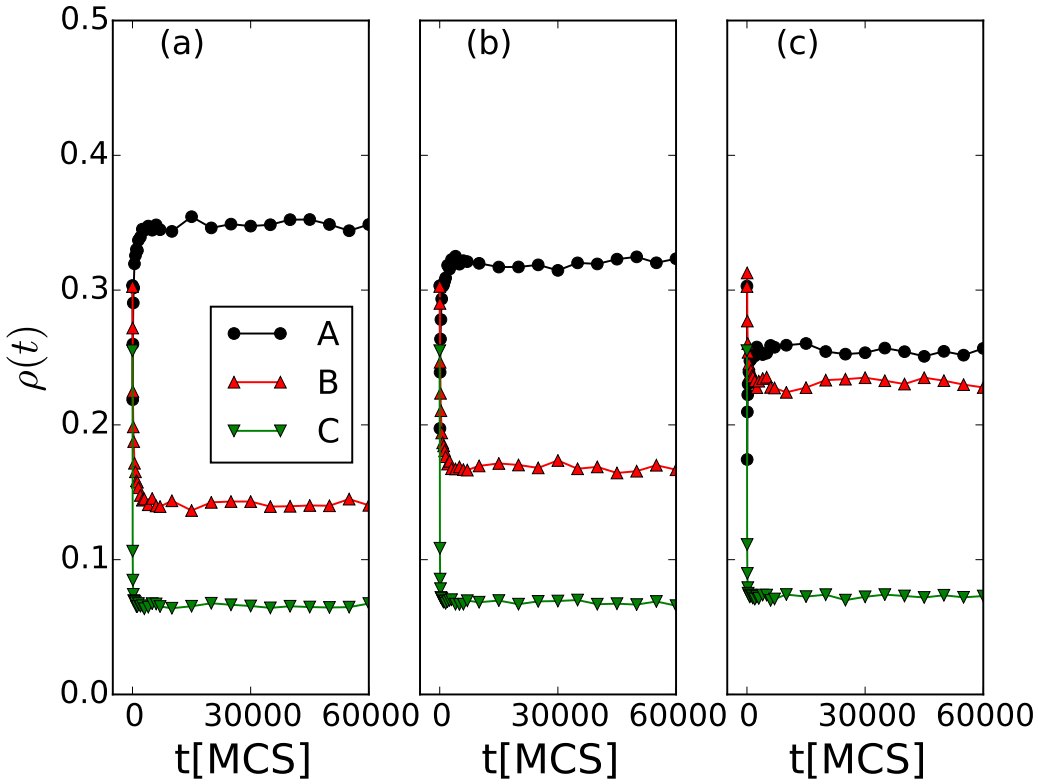

Figure 4.12: Adapted from paper [29] Fig.12. Data obtained from single Monte Carlo simulation runs in a zero-dimensional system with direct competition, evolutionary dynamics, and temporal correlations: Time record of population densities with $\omega_{\eta A} = 0.1$, $\omega_{\eta B} = 0.15$, $\omega_{\mu B} = 0.1$ and $\omega_{\mu A} = 0.132, 0.140, 0.160$ from left to right with species indicated as A in black dots, B in red triangles up, and C green triangles down.

triangles up, and green triangles down), and measure the final distribution of η and μ when the system reaches stationarity after 50 000 MCS. Figs. 4.13(a) and (c) show the resulting distributions for predator species A, while (b) and (d) those for B. Since both μ and η are in the range $[0, 1]$, we divide this interval evenly into 1 000 bins, each of length 0.001. The distribution frequency P is defined as the number of individuals whose character values fall in each of these bins, divided by the total particle number of that species. In Fig. 4.13(a), the eventual distribution of μ_A is seen to become slightly less optimized as $\omega_{\mu A}$ is increased from 0.144 to 0.156 since there is a lower fraction of low μ_A values in the green curve as compared with the red one. Since species A has a larger death rate, its final stable population density decreases as μ_A increases. In parallel, the distribution of η_A becomes optimized as shown in Fig. 4.13(c), as a result of natural selection: Species A has to become more efficient in predation to make up for its disadvantages associated with its higher death rates. Predator

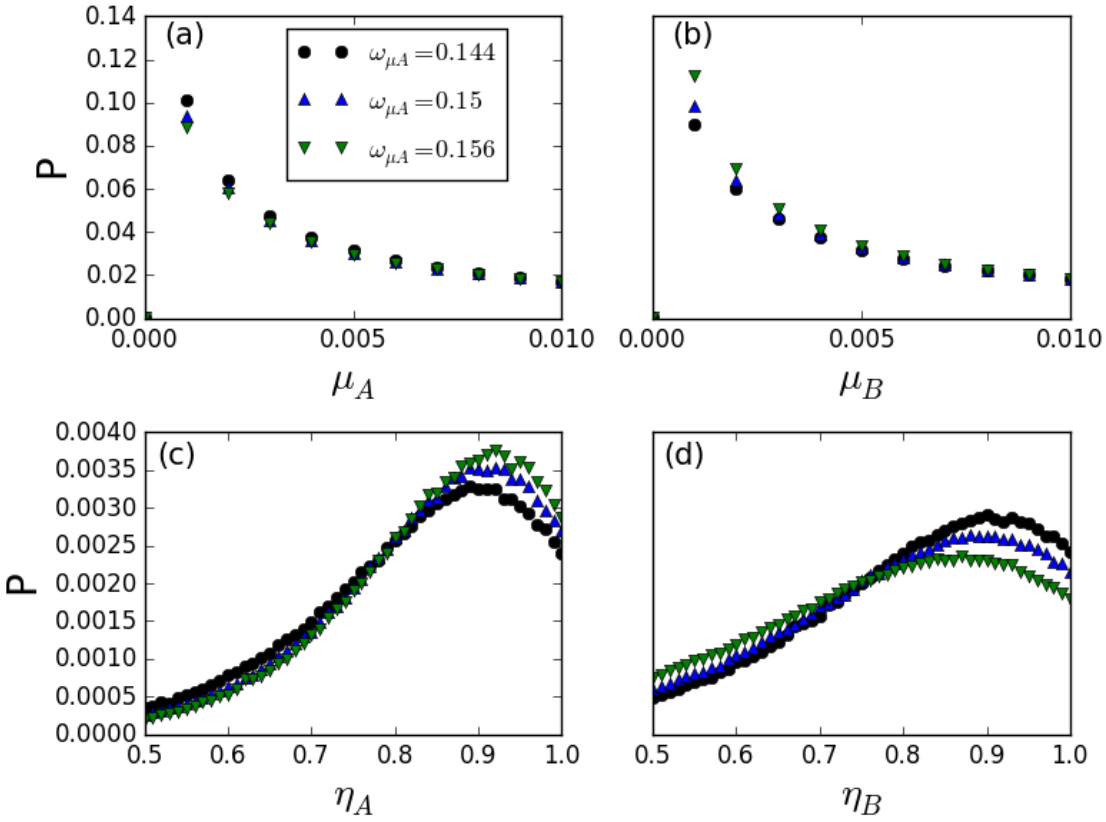

Figure 4.13: Adapted from paper [29] Fig.13. Monte Carlo simulations with direct predator competition: The final distribution of η and μ when the system becomes stable after 50 000 Monte Carlo Steps with $\omega_{\eta A} = 0.15$, $\omega_{\eta B} = 0.1$, $\omega_{\mu B} = 0.1$ and $\omega_{\mu A} = [0.144, 0.15, 0.156]$ indicated in red black dots, blue triangles up, and green triangles down. (a) and (c) depict the distribution of characters of predator species A, while (b) and (d) that of B. The interval $[0, 1]$ is divided evenly into 1 000 histograms bins; the quantity P represents the proportion of individuals with rates in the corresponding bins.

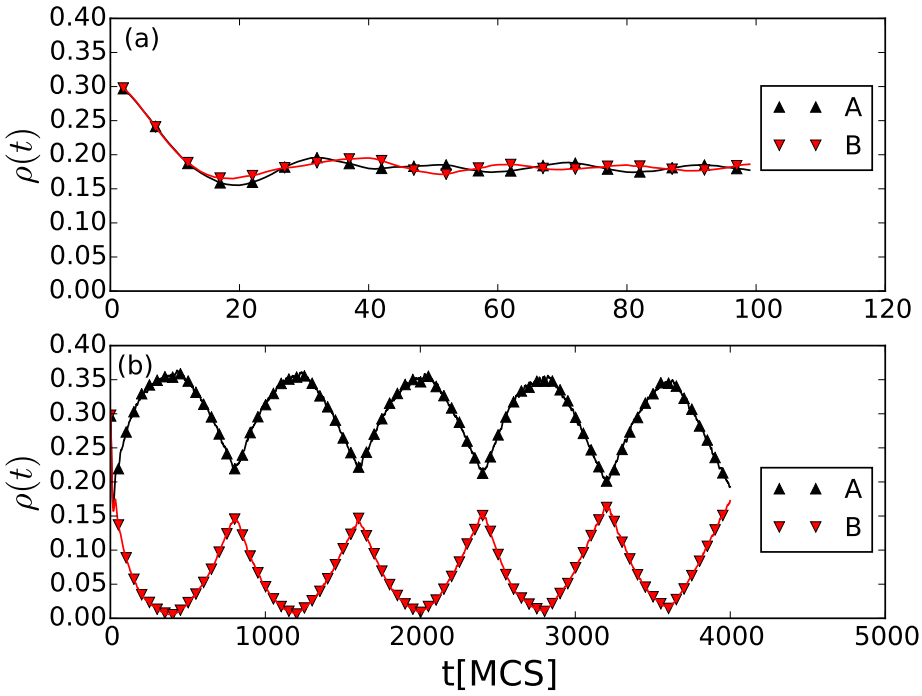

Figure 4.14: Adapted from paper [29] Fig.14. Monte Carlo simulations showing the temporal record of both predator population densities when the distribution widths $\omega_{\eta A}$ and $\omega_{\eta B}$ periodically exchange their values between 0.2 and 0.3. The other parameters are set to $\mu_A = \mu_B = 0.125$, $\sigma = 1.0$, and $\omega_C = \omega_{\mu A} = \omega_{\mu B} = 0$. The switch periods are $T = 10$ MCS in (a) and $T = 400$ MCS in (b).

species B is also influenced by the changes in species A. Since there is reduced competition from A in the sense that its population number decreases, the B predators gain access to more resources, thus lending its individuals with low predation efficiencies better chances to reproduce, and consequently rendering the distribution of η_B less optimized, see Fig. 4.13(d). This observation can be understood as predator species B needs no longer become as efficient in predation because they enjoy more abundant food supply. In that situation, since species B does not perform as well as before in predation, their death rate μ_B distribution in turn tends to become better optimized towards smaller values, as is evident in Fig. 4.13(b).

4.4.5 Periodic environmental changes

Environmental factors also play an important role in population abundance. There already exist detailed computational studies of the influence of spatial variability on the two-species lattice LV model [46, 47, 62]. However, rainfall, temperature, and other weather conditions that change in time greatly determine the amount of food supply. A specific environmental condition may favor one species but not others. For example, individuals with larger body

sizes may usually bear lower temperatures than small-sized ones. Since animals have various characters favoring certain natural conditions, one may expect environmental changes to be beneficial for advancing biodiversity.

We here assume a two-predator system with species A stronger than B so that the predator B population will gradually decrease as discussed in section 4.3. Yet if the environment changes and turns favorable to species B before it goes extinct, it may be protected from extinction. According to thirty years of observation of two competing finch species on an isolated island ecology [57], there were several instances when environmental changes saved one or both of them when they faced acute danger of extinction. We take $\omega_{\eta A}$ and $\omega_{\eta B}$ as the sole control parameters determining the final states of the system, holding all other rates fixed in our model simulations. Even though the environmental factors cannot be simulated directly here, we may effectively address environment-related population oscillations by changing the predation efficiency distribution widths ω. We initially set $\omega_{\eta A} = 0.2$ and $\omega_{\eta B} = 0.3$, with the other parameters held constant at $\mu_A = \mu_B = 0.125$, $\sigma = 1.0$, and $\omega_C = \omega_{\mu A} = \omega_{\mu B} = 0$. In real situations the environment may alternate stochastically; in our idealized scenario, we just exchange the values of $\omega_{\eta A}$ and $\omega_{\eta B}$ periodically for the purpose of simplicity. The population average of the spontaneous death rate is around 0.02, therefore its inverse ≈ 50 MCS yields a rough approximation for the individuals' typical dwell time on the lattice. When the time period T for the periodic switches is chosen as 10 MCS, which is shorter than one generation's life time, the population densities remain very close to their identical mean values, with small oscillations; see Fig. 4.14(a). Naturally, neither species faces the danger of extinction when the environmental change frequency is high. In Fig. 4.14(b), we study the case of a long switching time $T = 400$ MCS, or about eight generations. As one would expect, the B population abundance decreases quickly within the first period. Before the B predators reach total extinction, the environment changes to in turn rescue this species B. This example shows that when the environment stays unaltered for a very long time, the weaker species that cannot effectively adapt to this environment would eventually vanish while only the stronger species would survive and strive. When the time period T close matches the characteristic decay time t_c, see Fig. 4.14(b), one observes a resonant amplification effect with large periodic population oscillations enforced by the external driving.

4.5 Conclusions

In this part we use detailed Monte Carlo simulations to study an ecological system with two predator and one prey species on a two-dimensional square lattice. The two predator species may be viewed as related families, in that their reactions are similar, including predation, spontaneous death, and reproduction. The most important feature in this model is that there is only one mobile and reproducing food resource for all predators to compete for. We design various model variants with the goal of finding the key properties that stabilize a three-species coexistence state, and thus facilitate biodiversity in this simple model

system. We find no means to obtain coexistence when all reaction rates are fixed or individuals from the same species are all homogeneous, which clearly indicates the importance of demographic variability and evolutionary population adaptation. When dynamical optimization of the individuals in the reproduction process is introduced, they may develop various characters related to their predation and reproduction efficiencies. However, this evolutionary dynamics itself cannot stabilize coexistence for all three species, owing to the fixed constraint that both predator kind compete for the same food resource. In our model, direct competition between predator species is required to render a three-species coexistence state accessible, demonstrating the crucial importance of combined mutation, competition, and natural selection in stabilizing biodiversity.

We observe critical slowing-down of the population density decay near the predator extinction threshold, which also serves as an indicator to locate the coexistence region in parameter space. When the system attains its quasi-steady coexistence state, the spatial properties of the particle distribution remain stable even as the system evolves further. Character displacements hence occur as a result of inter-species competition and natural selection in accord with biological experiments. Through comparison of the coexistence regions of the full lattice model and its zero-dimensional representation, we find that spatial extent may decrease the ecosystem's stability, because the two predator species can effectively block each other from reaching their prey. We also study the influence of environmental changes by periodically switching the rate parameters of the two competing predator species. The system may then maintain three-species coexistence if the period of the environmental changes is smaller than the relaxation time of the population density decay. Matching the switching period to the characteristic decay time can induce resonantly amplified population oscillations.

Stable coexistence states with all three species surviving with corresponding constant densities are thus only achieved by introducing both direct predator competition and evolutionary adaptation in our system. In sections 4.3 and 4.4, we have explored character displacement without direct competition as well as competition without character displacement, yet a stable three-species coexistence state could not be observed in either case. Therefore it is necessary to include both direct competition and character displacement to render stable coexistence states possible in our model. However, even both predator species A and B can only coexist in a small parameter interval for their predation efficieny distribution widths ω, because they represent quite similar species that compete for the same resources. In natural ecosystems, of course other factors such as distinct food resources might also help to achieve stable multi-species coexistence.

Chapter 5

Spatial patterns formed by killer and prey E. coli strains

The contents of this chapter constitute a section of the publication:

Datla U S, Mather W H, Chen S, Shoultz I W, Täuber U C, Jones C N, Butzin N C, 2017, "The spatiotemporal system dynamics of acquired resistance in an engineered microecology", Scientific Reports, 7, 16071, "Copyright (2017) by Springer Nature", a link to the Creative Commons license: http://creativecommons.org/licenses/by/4.0/

This chapter only includes my contribution to the paper: writing the simulation codes, performing Monte Carlo simulations, analyzing the data, and plotting graphs to visualize the results. Dr. Mather and Udaya Sree Datla assisted in building the mathematical model.

5.1 Introduction

Despite the simplicity of the reaction rules for each individual particle, their collective behaviors may display complex macroscopic patterns. For example, traveling waves and reaction fronts are observed in the lattice LV model; and spirals exist in the three-species cyclic competition models. Biologically more relevant problems include investigating the formation of ecological structures, such as the shape of fish groups in the ocean and the patterns on animals' skin. In some instances, one idealized mathematical or computational model is good enough to reproduce the characteristic properties of the structures, thus serving an efficient way to study their formation. Synthetic biology, which combines biological and engineering technologies, allows scientists to design a microecological system of species reacting with desired rules in a well-controlled laboratory environment. Our collaborators, Udaya et al., applied these techniques to set up a killer-prey system and then observed complex spatio-temporal patterns. We participated in this project by providing a Monte Carlo simulation model that reproduced the distribution of cells as they observed in the experiment. The contents of this computational simulation are publicated as a part of reference [30].

They utilized genetic engineering techniques to build an artificial biological system consisting of the killer and prey E. coli strains, NB003 and DZ10 respectively, on a circular plate. The killer strain was engineered to secrete molecules named AHL which may kill the prey upon entering, and then release them into the environment constitutively. The prey was engineered to have the ability to mutate to be resistant to AHL. With the two E. coli strains prepared, the experiment followed these steps: initially the prey cells were uniformly distributed on the plate; then a killer colony was placed at the center; neither of them had the ability to move because the water on the plate was far from enough for the cells to 'swim' in, i.e., the cells were fixed at the locations wherever they were generated.

The plate was scanned once per hour to make quantitative image analysis of the time-lapse. We did not see any noticeable growth of the killer colony. There was a concentric 'kill zone' surrounding the killer colony. Around five prey colonies grew in the killing zone with their sizes much larger than other ones further from the plate center. Other prey colonies dispersed outside the kill zone, with both their count and population densities gradually increasing outward.

5.2 Monte Carlo simulation model and results

The spatial structure observed in the experiment is believed to reveal the killer-prey reaction process with acquired resistance of the mutant prey. At the beginning of the experiment, the generated AHL molecules diffused freely into their surrounding areas, wherein most prey cells were killed, thus generating a kill zone. Since the prey cells underwent constant mutation, they then became resistant to AHL, thus there were several mutated prey cells finally growing

into large colonies since they did not have competitors for nutrients in the kill zone. In order to verify this assumption, as well as to have an overall picture of the dynamical process, other than our collaborators' experimental efforts, we designed an idealized computational simulation model with several simple reactions corresponding to real cellular interactions. If we denote the killer as K, food as F, AHL as A, prey as P, and mutant prey as M, their reactions read:

$$\begin{aligned} K + F &\xrightarrow{\mu} K + A\,, \\ M + F &\xrightarrow{\nu} M + M\,, \\ P &\xrightarrow{\lambda} M\,, \\ P + A &\xrightarrow{1-\lambda} A\,, \\ P + F &\xrightarrow{\nu} P + P\,. \end{aligned} \tag{5.1}$$

The model is implemented on a two-dimensional square lattice with circular reflecting boundary conditions. A reasonable radius of the system, 200 lattice sites, is chosen so as to be large enough to reproduce the experimental pictures and computationally time-saving. Even though the cells may grow several layers upward in the real system, we apply occupation restrictions at each lattice site for the purpose of simplicity: each lattice site could be occupied by one cell, which could be a killer (K), prey (P), or mutated prey (M), or stays empty. The cells are non-mobile to account for the experimental setup. Besides the three cell species, there are two kinds of molecules present: food (F) and AHL (A). There is no limit on the occupation of molecules since they are of much smaller sizes than the cells. They diffuse randomly in the system. Note that there is no reproduction process for the killer. The reason for that is we do not observe growth of the killer colony in the experiment, which means the reproduction rate of the killer is low compared with the prey. For simplicity, we do not include their reproduction process in the model. Therefore they do not die, but only produce AHL by consuming food molecules. Both the normal and resistant prey, P and M, could reproduce with available food. The normal prey would either gain resistance to AHL or be killed by them. Initially there is no AHL in the system, only 20 food molecules on each site. The above reactions are incorporated in stochastic Monte Carlo simulations, with the details of the algorithm presented bellow,

1. Randomly pick a cell (K, P, or M) and generate a random float number r in the range $[0, 1]$, for cases that

   - There is a killer K on the cell. If the number of food molecules on this site is positive and $r < \mu$, this killer would consume one food molecule and then produce an AHL, which is to reduce the food molecule number on this site by 1 and increase the AHL number by 1;
   - There is a mutated prey M on the cell. If there are food molecules available, $r < \nu$, and there are empty sites on its four nearest neighbors, it will consume

one food molecule and then generate a new M particle on a randomly selected empty site;

- There is a normal prey P on the cell. If $r < \lambda$, this particle changes to a mutated prey M. Otherwise, when there are AHL molecules on this site, this cell would be removed from the system and then the state of the site becomes empty. When there is no AHL on the site, there is a probability ν that this P cell reproduces a new P particle on one of its empty neighbors by consuming one food molecule F.

2. After the above reactions are performed, the food or AHL molecules on the site would diffuse to the neighbor sites with a probability D. In our simulation, D is fixed as 1.0, thus all molecules would move to their neighbor sites at random.

3. If the total number of all cells including K, P, and M is currently N in the system, the simulation time would be updated by $1.0/N$ after the above reactions. One Monte Carlo step is considered finished when the integer part of the simulation time increases by 1. And step (1) and (2) would be repeated until a pre-given number of MCS is completed.

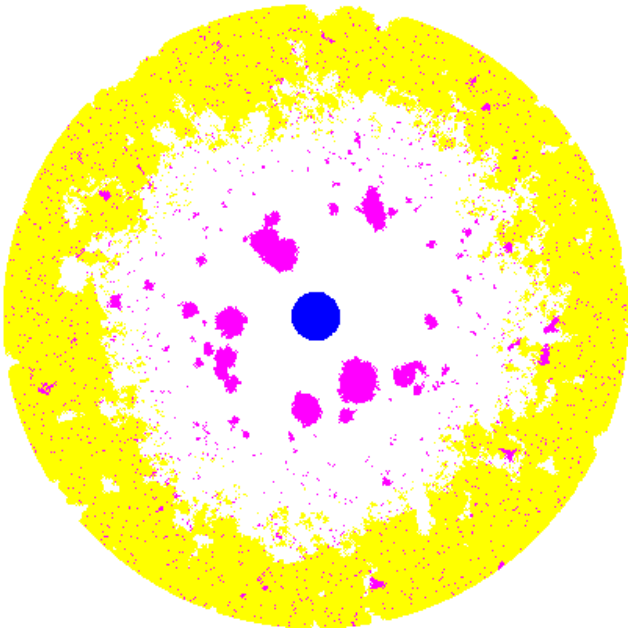

Figure 5.1: Adapted from paper [30] Fig.3. The distribution of the cells when the simulation of the killer-prey system runs for 3000 MCS with reaction probabilities $\mu = 0.1$, $\nu = 0.02$, and $\lambda = 0.00001$. The simulation is performed on a two-dimensional lattice with a circular reflecting boundary. The radius of the system is 200 lattice sites. Killers are indicated with the blue color, mutated prey with red, and normal prey with yellow.

Fig. 5.1 shows the distribution of the cells after the simulation runs for 3000 MCS with the reaction probabilities $\mu = 0.1$, $\nu = 0.02$, and $\lambda = 0.00001$. The blue killer cells are centered at the plate surrounded by a kill zone where a few red mutated prey colonies grow to be large. Hundreds of tiny red colonies are located outside the kill zone. In the areas far from the killers, there are yellow normal prey surviving because AHL molecules have not yet diffused there. This simulation qualitatively reproduces the spatial structures of the kill zone and the distribution of cells as already observed in the experiments, thus demonstrating that the killer-prey reactions together with acquired resistance of the prey are sufficient to generate the spatial patterns observed in the experiment. The computational model could be further investigated to provide insights about the future work of the experiments.

Chapter 6

Summary

This thesis includes four research projects about non-equilibrium critical dynamics, boundary and disorder effects, noise-induced pattern formation, and biodiversity in two- and three-species predator-prey systems. We utilize the tool of Monte Carlo simulation to investigate the stochastic lattice Lotka–Volterra model and its variants.

The first project, described in chapter 2, studies the critical dynamics near the active-to-absorbing phase transition point which is introduced by the site occupation restriction in the stochastic lattice LV model. The temporal evolution of the predator species population density shows a transition from a fast exponential decay to a slow algebraic decay when the system undergoes a phase transition from a two-species coexistence state to an absorbing state with the predator species going extinct. Therefore, its relaxation time, i.e., the characteristic time for the predator population density to reach its stationary value, diverges when the control parameter approaches the critical value. The two-time autocorrelation functions, measured at waiting times s and observation times t, do not overlap when plotted against $t - s$, indicating that time translation invariance is broken. However, when they are scaled by a factor s^b, where b represents the scaling exponent, they collapse when plotted versus t/s, demonstrating that simple aging dynamic scaling holds here. Indeed, critical aging is considered to occur when there is critical slowing-down, breaking of time translation invariance, and dynamic scaling. Since the critical and aging exponents measured in the system agree with those of Directed Percolation (DP), the lattice LV model at the phase transition point belongs to the DP class. These critical phenomena have a potential application in providing warning signals when an endangered species is close to extinction in its natural ecological habitat.

Aging is due to critical slowing-down in our system. In general, it can emerge whenever a system's relaxation kinetics is slow and time translation invariance is broken, say by a quench from an initial state that is fundamentally different from the long-time asymptotic stationary state the system tries to reach. For example, it is also observed in systems such as the May-Leonard type six-species model with coarsening [65], Coulomb glass in disordered

semiconductors [66], and Bose glass in type-II superconductors with defects [66], to list but a few. There is also a case that the stochastic predator-prey model can recapitulate the phenomenology of the laminar-turbulence transition even though they originate from unrelated areas, as demonstrated in reference [67]. Therefore, it is reasonable to compare the LV model and others in order to find their connections if they exist.

There are still some open questions arising from our research. In chapter 4, the measured exponents at the critical points of one predator extinction transition do not agree with DP values, which is contradicting our previous experience that active-absorbing phase transitions usually belong to the DP class. This might be due to demographic variability, which needs to be explored more in the future. Another possible research direction is to change the model so that it switches between different universality classes, which is related to control theory. Considering the relative simplicity of the LV model, it is an ideal system to work with in the field of population dynamics and non-equilibrium statistical physics in the future.

Inspired by seeing the dramatic influences of spatial and temporal correlations on the dynamical properties of a system, as demonstrated by the difference between the lattice model and the mean-field model, this thesis also explores the effects of a spatial boundary, periodic fluctuations, and demographic variabilities.

Spatial inhomogeneity is very common in ecological systems since the natural environment varies by location. In chapter 3 we construct such a system in which a straight border evenly splits the system into two parts, with a two-species coexistence state on one side and a predator extinction state on the other side. We measure the predator population density, correlation length, and relaxation time in various parts of the system. Their values in the boundary region largely differ from those deep inside the coexistence area, indicating the enormous influence of spatial inhomogeneity. Since the boundary effects only persist for a spatial distance of about one correlation length, we split the system into small pieces, like a checkerboard, then observe the boundary effects to gradually vanish, as expected.

Temporal fluctuations, such as the irregular changes of the temperature, play an important role in ecological systems as well. In chapter 4, we periodically switch the control parameters, helping to stabilize the system which would otherwise fall into an absorbing state. All our simulations incorporate temporal stochasticity since the reactions occur in a random way.

Considering that reproduction of identical offspring occurs rarely in nature, demographic variability is added to our simulation model in order to render it closer to real ecological systems. As in chapter 4, the particles from a single species vary in their predation efficiency, death rates, and reproduction rates. This demographic variability is introduced to simulate a 'Darwinian evolution' process that an offspring particle may be different from its parent, and thus the species on average becomes stronger after several generations. Chapter 4 focuses on the interplay between evolution and interspecific competition in an idealized two-predator-one-prey model. We find that evolution or direct competition between the two predator species cannot stabilize a three-species coexistence state in a system where two related predator species compete for the same food resource, but the combination of the two

does. Hopefully, this part of our work will finally contribute to better understanding the emergence and stability of biodiversity in ecology.

We have studied spatial inhomogeneity and temporal fluctuations separately here; it might be interesting to study a system with mixed variabilities. We have not yet performed a systematic study of the extent to which these perturbations drive the system away from the mean-field model. Some future work could focus on this issue. For example, in order to study how fast the diffusion of particles should be so as to render the system close to mean-field predictions, we could introduce additional diffusion or jumping for the particles. When the diffusion rate is 0, the particles are fixed on their sites, thus spatial structures form. When the diffusion rate approaches infinity, each pair of particles have equal chance to meet, much like an infinite-dimensional system. We can tune the diffusion rate between 0 and positive infinity to study how the system changes along the way. This method can also explore finite-size effects, site restriction effects, and other perturbations introduced by the simulation algorithm.

In chapter 5, we utilize a simplified computational simulation model to reproduce the spatio-temporal patterns of the cell distribution in a biological experiment of two killer and prey E. coli stains with acquired resistance of the prey strain. This model only contains reaction rules relevant to the experiments. These include the killing of the normal prey by AHL molecules secreted by the predator cells, the mutation of the normal prey so that they gain resistance to AHL, and the reproduction of the cells. This idealized model shows the formation of a kill zone around the killer colony and the growth of large mutant prey colonies inside the kill zone in a similar way to the experiment. The model suffices to reproduce the dynamical properties of the experiment. In the future, we might explore the model more in hope of finding valuable insights that aid interpretations of experiments. The LV model and its variants are sometimes criticized for being over-simplified and ecologically unrealistic. This is partially due to the natural environment being too complex to be simulated, as well as the data for wild animals being difficult to collect. Synthetic biology as addressed in chapter 5 sheds some light on this problem. Genetic engineering technologies can help design certain species reacting with desired rules. Experiments can be performed in well-controlled laboratory environments, thus scientists can do accurate measurements. Therefore, synthetic biology bridges the gap between simple mathematical models and real complex ecological systems, which might gain more attention in the future.

In general, we study problems about critical dynamics at the phase transition point, noise-induced pattern formation, and the effects of a spatial boundary, periodic fluctuations, and demographic variabilities. They belong to a large area of non-equilibrium statistical physics which is of interest to physicists. We hope to find more dynamical properties with the models studied in population dynamics. We also want to further modify these models to study ecological or biological problems in the real world with the help of modern experimental technologies.

Bibliography

[1] Lotka A J, 1920, Undamped oscillations derived from the law of mass action, *Journal of the American Chemical Society*, **42**, 1595 (Cited on pages 1, 10, 28, and 41.)

[2] Volterra V, 1926, Fluctuations in the abundance of a species considered mathematically, *Nature*, **118**, 558 (Cited on pages 1, 10, 28, and 41.)

[3] May R M, 1973, *Stability and complexity in model ecosystems* vol 6, (Princeton: Princeton University Press) (Cited on pages 3 and 10.)

[4] Maynard Smith J, 1974, *Models in ecology*, (Cambridge: Cambridge University Press) (Cited on pages 3 and 10.)

[5] Boccara N, Roblin O, Roger M, 1994, Automata network predator-prey model with pursuit and evasion, *Physical Review* E, **50**, 4531 (Cited on pages 4, 10, 11, 28, and 41.)

[6] Durrett R, 1999, Stochastic spatial models, *SIAM Review*, **41**, 677 (Cited on pages 4, 10, 28, and 41.)

[7] Provata A, Nicolis G, Baras F, 1999, Oscillatory dynamics in low-dimensional supports: a lattice Lotka—Volterra model, *The Journal of Chemical Physics*, **110**, 8361 (Cited on pages 4, 10, 28, and 41.)

[8] Rozenfeld A F, Albano E V, 1999, Study of a lattice-gas model for a prey–predator system, *Physica* A, **266**, 322 (Cited on pages 4, 10, 28, and 41.)

[9] Lipowski A 1999, Oscillatory behavior in a lattice prey-predator system, *Physical Review* E, **60**, 5179 (Cited on pages 4, 10, 28, and 41.)

[10] Lipowski A, Lipowska D, 2000, Nonequilibrium phase transition in a lattice prey-predator system, *Physica* A, **276**, 456 (Cited on pages 4, 10, 11, 28, and 41.)

[11] Monetti R, Rozenfeld A, Albano E, 2000, Study of interacting particle systems: the transition to the oscillatory behavior of a prey-predator model, *Physica* A, **283**, 52 (Cited on pages 4, 10, 11, 28, and 41.)

[12] Droz M, Pękalski A, 2001, Coexistence in a predator-prey system, *Physical Review* E, **63**, 051909 (Cited on pages 4, 10, 11, 28, and 41.)

[13] Antal T, Droz M, 2001, Phase transitions and oscillations in a lattice prey-predator model, *Physical Review* E, **63**, 056119 (Cited on pages 4, 10, 28, and 41.)

[14] Kowalik M, Lipowski A, Ferreira A L, 2002, Oscillations and dynamics in a two-dimensional prey-predator system, *Physical Review* E, **66**, 066107 (Cited on pages 4, 10, 28, and 41.)

[15] Mobilia M, Georgiev I T, Täuber U C, 2006, Fluctuations and correlations in lattice models for predator-prey interaction, *Physical Review* E, **73**, 040903 (Cited on pages 4, 10, 11, 12, 28, 41, 42, and 43.)

[16] Washenberger M J, Mobilia M, Täuber U C, 2007, Influence of local carrying capacity restrictions on stochastic predator–prey models, *Journal of Physics: Condensed Matter*, **19**, 065139 (Cited on pages 4, 10, 11, 28, 32, and 41.)

[17] McKane A J, Newman T J, 2005, Predator-prey cycles from resonant amplification of demographic stochasticity, *Physical Review Letters*, **94**, 218102 (Cited on pages 4, 10, and 28.)

[18] Mobilia M, Georgiev I T, Täuber U C, 2007, Phase transitions and spatio-temporal fluctuations in stochastic lattice Lotka–Volterra models, *Journal of Statistical Physics*, **128**, 447 (Cited on pages 4, 6, 10, 11, 13, 18, 20, 28, and 41.)

[19] Dobramysl U, Mobilia M, Pleimling M, Täuber U C, 2017, Stochastic population dynamics in spatially extended predator-prey systems, to appear in *Journal of Physics A: Mathematical and Theoretical* [arXiv:1708.07055] (Cited on pages 4, 41, and 42.)

[20] Chen S, Täuber U C, 2016, Non-equilibrium relaxation in a stochastic lattice Lotka–Volterra model, *Physical Biology*, **13**, 025005 (Cited on pages 5, 7, 12, 15, 16, 18, 19, 22, 24, 28, 30, 41, 42, and 62.)

[21] Täuber U C, 2014, *Critical dynamics – A field theory approach to equilibrium and non-equilibrium scaling behavior*, (Cambridge: Cambridge University Press) (Cited on pages 4, 5, 11, 17, 18, 23, 47, and 61.)

[22] Henkel M, Hinrichsen H, Lübeck S, 2008, *Non-equilibrium phase transitions* vol 1: Absorbing phase transitions, (Bristol, UK: Springer) (Cited on pages 5, 11, 17, 18, 21, 47, and 61.)

[23] Henkel M, Pleimling M, 2010, *Non-equilibrium phase transitions* vol 2: Ageing and dynamical scaling far from equilibrium, (Bristol, UK: Springer) (Cited on pages 5, 11, 21, and 23.)

[24] Täuber U C, 2012, Population oscillations in spatial stochastic Lotka–Volterra models: a field-theoretic perturbational analysis, *Journal of Physics A: Mathematical and Theoretical*, **45**, 405002 (Cited on pages 6, 10, 11, and 18.)

[25] Brown W L, Wilson E O, 1956, Character displacement, *Systematic Zoology*, **5**, 49 (Cited on pages 6, 41, and 65.)

[26] Melville J, 2002, Competition and character displacement in two species of scincid lizards, *Ecology letters*, **5**, 386 (Cited on pages 6, 10, 41, and 55.)

[27] Balagaddé F K et al. 2008, A synthetic Escherichia coli predator–prey ecosystem, *Molecular systems biology*, **4**, 187 (Cited on page 6.)

[28] Heiba B, Chen S, Täuber U C, 2018, Boundary effects on population dynamics in stochastic lattice Lotka–Volterra models, *Physica A*, **491**, 582 (Cited on pages 7, 31, 33, 34, 35, 36, 37, and 38.)

[29] Chen S, Dobramysl U, Täuber U C, 2017, Evolutionary dynamics and competition stabilize three-species predator-prey communities, submitted to Ecological Complexity [arXiv:1711.05208] (Cited on pages 7, 8, 44, 45, 47, 48, 53, 55, 56, 60, 61, 63, 64, 66, 67, and 68.)

[30] Datla U S, Mather W H, Chen S, Shoultz I W, Täuber U C, Jones C N, Butzin N C, 2017, The spatiotemporal system dynamics of acquired resistance in an engineered microecology, *Scientific Reports*, **7**, 16071 (Cited on pages 7, 8, 72, and 74.)

[31] Hofbauer J, Sigmund K, 1998, *Evolutionary games and population dynamics*, (Cambridge: Cambridge University Press) (Cited on page 10.)

[32] Neal D, 2004, *Introduction to population biology*, (Cambridge: Cambridge University Press) (Cited on page 10.)

[33] Matsuda H, Ogita N, Sasaki A, Satō K, 1992, Statistical mechanics of population – the lattice Lotka–Volterra model, *Progress of Theoretical Physics*, **88**, 1035 (Cited on pages 10, 28, and 41.)

[34] Satulovsky J E, Tomé T, 1994, Stochastic lattice gas model for a predator-prey system, *Physical Review* E, **49**, 5073 (Cited on pages 10, 11, 28, and 41.)

[35] Dai L, Vorselen D, Korolev K S, Gore J, 2012, Generic indicators for loss of resilience before a tipping point leading to population collapse, *Science*, **336**, 1175 (Cited on pages 11, 21, and 62.)

[36] Voigt C A, Ziff R M, 1997, Epidemic analysis of the second-order transition in the Ziff-Gulari-Barshad surface-reaction model, *Physical Review* E, **56**, R6241 (Cited on pages 18, 20, and 62.)

[37] Grassberger P, Zhang Y-C, 1996, Self-organized formulation of standard percolation phenomena, *Physica* A, **224**, 169 (Cited on pages 18, 20, 21, and 47.)

[38] Janssen H K, Täuber U C, 2005, The field theory approach to percolation processes, *Annals of Physics* (NY), **315**, 147 (Cited on pages 18 and 23.)

[39] Takeuchi K A, Kuroda M, Chaté H, Sano M, 2009, Experimental realization of directed percolation criticality in turbulent liquid crystals, *Physical Review* E, **80**, 051116 (Cited on pages 20 and 25.)

[40] Daquila G L, Täuber U C, 2012, Nonequilibrium relaxation and critical aging for driven Ising lattice gases, *Physical Review Letters*, **108**, 110602 (Cited on pages 21 and 26.)

[41] Ramasco J J, Henkel M, Santos M A, da Silva Santos C A, 2004, Ageing in the critical contact process: a Monte Carlo study, *Journal of Physics A: Mathematical and General*, **37**, 10497 (Cited on pages 20, 23, and 25.)

[42] Skellam J G, 1951, Random dispersal in theoretical populations, *Biometrika*, **38**, 196 (Cited on page 28.)

[43] Dahmen K A, Nelson D R, Shnerb N M, 1999, Population dynamics and non-Hermitian localization, *Statistical Mechanics of Biocomplexity*, **527**, 124 (Cited on page 28.)

[44] Méndez, Campos D, 2008, Population extinction and survival in a hostile environment, *Physical Review* E, **77**, 022901 (Cited on page 28.)

[45] Fisher R A, 1937, The waves of advance of advantageous genes, *Annals of Eugenics*, **7**, 335 (Cited on page 28.)

[46] Dobramysl U, Täuber U C, 2008, Spatial variability enhances species fitness in stochastic predator-prey interactions, *Physical Review Letters*, **101**, 258102 (Cited on pages 28, 65, and 68.)

[47] Dobramysl U, Täuber U C, 2013, Environmental versus demographic variability in two-species predator-prey models, *Physical Review Letters*, **110**, 048105 (Cited on pages 28, 42, 50, 51, and 68.)

[48] Darwin C R, 1859, On the origin of species by means of natural selection, *John Murray* (Cited on page 41.)

[49] Schluter D, McPhail J D, 1992, Ecological character displacement and speciation in sticklebacks, *American Naturalist*, **140**, 85 (Cited on page 41.)

[50] Taper M L, Case T J, 1992, Coevolution among competitors, *Oxford Surveys in Evolutionary Biology*, **8**, 63 (Cited on page 41.)

[51] Lack D, 1947, Darwin's finches, *Cambridge University Press* (Cited on pages 41 and 65.)

[52] Grant P R, 1975, The classic case of character displacement, *Evolutionary Biology*, **8**, 237 (Cited on pages 41 and 65.)

[53] Arthur W, 1982, The evolutionary consequences of interspecific competition, *Advances in Ecological Research*, **12**, 127 (Cited on pages 41 and 65.)

[54] Maynard Smith J, 1982, Evolution and the theory of games, *Cambridge University Press* (Cited on page 41.)

[55] Frachebourg L, Krapivsky P L, E. Ben-Naim, 1996, Spatial organization in cyclic Lotka–Volterra systems, *Physical Review Letter*, **77**, 2125 (Cited on page 41.)

[56] Shih H Y, Goldenfeld N, 2014, Path-integral calculation for the emergence of rapid evolution from demographic stochasticity, *Physical Review* E, **90**, 050702 (Cited on page 42.)

[57] Grant R P, Grant B R, 2006, Evolution of Character Displacement in Darwin's finches, *Science*, **313**, 224 (Cited on pages 46, 65, and 69.)

[58] Rice A M, Leichty A R, Pfennig D W, 2009, Parallel evolution and ecological selection: replicated character displacement in spadefoot toads, *Proceedings of the Royal Society* B, **276**, 4189 (Cited on pages 46 and 65.)

[59] Stuart Y E, Campbell T S, Hohenlohe P A, Reynolds R G, Revell L J, Losos J B, 2014, Rapid evolution of a native species following invasion by a congener, *Science*, **346**, 463 (Cited on pages 46 and 65.)

[60] Tan J, Slattery M R, Yang X, Jiang L, 2016, Phylogenetic context determines the role of competition in adaptive radiation, *Proceedings of the Royal Society* B, **283** (Cited on pages 46 and 65.)

[61] Broadbent S R, Hammersley J M, 1957, Percolation Processes, *Mathematical Proceedings of the Cambridge Philosophical Society*, **53**, 629 (Cited on page 47.)

[62] Dobramysl U, Täuber U C, 2013, Environmental versus demographic variability in stochastic predator-prey models, *Journal of Statistical Mechanics*, **2013**, P10001 (Cited on pages 50, 51, and 68.)

[63] He A, Mobilia M, Täuber U C, 2011, Coexistence in the two-dimensional May–Leonard model with random rates, *European Physical Journal B*, **82**, 97 (Cited on page 65.)

[64] Strauss S Y, Lau J A, Schoener T W, Tiffin P, 2008, Evolution in ecological field experiments: implications for effect size, *Ecology Letters*, **11**, 199 (Cited on page 65.)

[65] Brown B L, Pleimling M, 2017, Coarsening with non-trivial in-domain dynamics: correlations and interface fluctuations, *Physical Review* E, **96**, 012147 (Cited on page 76.)

[66] Assi H, Chaturvedi H, Pleimling M, Täuber U C, 2016, Structural relaxation and aging scaling in the Coulomb and Bose glass models, *The European Physical Journal* B, **89**, 252 (Cited on page 77.)

[67] Goldenfeld N, Shih H Y, 2017, Turbulence as a problem in non-equilibrium statistical mechanics, *Journal of Statistical Physics,* **167**, 575 (Cited on page 77.)